5

Fundamentals of Poroelasticity

E. DETOURNAY

University of Minnesota, Minneapolis, MN, USA

and

ALEXANDER H.-D. CHENG

University of Delaware, Newark, DE, USA

5.1 INTRODUCTION

The presence of a freely moving fluid in a porous rock modifies its mechanical response. Two mechanisms play a key role in the interaction between the interstitial fluid and the porous rock: (i) an increase of pore pressure induces a dilation of the rock; and (ii) compression of the rock causes a rise of pore pressure, if the fluid is prevented from escaping the pore network. These coupled mechanisms bestow an apparent time-dependent character to the mechanical properties of the rock. Indeed, if excess pore pressure induced by compression of the rock is allowed to dissipate through diffusive fluid mass transport, further deformation of the rock progressively takes place. It also appears that the rock is more compliant under drained conditions (when excess pore pressure is completely dissipated) than undrained ones (when the fluid cannot escape the porous rock).

Interest in the role of these coupled diffusion–deformation mechanisms was initially motivated by the problem of 'consolidation' – the progressive settlement of a soil under surface surcharge [1–4]. However, the role of pore fluid has since been explored in scores of geomechanical processes: subsidence due to fluid withdrawal [5, 6], tensile failure induced by pressurization of a borehole [7, 8], propagation of shear and tensile fractures in fluid-infiltrated rock with application to earthquake mechanics [8–10], *in situ* stress determination [7, 11], sea bottom instability under water wave loading [12–14], and hydraulic fracturing [15–17], to cite a few.

The earliest theory to account for the influence of pore fluid on the quasi-static deformation of soils was developed in 1923 by Terzaghi [1] who proposed a model of one-dimensional consolidation. This theory was generalized to three dimensions by Rendulic [2] in 1936. However, it is Biot who in 1935 [3] and 1941 [4] first developed a linear theory of poroelasticity that is consistent with the two basic mechanisms outlined above. Essentially the same theory has been reformulated several times by Biot himself [18–21], by Verruijt [5] in a specialized version for soil mechanics, and also by Rice and Cleary [8] who linked the poroelastic parameters to concepts that are well understood in rock and soil mechanics. In particular, the presentation of Rice and Cleary [8] emphasizes the two

limiting behaviors, drained and undrained, of a fluid-filled porous material; this formulation considerably simplifies the interpretation of asymptotic poroelastic phenomena. Alternative theories have also been developed using the formalism of mixtures theory [22–26], but in practice they do not offer any advantage over the Biot theory [8, 26].

This chapter is concerned with the formulation and analysis of coupled deformation–diffusion processes, within the framework of the Biot theory of poroelasticity. Four major sections cover the following topics: (i) the constitutive equations, presented in an effort to unify and to relate various approaches proposed in the literature; (ii) the linear quasi-static theory of poroelasticity, using a formulation inspired partially by Rice and Cleary's work [8]; (iii) analytical and numerical methods for solving initial/boundary value problems; and (iv) solution and discussion of some fundamental problems. Other issues such as anisotropy, nonlinearity, and in particular, aspects of the role of pore fluid on rock strength and failure mechanism [9, 27], are only briefly addressed in the context of this presentation.

5.2 MECHANICAL DESCRIPTION OF A POROELASTIC MATERIAL

As a necessary preliminary to a presentation of the constitutive equations, mass and momentum balance laws, we briefly introduce here the basic kinematic and dynamic quantities that are used in the mechanical description of a fluid-filled porous rock. Consistent with the classical continuum approach, any quantity that appears in this description is taken to be averaged over a certain length scale l. This length scale l, which underpins the continuum model, is assumed to be large (at least by a factor of 100) with respect to the length scale of the microstructure (*i.e.* the typical dimension of the pores or rock grains), yet small enough to allow the introduction of genuine macroscopic scale material heterogeneity.

The Biot model of a fluid-filled porous material is constructed on the conceptual model of a coherent solid skeleton and a freely moving pore fluid (in other words both solid and fluid phases are fully connected). This conceptual picture dictates the choice of the kinematic quantities: a solid displacement vector u_i which tracks the movement of the porous solid with respect to a reference configuration, and a specific discharge vector q_i which describes the motion of the fluid *relative* to the solid. The specific discharge q_i is formally defined as the rate of fluid volume crossing a unit area of porous solid whose normal is in the x_i direction. Two 'strain' quantities are also introduced to follow the deformation and the change of fluid content of the porous solid with respect to an initial state: the usual small strain tensor ε_{ij} and the variation of fluid content ζ, defined as the variation of fluid volume per unit volume of porous material due to diffusive fluid mass transport: ε_{ij} is positive for extension, while a positive ζ corresponds to a 'gain' of fluid by the porous solid. The strain quantities are related to the original kinematic variables u_i and q_i according to a compatibility expression

$$\varepsilon_{ij} = \tfrac{1}{2}(u_{i,j} + u_{j,i}) \tag{1}$$

and the fluid mass balance relation (see Section 5.4.1.3)

$$\frac{\partial \zeta}{\partial t} = -q_{i,i} \tag{2}$$

where t represents time. The following conventions have been adopted in writing these two equations: a comma followed by subscripts denotes differentiation with respect to spatial coordinates and repeated indices in the same monomial imply summation over the range of the indices (generally 1–3, unless otherwise indicated).

Consider now the basic dynamic variables: the total stress tensor σ_{ij}, and the pore pressure p, which is a scalar. The stress is defined in the usual way: σ_{ij} is the *total force* in the x_j direction per unit area whose normal is in the x_i direction. (Consistent with the strain convention, a positive normal stress implies tension.) The pore pressure in a material element is defined as the pressure in a hypothetical reservoir which is in equilibrium with this element (*i.e.* no fluid exchange takes place between the reservoir and the material element) [8]. Note that the stress and pore pressure are the conjugate quantities of the strain and the variation of fluid content, respectively; in other words the work increment associated with the strain increment $\mathrm{d}\varepsilon_{ij}$ and $\mathrm{d}\zeta$, in the presence of the stress σ_{ij} and p, is

$$\mathrm{d}W = \sigma_{ij}\,\mathrm{d}\varepsilon_{ij} + p\,\mathrm{d}\zeta \tag{3}$$

In the Biot model, description of stress and strain in the fluid is thus limited to their isotropic component. The shear stress at the contact between fluid and solid, associated with a local velocity gradient in the fluid is not considered in this formulation. Furthermore, the definition of the pore pressure places some restrictions on the time scale at which coupled diffusion–deformation processes can be analyzed, since the pore pressure must first be locally equilibrated between neighboring pores, over the length scale l (time scale and length scale are linked through a diffusivity coefficient, which depends among other things on the viscosity of the interstitial fluid). It is therefore in the modeling of quasi-static processes that the Biot model finds its full justification, even though it has been extended to the dynamic range [28].

5.3 CONSTITUTIVE EQUATIONS

This section deals principally with the volumetric response of a linear isotropic poroelastic material. The description of this seemingly simple material has been the object of many different formulations. Here we relate some of these approaches, considering first a 'continuum' formulation where the fluid-filled material is treated as a whole, then a 'micromechanical formulation' where the individual contributions of the solid and fluid constituents are explicitly taken into account. Many material constants are introduced in this presentation of the volumetric response, but only three of these parameters are actually independent. The three basic material constants that have been selected to constitute the reference set are the drained bulk modulus K, the undrained bulk modulus K_u, and the Biot coefficient α. (Correspondences between the basic material constants K, K_u, and α and the coefficients appearing in the various formulations proposed by Biot can be found in Appendix A.)

5.3.1 Continuum Formulation

5.3.1.1 Poroelastic constitutive equations

The Biot formulation of the constitutive equations for a fluid-filled porous material is based on the assumptions of linearity between the stress (σ_{ij}, p) and the strain (ε_{ij}, ζ), and reversibility of the deformation process (meaning that no energy is dissipated during a closed loading cycle). With the respective addition of the scalar quantities p and ζ to the stress and strain group, the linear constitutive relations can be obtained by extending the known elastic expressions. In particular, the most general form of the isotropic material response is

$$\varepsilon_{ij} = \frac{\sigma_{ij}}{2G} - \left(\frac{1}{6G} - \frac{1}{9K}\right)\delta_{ij}\sigma_{kk} + \frac{1}{3H'}\delta_{ij}p \tag{4a}$$

$$\zeta = \frac{\sigma_{kk}}{3H''} + \frac{p}{R'} \tag{4b}$$

Without the pore pressure, equation (4a) degenerates to the classical elastic relation. The parameters K and G are thus identified as the bulk and the shear modulus of the drained elastic solid. The additional constitutive constants H', H'' and R' characterize the coupling between the solid and fluid stress and strain. One of these constants can however be eliminated. Indeed, the assumption of reversibility implies that the work increment

$$\mathrm{d}W = \sigma_{ij}\,\mathrm{d}\varepsilon_{ij} + p\,\mathrm{d}\zeta = \varepsilon_{ij}\,\mathrm{d}\sigma_{ij} + \zeta\,\mathrm{d}p \tag{5}$$

is an exact differential [4]; the Euler conditions

$$\frac{\partial \varepsilon_{ij}}{\partial p} = \frac{\partial \zeta}{\partial \sigma_{ij}} \tag{6}$$

combined with equations (4) lead to the equality $H'' = H'$. The isotropic constitutive law therefore involves only four constitutive constants G, K, H' and R'. (H' and R' were originally denoted as H and R in Biot's 1941 paper [4]. Since the same symbols were later redefined [18], the prime superscripts have been added here to avoid any confusion; see Appendix A.)

The constitutive equations of an isotropic poroelastic material (equations 4) can actually be separated into a deviatoric response

$$e_{ij} = \frac{1}{2G} s_{ij} \tag{7}$$

and a volumetric one

$$\varepsilon = -\left(\frac{P}{K} - \frac{p}{H'}\right) \tag{8a}$$

$$\zeta = -\left(\frac{P}{H'} - \frac{p}{R'}\right) \tag{8b}$$

where s_{ij} and e_{ij} denote the deviatoric stress and strain, P the mean or total pressure (isotropic compressive stress), and ε the volumetric strain

$$s_{ij} = \sigma_{ij} + P\delta_{ij} \tag{9a}$$

$$e_{ij} = \varepsilon_{ij} - \frac{\varepsilon}{3}\delta_{ij} \tag{9b}$$

$$P = -\frac{\sigma_{kk}}{3} \tag{9c}$$

$$\varepsilon = \varepsilon_{kk} \tag{9d}$$

It is apparent from equation (7) that for an isotropic poroelastic material, the deviatoric response is purely elastic. The coupled effects which involve constants H' and R' appear only in the volumetric stress–strain relationship (equations 8). This is, however, a particularity of isotropic materials (further information on the constitutive equations of anisotropic material can be found in refs. 18, 27 and 29). The remainder of this section will be exclusively devoted to an analysis of the volumetric response of a linear isotropic poroelastic material.

5.3.1.2 Volumetric response

(i) Drained and undrained response

A key feature of the response of fluid-infiltrated porous material is the difference between undrained and drained deformation. These two modes of response represent limiting behaviors of the material: the undrained response characterizes the condition where the fluid is trapped in the porous solid such that $\zeta = 0$, while the drained response corresponds to zero pore pressure $p = 0$. (For the time being, the drained conditions will be assumed to correspond to $p = 0$; this can, however, be relaxed to include any initial pore pressure field that is in equilibrium.)

From equation (8b), it is apparent that a pore pressure p proportional to the total pressure P is induced under the undrained condition $\zeta = 0$

$$p = BP \tag{10}$$

where the coefficient $B = R'/H'$ is known as the Skempton pore pressure coefficient [30]. Substituting p in equation (8a) by the value given in equation (10) indicates that the volumetric strain is proportional to the total pressure P under the undrained condition ($\zeta = 0$)

$$\varepsilon = -\frac{P}{K_u} \tag{11}$$

where

$$K_u = K\left(1 + \frac{KR'}{H'^2 - KR'}\right) \tag{12}$$

is the undrained bulk modulus of the material.

Under the drained condition $p = 0$, the volumetric strain is also proportional to the total pressure (see equation 8a)

$$\varepsilon = -\frac{P}{K} \tag{13}$$

So under both drained and undrained conditions, the poroelastic material behaves as an elastic one, the undrained material being, however, stiffer (in its volumetric response) than the drained one. Substituting equation (13) in equation (8b), with $p = 0$, leads to

$$\zeta = \alpha\varepsilon \tag{14}$$

where $\alpha = K/H'$. This equation gives a meaning to the constant α as the ratio of the fluid volume gained (or lost) in a material element to the volume change of that element, when the pore pressure is allowed to return to its initial state. Equation (14) also points to the fact that α cannot be larger than 1, since the volume of fluid gained (or lost) by an element cannot be greater than the total volume change of that element (under the linearized approximation).

The three volumetric constitutive constants, K, K_u and α, which will be chosen in place of K, H' and R' as the basic set, have thus physical meanings that are associated with the drained and undrained responses of the material. The range of variation of α is $[0, 1]$ and K_u is $[K, \infty]$.

(ii) Fast and slow loading

The undrained and drained responses also characterize the instantaneous and long-term behaviors of the poroelastic material under the particular conditions of a suddenly applied constant loading. Consider the 'instantaneous' response of the poroelastic material to such a step loading. Just after imposition of a load, the pore fluid has not had the time to move between neighboring material elements, other than within some local pore scale, hence $\zeta = 0$. After a long time, the pore pressure will equilibrate with the pore pressure imposed at the boundary. Assuming this pore pressure to be zero, the long-term response of the material will be characterized by the disappearance of the pore pressure everywhere, *i.e.* $p = 0$. Because of the stiffness contrast between undrained and drained response, the volumetric deformation will evolve from the short-term value (equation 11) to the long-term one (equation 13).

In the most general manner, the undrained response denotes conditions where the time scale characteristic of the loading is too short to allow fluid movement to take place between material elements by diffusive mass transport, while the drained response characterizes conditions where the pore pressure field is in steady state equilibrium.

(iii) Alternative expressions for the volumetric response

For further reference, it is useful to write the volumetric relations (equations 8) using the basic set of constants, α, K and K_u

$$\varepsilon = -\frac{1}{K}(P - \alpha p) \tag{15a}$$

$$\zeta = -\frac{\alpha}{K}\left(P - \frac{p}{B}\right) \tag{15b}$$

where

$$B = \frac{K_u - K}{\alpha K_u} \tag{16}$$

The volumetric relations can inversely be written as

$$P = \alpha M\zeta - K_u\varepsilon \tag{17a}$$

$$p = M(\zeta - \alpha\varepsilon) \tag{17b}$$

where

$$M = \frac{K_u - K}{\alpha^2} = \frac{H'^2R'}{H'^2 - KR'} \tag{18}$$

The constant M is sometimes called the Biot modulus; it is the inverse of a storage coefficient

[31, 32], defined as the increase of the amount of fluid (per unit volume of rock) as a result of a unit increase of pore pressure, under constant volumetric strain

$$\frac{1}{M} = \left.\frac{\partial \zeta}{\partial p}\right|_{\varepsilon} \tag{19}$$

5.3.2 Micromechanical Approach

The constitutive model presented in the previous section describes the response of a porous material as a whole, without explicitly taking into account the individual contributions of its solid and fluid constituents. In other words, the 'lumped' continuum model relates the bulk response to the bulk material properties. The shortcomings of this approach are that the bulk material constants are tied to a specific solid–pore–fluid system. It is, for example, not known how these bulk constants are influenced by change in the compressibility of the fluid or in the porosity of the rock.

It is thus desirable to look into the 'micromechanics' of the solid–pore–fluid system to elicit the dependence of the bulk material coefficients on the micromechanical ones. At the cost of more measurements, one can gain additional insight to the interaction among the constituents. This approach leads also to the establishment of the limiting behaviors furthermore, it can provide guidelines to extend the theory into the nonlinear range.

The emphasis below is restricted to the poroelastic coupling of the material response. Hence only the volumetric response of the poroelastic material, subject to a total pressure P and a pore pressure p is examined (assuming that prior to loading, there is zero stress and pore pressure). This loading will be designated by the notation $\{P, p\}$, to emphasize the independence of the two load components. An alternative to the loading decomposition $\{P, p\}$ will be also considered here. The loading $\{P, p\}$ can be recombined into two components: (i) a Terzaghi effective pressure $P' = P - p$, and (ii) a 'Π-pressure' $p' = p$ which corresponds to a confining pressure and a pore pressure of same magnitude p. This particular loading will henceforth be denoted as 'Π-loading', and the alternative loading decomposition will be denoted as $[P', p']$.

5.3.2.1 Volumetric response of fluid-infiltrated porous solids

(i) Porous solid and pore volume

Let us consider a 'sample' of porous material of volume V, containing an *interconnected* pore space of volume V_p. The combined volume of the solid phase and isolated pores is denoted by V_s, with $V = V_p + V_s$. Assuming full saturation, the volume of fluid which can freely circulate in the sample is thus $V_f = V_p$. The porosity ϕ is defined as the ratio V_p/V.

The volumetric response of the porous material to the loading $\{P, p\}$ can be described in terms of $\Delta V/V$ and $\Delta V_p/V_p$, the volumetric strain of the bulk material and of the pore space, respectively. Simply by invoking linearity between stress and strain, the following relations can be written

$$\frac{\Delta V}{V} = -\frac{1}{K}(P - \alpha p) \tag{20a}$$

$$\frac{\Delta V_p}{V_p} = -\frac{1}{K_p}(P - \beta p) \tag{20b}$$

where K_p is the bulk modulus for the pore volumetric strain and β a dimensionless effective stress coefficient. A comparison of equation (20a) with equation (15a) reveals that the coefficients of K and α are those defined before. The coefficients appearing in equations (20) are, however, not all independent. By invoking the Betti–Maxwell reciprocal theorem, it can indeed be proven that the increase in total volume ΔV due to the application of a pore pressure p is the same (to a minus sign) as the decrease in the pore volume ΔV_p due to the application of a confining pressure P of equal magnitude [33, 34]

$$\left.\frac{\partial V}{\partial p}\right|_{P} = -\left.\frac{\partial V_p}{\partial P}\right|_{p} \tag{21}$$

Substituting equations (20) into equation (21), we obtain

$$K_p = \frac{\phi}{\alpha} K \tag{22}$$

The constitutive relations (equations 20) can alternatively be expressed in terms of the two loading components P' and p'

$$\frac{\Delta V}{V} = -\frac{P'}{K} - \frac{p'}{K_s'} \tag{23a}$$

$$\frac{\Delta V_p}{V_p} = -\frac{P'}{K_p} - \frac{p'}{K_s''} \tag{23b}$$

Comparison with equations (20) shows that

$$\alpha = 1 - \frac{K}{K_s'} \tag{24a}$$

$$\beta = 1 - \frac{K_p}{K_s''} \tag{24b}$$

The coefficients K_s' and K_s'' are two bulk moduli, which under certain circumstances can be both identified with the bulk modulus K_s of the solid constituent (see Section 5.3.2.2).

(ii) Solid constituent and porosity

The load decomposition $[P', p']$ suggests an alternative description of the volumetric response of the porous solid in terms of $\Delta V_s/V_s$ and $\Delta\phi/(1-\phi)$, two quantities that measure respectively the volumetric deformation of the solid phase, and the relative deformation of the pore space and the porous solid [35]. Using the definition $V = V_p + V_s$ and $\phi = V_p/V$, it is easily deduced that

$$\frac{\Delta V}{V} = \frac{\Delta V_s}{V_s} + \frac{\Delta\phi}{1-\phi} \tag{25a}$$

$$\frac{\Delta V_p}{V_p} = \frac{\Delta V_s}{V_s} + \frac{\Delta\phi}{\phi(1-\phi)} \tag{25b}$$

The constitutive relations for the solid phase and the porosity can then be established using the above decomposition and equations (23),

$$\frac{\Delta V_s}{V_s} = -\frac{P'}{(1-\phi)K_s'} - \frac{1}{1-\phi}\left(\frac{1}{K_s'} - \frac{\phi}{K_s''}\right)p' \tag{26a}$$

$$\frac{\Delta\phi}{1-\phi} = -\frac{P'}{K_\phi} + \frac{\phi}{1-\phi}\left(\frac{1}{K_s'} - \frac{1}{K_s''}\right)p' \tag{26b}$$

where we have introduced the notation

$$\frac{1}{K_\phi} = \frac{1}{K} - \frac{1}{1-\phi}\frac{1}{K_s'} \tag{27}$$

The advantage of writing the volumetric constitutive response of the porous material in the above form becomes obvious for the particular case $K_s' = K_s''$, discussed in Section 5.3.2.2.

(iii) Fluid volumetric response

On the assumption that the pore space of the porous material is completely filled by a fluid, the pore volume change is equal to the variation of fluid volume trapped in the pore space, *i.e.* $\Delta V_p = \Delta V_f$. The variation of fluid volume ΔV_f can actually be decomposed into two parts

$$\Delta V_f = \Delta V_f^{(1)} + \Delta V_f^{(2)} \tag{28}$$

where $\Delta V_f^{(1)}$ is the component associated to the compression or dilation of the interstitial fluid and $\Delta V_f^{(2)}$ is the component due to fluid exchange between the sample of porous material and the

outside. Introducing the bulk modulus of the fluid K_f, $\Delta V_f^{(1)}$ can be expressed in terms of the pore pressure as

$$\frac{\Delta V_f^{(1)}}{V_f} = -\frac{p}{K_f} \tag{29}$$

The second component $\Delta V_f^{(2)}$ is actually related to the variation of fluid content ζ introduced earlier, *i.e.*

$$\zeta = \frac{\Delta V_f^{(2)}}{V} = \frac{\phi \Delta V_f^{(2)}}{V_f} \tag{30}$$

Using equations (23b), (29) and (30), a constitutive relation can be derived for ζ

$$\zeta = -\frac{\phi}{K_p}\left(P - \frac{p}{B}\right) \tag{31}$$

where

$$\frac{1}{B} = 1 - \frac{K_p}{K_s''} + \frac{K_p}{K_f} \tag{32}$$

The original equation for ζ (equation 15b) has thus been reconstructed from a different viewpoint.

(iv) Parameter correspondences and limiting cases

The previous construction has provided an alternative meaning to the poroelastic constants. Table 1 summarizes the correspondence between continuum and micromechanical quantities. These

Table 1 Relation Among Bulk Continuum and Micromechanical Coefficients

$$\alpha = 1 - \frac{K}{K_s'}$$

$$= 1 - \frac{K_p}{\phi K_s' + K_p}$$

$$K_u = K\left[1 + \frac{\left(1 - \frac{K}{K_s'}\right)^2}{\frac{K}{K_s'}\left(1 - \frac{K}{K_s'}\right) + \phi\left(\frac{K}{K_f} - \frac{K}{K_s''}\right)}\right]$$

$$B = 1 - \frac{\phi\left(\frac{K}{K_f} - \frac{K}{K_s''}\right)}{\left(1 - \frac{K}{K_s'}\right) + \phi\left(\frac{K}{K_f} - \frac{K}{K_s''}\right)}$$

$$= 1 - \frac{\frac{K_p}{K_f} - \frac{K_p}{K_s''}}{1 + \frac{K_p}{K_f} - \frac{K_p}{K_s''}}$$

$$K = K_s'\left(1 - \frac{\phi K_s'}{\phi K_s' + K_p}\right)$$

$$= \frac{K_p}{\phi}\left(1 - \frac{K_p}{K_p + \phi K_s'}\right)$$

$$= K_\phi\left[1 - \frac{K_\phi}{(1-\phi)K_s' + K_\phi}\right]$$

$$\frac{1}{M} = \frac{K}{K_s'}\left(\frac{1}{K} - \frac{1}{K_s'}\right) + \phi\left(\frac{1}{K_f} - \frac{1}{K_s''}\right)$$

equations can be used to evaluate the dependence of the bulk continuum constants α, B, K, K_u and M on the porosity and the compressibilities of the fluid, solid and pores. In particular, simplified expressions for the poroelastic parameters can be extracted for limiting cases.

(a) Incompressible solid constituent ($K/K_s' \ll 1$ and $K/K_s'' \ll 1$). The compressibility of the solid phase is negligible compared to that of the drained bulk material. The simplified expressions for α, B, K_u, and M are

$$\alpha = 1 \tag{33a}$$

$$K_u = K\left(1 + \frac{K_f}{\phi K}\right) \tag{33b}$$

$$B = 1 - \frac{1}{1 + \dfrac{K_f}{\phi K}} \tag{33c}$$

$$M = \frac{K_f}{\phi} \tag{33d}$$

The resultant model is equivalent to Verruijt's [5], where the ratio K_f/ϕ is the only relevant poroelastic constant. We also note that the following relation which links the bulk modulus of the porous solid K to K_ϕ and K_p

$$K = K_\phi = \frac{K_p}{\phi} \tag{34}$$

(b) Incompressible fluid and solid constituents ($K/K_s' \ll 1$, $K/K_s'' \ll 1$ and $K/K_f \ll 1$). Equations (33) for the incompressible solid constituent case reveal that if the compressibility of the fluid can further be neglected, then $B = 1$, $K_u \to \infty$, and $M \to \infty$. For this limiting situation all the poroelastic parameters assume their upper bound values.

(c) Highly compressible fluid constituent ($K_f/K \ll 1$). The approximated expressions for B, K_u, and M are

$$K_u = K\left(1 + \frac{\alpha^2 K_f}{\phi K}\right) \tag{35a}$$

$$B = \frac{\alpha K_f}{\phi K} = \frac{K_f}{K_p} \tag{35b}$$

$$M = \frac{K_f}{\phi} \tag{35c}$$

In the limit $K_f \to 0$, the parameter $B \to 0$, $K_u \to K$, and $M \to 0$; in other words, the porous material behaves as an elastic material without fluid.

5.3.2.2 *Invariance of porosity under* Π*-loading*

We now consider an ideal porous material characterized by a fully connected pore space and by a microscopically homogeneous and isotropic matrix material. If a Π-loading is applied to this material, the resulting stress corresponds to a uniform pressure p everywhere in the solid constituent. In other words, this material deforms under Π-loading as if all the pores were filled with solid material [33, 36]. Hence, the solid component and the skeleton experience a uniform volumetric strain without any shape change, and

$$\frac{\Delta V_s}{V_s} = \frac{\Delta V_p}{V_p} = \frac{\Delta V}{V} \tag{36}$$

The above relation implies that there is no change in porosity under Π-loading in this ideal material. Applying equation (36) to equations (23) with $P' = 0$, we clearly observe the identity between the two solid moduli

$$K_s' = K_s'' = K_s \tag{37}$$

where K_s is now identified as the modulus of solid material. The above equivalence between the K_s' and K_s'' actually serves as the definition of this ideal porous material, which appears to have been first discussed by Gassmann [37].

With the identity in equation (37), the constitutive equations (equations 26) simplify to

$$\frac{\Delta V_s}{V_s} = -\frac{P_s}{K_s} \tag{38a}$$

$$\frac{\Delta \phi}{1-\phi} = -\frac{P'}{K_\phi} \tag{38b}$$

where

$$P_s = \frac{1}{1-\phi}(P - \phi p) \tag{39}$$

These are the constitutive laws derived by Carroll [35, 38]. Equation (38a) shows that the volumetric strain of the solid phase is proportional to the solid pressure P_s, defined as the isotropic component of the compressive stress averaged over the solid phase. Equation (38b) reveals that the porosity variation is controlled by the Terzaghi effective pressure $P' = P - p$. In particular, for a sample under Π-loading, there is no porosity variation $\Delta\phi = 0$, since $P' = 0$.

Equation (37) brings some simplification of the relation between the bulk continuum and micromechanical parameters. The specialization of results in Table 1 is now summarized in Table 2, where the ratio K_s/K has been replaced by $(1 - \alpha)$. Generalization of this theory to deviatoric loading and anisotropic elastic material can be found in the work of Katsube and Carroll [38, 39].

It is instructive to consider the case of an elastic isotropic material with spherical pores [35, 38]. Using the expression for the effective bulk modulus derived by Mackenzie [40], it can be shown that

$$K_\phi = \frac{4G_s(1-\phi)}{3\phi} \tag{40}$$

where G_s is the shear modulus of the solid phase. Hill [41, 42] proved that equation (40) gives an upper bound for the effective bulk modulus of a porous solid, irrespective of the pore configuration. Equation (40) shows that the modulus K_ϕ depends only on the solid shear modulus G_s (and not on K_s), implying that porosity variation in an elastic material with spherical pores is due entirely to the shear stresses induced in the solid phase by the application of an effective pressure P'. These shear stresses, which have zero volume average, are associated to the stress concentration around the pores [35].

How good is the approximation introduced by assuming that $K_s' = K_s''$? The bulk moduli of the major mineralogical components of most rocks do not differ by a large amount, and thus any significant difference between these two moduli is likely to be the consequence of the existence of a nonconnected pore space. The little experimental evidence available does not contradict, however, the validity of this assumption. Nur and Byerlee [36] reported tests on a low porosity Westerly granite ($\phi \cong 1\%$) indicating that the bulk modulus K_s' identical to the grain modulus. Experiments

Table 2 Expressions for α, K_u, B and M for the Particular Case where ϕ is Invariant under Π-Loading

$\alpha = 1 - \dfrac{K}{K_s}$
$K_u = K\left[1 + \dfrac{\alpha^2 K_f}{(1-\alpha)(\alpha-\phi)K_f + \phi K}\right]$
$B = \dfrac{\alpha K_f}{[\alpha - \phi(1-\alpha)]K_f + \phi K}$
$\dfrac{1}{M} = \dfrac{\phi}{K_f} + \dfrac{\alpha - \phi}{K_s}$

performed by Zimmerman *et al.* [43] on various sandstones also support this hypothesis. In closing, it is noted that the assumption $K_s' = K_s''$ is certainly a convenient one. The error linked to the assumption is assumably modest, especially in view of the nonlinear effects which are discussed next.

5.3.2.3 Nonlinear volumetric deformation of porous rocks

Many experimental results suggest that the volumetric response of porous rocks to the change of total pressure and pore pressure is actually nonlinear [43–45]. The linear relations considered so far are merely approximations, applicable to 'small' stress variations. The nonlinear behavior is generally associated with the closing/opening of crack-like pores (characterized by the small aspect ratio of the minor to major axis of the pore), but in very porous and weak rocks, it is caused by progressive pore collapse. The main concern here is to establish whether or not the dependence of the compressibilities on the total pressure P and the pore pressure p can be reduced to an 'effective' pressure instead (*i.e.* a quantity depending linearly on P and p), and to establish bounds on the variation of the compressibilities with porosity.

Investigations of the nonlinear deformation of porous rocks have mainly been motivated by the need to quantify the effect of pore pressure decline during depletion of an oil or gas reservoir on pore volume and the volume of the rock (the latter in relation with the study of the mechanism of subsidence). We also adopt here a notation in terms of compressibility instead of stiffness that is consistent with the one used in these studies.

Under increasing confining pressure and/or decreasing pore pressure, crack-like pores close progressively (those with the smallest aspect ratio first) and once closed do not contribute any more to the compressibility of the rock. Pores that are approximately equidimensional do not close, however, provided that the solid material remains elastic. To accommodate this nonlinear deformation, the volumetric response of the porous material is now written in incremental form, for an infinitesimal transition of the loading from $\{P, p\}$ to $\{P + \mathrm{d}P, p + \mathrm{d}p\}$

$$\frac{\mathrm{d}V}{V^0} = -C_{bc}(P, p)\,\mathrm{d}P + C_{bp}(P, p)\,\mathrm{d}p \tag{41a}$$

$$\frac{\mathrm{d}V_p}{V_p^0} = -C_{pc}(P, p)\,\mathrm{d}P + C_{pp}(P, p)\,\mathrm{d}p \tag{41b}$$

where the superscript 0 for the bulk and pore volumes refers to stress-free conditions (to ensure a 'small strain' formulation). The compliance coefficients C_{bc} and C_{bp} are the bulk compressibilities while C_{pc} and C_{pp} are pore compressibilities. The compressibilities are related to the previously defined parameters by

$$C_{bc} = \frac{1}{K} \quad C_{bp} = \frac{\alpha}{K} \quad C_{pc} = \frac{1}{K_p} \quad C_{pp} = \frac{\beta}{K_p} \tag{42}$$

If the deformation induced by the infinitesimal load $\{\mathrm{d}P, \mathrm{d}p\}$ is reversible and independent of the manner in which it is applied, then equation (22) between two of the poroelastic constants still holds, *i.e.* in the present notation

$$C_{bp} = \phi C_{pc} \tag{43}$$

As implied by the notation used in equation (41), all the coefficients depend on the confining pressure and pore pressure. With some weak assumptions it is, however, possible to demonstrate that the compressibilities are actually only functions of the Terzaghi effective pressure P' [43]. This can be established by writing equations (41) in a different form (compare equations 20 and 23)

$$\frac{\mathrm{d}V}{V^0} = -C_{bc}(P', p')\,\mathrm{d}P' - C_s'(P', p')\,\mathrm{d}p' \tag{44a}$$

$$\frac{\mathrm{d}V_p}{V_p^0} = -C_{pc}(P', p')\,\mathrm{d}P' - C_s''(P', p')\,\mathrm{d}p' \tag{44b}$$

It is clear that

$$C_s' = C_{bc} - C_{bp} \tag{45a}$$

$$C_s'' = C_{pc} - C_{pp} \tag{45b}$$

Consider the following assumptions. (1) There is no porosity variation under Π-loading. (2) The compressibility of the solid phase is constant (independent of stress). (3) The volume variations dV and dV_p induced by the loading $\{dP, dp\}$ do not depend on the stress path followed. In other words, dV and dV_p are exact differentials.

Assumption 1 leads to the equality $dV/V^0 = dV_p/V_p^0$ under the condition $dP' = 0$, hence

$$C_s' = C_s'' = C_s = \frac{1}{K_s} \tag{46}$$

In the above, C_s is the compressibility of the solid phase. Assumption 3 implies that Euler conditions $\partial C_{bc}/\partial p' = \partial C_s/\partial P'$ and $\partial C_{pc}/\partial p' = \partial C_s/\partial P'$ exist. Since C_s is a constant (assumption 2), we find

$$\frac{\partial C_{bc}}{\partial p'} = \frac{\partial C_{pc}}{\partial p'} = 0 \tag{47}$$

It is finally concluded that the bulk and pore compressibilities depend only on the Terzaghi effective pressure P'. This conclusion is supported by many experimental results obtained by Zimmerman *et al.* [43] and others. Also, the above relations (equations 43, 45 and 46) show that once ϕ and C_s are known, it is enough to measure only one compressibility (the other compressibilities being then directly determined).

Equation (45a) shows $C_{bc} = C_s + \phi C_{pc}$, suggesting that the bulk compressibility C_{bc} is always larger than the solid phase compressibility C_s. The pore compressibility C_{pc}, and thus the bulk compressibility, decrease with increasing confining pressure until all the crack-like pores are closed. The compressibilities then approach constant values. Experiments on consolidated sandstones [43] indicate that this effect takes place at a confining pressure of about 50 MPa. For a rock like the Westerly granite, which is made up almost exclusively of crack-like pores, all the cracks are closed at a confining pressure of about 200 MPa and the bulk compressibility of the rock is then virtually identical to the compressibility of the mineral constituents, C_s.

Although it has been shown that $C_{bc} \geq C_s (K_s \geq K)$, one can establish more precise bounds for the bulk modulus K. Hashin and Shreikman [46] considered a material which is both microscopically and macroscopically isotropic, and constructed the upper bound

$$\frac{K}{K_s} \leq 1 - \frac{3\phi}{2 + \phi} \tag{48}$$

The lower bound for K is clearly zero, as one can have a connected network of long and thin cracks embedded in the media such that it can be closed without resistance. From equation (48), bounds for the following quantities can also be derived [43]

$$\frac{K_p}{K_s} \leq \frac{2}{3} - \frac{2\phi}{3} \tag{49a}$$

$$\alpha \geq \frac{3\phi}{2 + \phi} \tag{49b}$$

$$\beta \geq \frac{1}{3} + \frac{2\phi}{3} \tag{49c}$$

5.3.3 Laboratory Measurements

The principle of measuring the poroelastic coefficients that characterize the volumetric response of an isotropic porous rock is now discussed. In view of the nonlinear response of rocks, the poroelastic constants must be understood as incremental or tangent parameters. They need thus to be determined by measuring the response to a small load increment of a rock sample, initially subject to a confining pressure P_0 and a pore pressure p_0. It practice, it can generally be assumed that the incremental (or tangent) coefficients depend only on the Terzaghi effective pressure $P_0 - p_0$, implying that all the measurements can actually be done at zero reference pore pressure, $p_0 = 0$.

Three types of tests are commonly used to determine the poroelastic parameters: (i) the drained test where the load increment is $\{\Delta P, 0\}$; (ii) the unjacketed test characterized by an equal increase of

Table 3 Test Description

Test	*Boundary conditions*	*Measurements*	*Poroelastic parameters*
Drained	$P = P^0 + \Delta P$	$\Delta V/V$	K
	$p = p^0$	$\Delta V_f/V$	α
Undrained	$P = P^0 + \Delta P$	$\Delta V/V$	K_u
	$\zeta = 0$	p	B
Unjacketed	$P = P^0 + \Delta p'$	$\Delta V/V$	K_s'
	$p = p^\circ + \Delta p'$	$\Delta V_f/V$	γ

the confining pressure and pore pressure, $[0, \Delta p']$; and (iii) the undrained test where a confining pressure ΔP is applied on the rock, but no fluid is allowed to enter or leave the core sample.

All these tests can be carried out in an apparatus that can be schematically described as follows. A jacketed core of rock set between two endcaps is placed in a pressure vessel where a confining pressure can be applied hydraulically. Endcaps can be designed either with drainage holes to enable control of the pore pressure through fluid mass exchange with the sample for the drained test, or solid for the undrained test (possibly mounted with a pressure transducer). See Zimmerman *et al.* [47] for a description of such an apparatus with control of both the confining pressure and pore pressure, and Green and Wang [48] for aspects pertaining to the undrained experiment. Note that the increments of pressure used in these experiments are typically of order of a few MPa. Table 3 summarizes the tests, testing conditions and parameters determined. Details are discussed next.

5.3.3.1 Drained test

In the drained test, the confining pressure is increased by ΔP, but the pore pressure p is maintained at the initial value p_0 on the boundary (or at least part of the boundary) of the rock core. As a result of the loading, an incremental pore pressure Δp is initially induced in the rock (equal to $B\Delta P$, assuming 'undrained' conditions during application of the load), and is then progressively dissipated as the pore pressure comes into equilibrium with the boundary condition. If the cylindrical sample is drained at both ends, the drainage path is approximately one-dimensional and the characteristic time for dissipation of the induced pore pressure is of order $L^2/4c$, where c is the diffusivity coefficient (see Section 5.4.3) and L the length of the core. Depending on the permeability of the rock, the diffusivity coefficient can be as high as $10^4\ \mathrm{cm^2\,s^{-1}}$ for a very permeable sandstone and as low as $10^{-4}\ \mathrm{cm^2\,s^{-1}}$ for a low porosity shale. For a core length of 5 cm, the time required for the pore pressure to reach equilibrium could thus vary from less than one second for a sandstone to the order of days for a shale.

Once the pore pressure is in equilibrium, two measurements can be made: ΔV, the volume change of the sample, and ΔV_f, the volume of fluid expelled from the rock. Since the fluid pressure before loading and at equilibrium is identical, no calibration of the measurement system for ΔV_f to compensate for pressure change is needed; furthermore ΔV_f should accurately represent the change of pore volume caused by the incremental loading $\{\Delta P, 0\}$. The volumetric change of the sample ΔV can be estimated using strain gauges mounted on the core in transverse and longitudinal directions, or from the oil volume change in the cell (this latter method requires, however, calibration to account for the compressibility of the confining fluid volume and the cell).

From the two measurements ΔV and ΔV_f ($= \Delta V_p$), the drained bulk modulus K and the α coefficient can be determined according to $K = V\Delta P/\Delta V$ and $\alpha = \Delta V_f/\Delta V$, respectively (see equations 20 and 22).

5.3.3.2 Undrained test

In this test, an incremental confining pressure ΔP is applied to the rock sample, without any fluid allowed to leave the sample. Two measurements can be made directly after application of the load: the volumetric change ΔV for the determination of K_u ($K_u = V\Delta P/\Delta V$) and the pore pressure

change Δp for B ($B = \Delta p/\Delta P$). Accurate determination of B requires that the 'dead' fluid volume, *i.e.* the volume of fluid exterior to the sample, be kept to a minimum, as the existence of this volume permits fluid to escape the core. According to Wissa [49], who conducted an experimental study of the pore measurement system, the ratio of dead fluid volume over the pore fluid volume should be less than 0.003.

5.3.3.3 Unjacketed test

In the original unjacketed test proposed by Biot and Willis [31], the core without a jacket is loaded by a fluid in a pressure vessel. The test can, however, be carried out with a jacketed core, as in the two other tests, simply by imposing equal increment $\Delta p'$ to the confining pressure and the pore pressure. As in the case of the drained test, two measurements can be made: ΔV and $\Delta V_f^{(2)}$, the amount of fluid injected. (The pore pressure field in the core has to be in equilibrium before these measurements become meaningful.) This time, however, because the pore pressure is changing, a calibration of the measuring system is needed to determine the variation of fluid volume inside the sample. From these measurements, two parameters can be determined: the unjacketed compressibility $\delta = 1/K_s' = \Delta V/V\Delta p'$ and a storage coefficient defined under condition of Π-loading, $\gamma = \Delta V_f^{(2)}/V\Delta p'$. The constant γ, denoted as the coefficient of fluid content by Biot and Willis [31], can be expressed in terms of the other poroelastic constants (see equations 30–32)

$$\gamma = \phi\left(\frac{1}{K_f} - \frac{1}{K_s''}\right) = \frac{1}{M} - \frac{\alpha(1-\alpha)}{K} \tag{50}$$

(Recall that M is the inverse of a storage coefficient defined under zero volumetric strain.) It has been pointed out by Biot and Willis [31] that if independent measurements of K_f and ϕ are made, the comparison between the two coefficients δ and γ serves as a check for the microscopic homogeneous condition ($K_s' = K_s''$).

5.3.3.4 Table of poroelastic constants

In Table 4, we list the micromechanical as well as the bulk continuum constants for several rocks, compiled from refs. 8, 50, 51 and 52. The parameters K_u, ν_u, B and c are dependent on the fluid; for that purpose, water with $K_f = 3.3 \times 10^3$ MPa is assumed. A note of caution, however, about the use of this table – the table is only intended to establish some basic idea about the range of realistic poroelastic constants. As discussed earlier, the poroelastic parameters are generally sensitive to the stress conditions under which they are measured. Measurement with static or dynamic techniques may also yield different results [51, 52]. These factors are not considered in the compilation of Table 4.

5.4 LINEAR ISOTROPIC THEORY OF POROELASTICITY

The focus of the preceding section was on the constitutive laws of poroelasticity. To construct a well-posed mathematical system for the description of the stress, pore pressure, flux and displacement in the medium, additional equations based on mass and momentum conservation principles need to be introduced. Together with the constitutive laws, these equations constitute the governing equations of the theory of poroelasticity. These equations are then reduced through substitution and elimination of variables to produce systems amenable for mathematical treatment, which are discussed below as field equations.

5.4.1 Governing Equations

5.4.1.1 Constitutive law

(i) Constitutive constants

In the preceding section on constitutive equations, the emphasis was placed on the volumetric response. This was reflected in the choice of bulk moduli K and K_u as part of the fundamental set of

Table 4 Poroelastic Constants for Various Materials

Material	G (N m^{-2})	ν	ν_u	K (N m^{-2})	K_u (N m^{-2})	B	c (m^2 s^{-1})	η	α	K_s (N m^{-2})	ϕ	k (md)
Ruhr sandstone	1.3×10^{10}	0.12	0.31	1.3×10^{10}	3.0×10^{10}	0.88	5.3×10^{-3}	0.28	0.65	3.6×10^{10}	0.02	2.0×10^{-1}
Tennessee marble	2.4×10^{10}	0.25	0.27	4.0×10^{10}	4.4×10^{10}	0.51	1.3×10^{-5}	0.08	0.19	5.0×10^{10}	0.02	1.0×10^{-4}
Charcoal granite	1.9×10^{10}	0.27	0.30	3.5×10^{10}	4.1×10^{10}	0.55	7.0×10^{-6}	0.08	0.27	4.5×10^{10}	0.02	1.0×10^{-4}
Berea sandstone	6.0×10^{9}	0.20	0.33	8.0×10^{9}	1.6×10^{10}	0.62	1.6×10^{0}	0.30	0.79	3.6×10^{10}	0.19	1.9×10^{2}
Westerly granite	1.5×10^{10}	0.25	0.34	2.5×10^{10}	4.2×10^{10}	0.85	2.2×10^{-5}	0.16	0.47	4.5×10^{10}	0.01	4.0×10^{-4}
Weber sandstone	1.2×10^{10}	0.15	0.29	1.3×10^{10}	2.5×10^{10}	0.73	2.1×10^{-2}	0.26	0.64	3.6×10^{10}	0.06	1.0×10^{0}
Ohio sandstone	6.8×10^{9}	0.18	0.28	8.4×10^{9}	1.3×10^{10}	0.50	3.9×10^{-2}	0.29	0.74	3.1×10^{10}	0.19	5.6×10^{0}
Pecos sandstone	5.9×10^{9}	0.16	0.31	6.7×10^{9}	1.4×10^{10}	0.61	5.4×10^{-3}	0.34	0.83	3.9×10^{10}	0.20	8.0×10^{-1}
Boise sandstone	4.2×10^{9}	0.15	0.31	4.6×10^{9}	8.3×10^{9}	0.50	4.0×10^{-1}	0.35	0.85	4.2×10^{10}	0.26	8.0×10^{2}

material constants. For the presentation of the linear theory, we introduce the drained and undrained Poisson ratios ν and ν_u and adopt instead $\{G, \alpha, \nu, \nu_u\}$ as the fundamental set. (Only four constants can be independently selected: one constant for the deviatoric response, three for the volumetric ones.) The drained and undrained Poisson ratios, ν and ν_u, are related to the moduli G, K, and K_u according to

$$\nu = \frac{3K - 2G}{2(3K + G)} \tag{51a}$$

$$\nu_u = \frac{3K_u - 2G}{2(3K_u + G)} \tag{51b}$$

The magnitude of the poroelastic effect is controlled by the values of the two constants α and ν_u (the range of variation for α is $[0, 1]$, and for ν_u $[\nu, 0.5]$). Two limiting cases have previously been defined: (i) the 'incompressible constituents' model, $\alpha = 1$ and $\nu_u = 0.5$, characterized by the strongest poroelastic effects; and (ii) the 'uncoupled' model, $\nu_u \cong \nu$, for which some of the poroelastic effects, such as the sensitivity of the volumetric response to the rate of loading, and the Skempton effect, disappear.

Three others parameters also play pivotal roles in the poroelastic equations: the Skempton pore pressure coefficient B, the Biot modulus M, and the poroelastic stress coefficient η. They can be expressed in terms of the fundamental constants as

$$B = \frac{3(\nu_u - \nu)}{\alpha(1 - 2\nu)(1 + \nu_u)} \tag{52a}$$

$$M = \frac{2G(\nu_u - \nu)}{\alpha^2(1 - 2\nu_u)(1 - 2\nu)} \tag{52b}$$

$$\eta = \frac{\alpha(1 - 2\nu)}{2(1 - \nu)} \tag{52c}$$

The ranges of these constants are $[0, 1]$ for B, $[0, \infty]$ for M, and $[0, 0.5]$ for η. It is also useful to introduce a storage coefficient S, which is related to M according to

$$S = \frac{(1 - \nu_u)(1 - 2\nu)}{M(1 - \nu)(1 - 2\nu_u)} \tag{53}$$

While M is defined under constant volumetric strain, S represents a storage coefficient defined under the particular conditions of uniaxial strain and constant normal stress in the direction of the strain [32]. Note that in the degenerate case $\nu_u \cong \nu$, $S = 1/M$.

(ii) Constitutive equations

The constitutive equations (equations 4) are now rewritten in terms of $\{G, \alpha, \nu, \nu_u\}$. For the sake of completeness, the various forms that these equations can take are recorded.

Consider first the constitutive response for the porous solid (equation 4a). Selecting the pore pressure p as the coupling term yields the strain–stress relation

$$2G\varepsilon_{ij} = \sigma_{ij} - \frac{\nu}{1 + \nu}\sigma_{kk}\delta_{ij} + \frac{\alpha(1 - 2\nu)}{1 + \nu}p\delta_{ij} \tag{54}$$

and the stress–strain equation

$$\sigma_{ij} + \alpha p\delta_{ij} = 2G\varepsilon_{ij} + \frac{2G\nu}{1 - 2\nu}\varepsilon\delta_{ij} \tag{55}$$

These relations are similar to those for a drained elastic solid with $(\sigma_{ij} + \alpha p\delta_{ij})$ playing the role of an 'effective stress' (the coefficient α is hence sometimes interpreted as an effective stress coefficient). Furthermore, equations (54) and (55) reduce to the drained elastic constitutive equations for vanishing p. On the other hand, if ζ is adopted as the coupling term, the constitutive expressions

become

$$2G\left(\varepsilon_{ij} - \frac{B}{3}\zeta\delta_{ij}\right) = \sigma_{ij} - \frac{\nu_u}{1+\nu_u}\sigma_{kk}\delta_{ij} \tag{56}$$

$$\sigma_{ij} = 2G\varepsilon_{ij} + \frac{2G\nu_u}{1-2\nu_u}\varepsilon\delta_{ij} - \alpha M\zeta\delta_{ij} \tag{57}$$

This time, the equations are like those for an undrained elastic solid, if ε_{ij} is replaced by the 'effective strain' $(\varepsilon_{ij} - B\zeta\delta_{ij}/3)$. The dual form of these equations clearly shows the elastic character of the poroelastic material in its two limiting behaviors, drained ($p = 0$) and undrained ($\zeta = 0$).

Now we list two different forms of the response equation for the pore fluid (equation 4b), depending on whether the mean stress or the volumetric strain is used as the coupling term

$$2G\zeta = \frac{\alpha(1-2\nu)}{1+\nu}\left(\sigma_{kk} + \frac{3}{B}p\right) \tag{58}$$

$$p = M(\zeta - \alpha\varepsilon) \tag{59}$$

(iii) Plane strain expressions

The above constitutive equations (equations 54–59) can be reduced to the case of plane strain $\varepsilon_{33} = \varepsilon_{13} = \varepsilon_{23} = 0$. Now the subscripts i, j and k take only the values 1, 2. From equation (54) the out-of-plane normal stress σ_{33} is given by

$$\sigma_{33} = \nu\sigma_{kk} - \alpha(1-2\nu)p \quad (k = 1, 2) \tag{60}$$

Equations (55), (57) and (59) remain the same (the range of the subscripts changes however). Equations (54), (56) and (58) become

$$2G\varepsilon_{ij} = \sigma_{ij} - \nu\sigma_{kk}\delta_{ij} + \alpha(1-2\nu)p\delta_{ij} \tag{61}$$

$$2G\left[\varepsilon_{ij} - \frac{(1+\nu_u)B}{3}\zeta\delta_{ij}\right] = \sigma_{ij} - \nu_u\sigma_{kk}\delta_{ij} \tag{62}$$

$$2G\zeta = \alpha(1-2\nu)\left[\sigma_{kk} + \frac{3}{B(1+\nu_u)}p\right] \tag{63}$$

(iv) Limiting cases

Of the two limiting parameter cases discussed earlier, it is of interest to examine the implications on the fluid response equation.

(a) The incompressible constituents model ($\alpha = 1$ and $\nu_u = 0.5$). Examination of equation (52b) for M suggests that $M \to \infty$ and equation (59) reduces to

$$\zeta = \varepsilon \tag{64}$$

The change of volume of the porous solid is thus equal to the volume of fluid exchanged.

(b) The uncoupled model ($\nu_u \approx \nu$). Here $M \to 0$. In order to have a nontrivial equation for the fluid response, we introduce the small parameter $\varepsilon = K_f/\phi K$ and look at the asymptotic behavior. In view of the previous results (equations 35), we have that $B \cong \alpha\varepsilon$, $K_u \cong K + \alpha^2 K\varepsilon$, $M \cong 1/S \cong K\varepsilon$ and $\nu_u \cong \nu + (1+\nu)(1-2\nu)\alpha^2\varepsilon/3$. There is thus a vanishingly small pore pressure induced by change of the mean stress during the undrained response, when $\varepsilon \to 0$. However, examination of equations (54) and (59) shows that $|\zeta| \gg |\varepsilon|$ under conditions where the mean stress is of the same order of magnitude as p. The equations (58) and (59) both reduce to the linearized equation of state of the pore fluid.

$$\zeta = \frac{\phi p}{K_f} = Sp \tag{65}$$

Note that for these two limiting cases, the solid response equations (equations 54 and 55) remain well-posed as they are expressed in terms of material constants that are independent of the compressibility of the fluid.

5.4.1.2 Transport law

The fluid transport in the interstitial space can be described by the well-known Darcy's law, which is an empirical equation for seepage flow in nondeformable porous media. It can also be derived from the Navier–Stokes equations by dropping the inertial terms [53]. Consistent with the current small deformation assumptions and by ignoring the fluid density variation effect (Hubert's Potential [54]), Darcy's law can be adopted here without modification

$$q_i = -\kappa(p_{,i} - f_i) \tag{66}$$

In this equation, $f_i = \rho_f g_i$ is the body force per unit volume of fluid (with ρ_f the fluid density, and g_i the gravity component in the i direction), and $\kappa = k/\mu$ the permeability coefficient or mobility coefficient (with k the intrinsic permeability having dimension of length squared, and μ the fluid dynamic viscosity).

The intrinsic permeability k is generally a function of the pore geometry. In particular, it is strongly dependent on porosity ϕ. According to the Carman–Kozeny law [55] which is based on the conceptual model of packing of spheres, a power law relation of $k \approx \phi^3/(1-\phi)^2$ exists. Other models based on different pore geometry give similar power laws (see ref. 56 for a review). Actual measurements on rocks, however, often yield power law relations with exponents for ϕ significantly larger than 3.

It is also of interest to investigate the relation between the permeability and the stress to which the rock is subjected. For a material which is porosity invariant under Π-loading, the following incremental constitutive equation applies (*cf.* equations 38b and 27 in Section 5.3.2.2)

$$\frac{\mathrm{d}\phi}{1-\phi} = -C_\phi(P')\mathrm{d}P' \tag{67}$$

where C_ϕ is the compliance for the porosity 'strain', given by

$$C_\phi(P') = C_{bc}(P') - \frac{C_s}{1-\phi} \tag{68}$$

Equation (67) can be integrated if the form of $C_{bc}(P')$ is explicitly known. Taking for example the Mackenzie model of an elastic material with spherical pores (*cf.* equation 40) gives

$$C_\phi = \frac{3\phi}{4G_s(1-\phi)} \tag{69}$$

Integrating equation (67) from a stress-free state then yields

$$\frac{\phi}{\phi_0} = \exp(-3P'/4G_s) \tag{70}$$

in which ϕ_0 is the porosity in the unstressed state and the shear modulus of the solid phase G_s is assumed to be constant. Considering a relation $k \approx \phi^a$, we obtain

$$k = k_0 \exp(-3P'/4G_s) = k_0 \exp(-bP') \tag{71}$$

where k_0 is the permeability under a stress-free state, and b should generally be regarded as an experimental constant. Equation (71) shows that k is a function of the effective confining pressure P' only. This type of exponential relationship, or some slight variation of it, has been quite successfully applied for fitting laboratory data.

Despite the above discussion on nonlinearity, the permeability is henceforth regarded as a stress-independent constant within the framework of linear theory.

5.4.1.3 Balance laws

(i) Equilibrium equations

Standard considerations of static equilibrium lead to the local stress balance equation

$$\sigma_{ij,j} = -F_i \tag{72}$$

where $F_i = \rho g_i$ is the body force per unit volume of the bulk material, $\rho = (1 - \phi)\rho_s + \phi\rho_f$ is the bulk density, ρ_s and ρ_f are the densities of the solid and the fluid phase, respectively.

(ii) Continuity equation for the fluid phase

Consideration of mass conservation of a compressible fluid yields the local continuity equation

$$\frac{\partial \zeta}{\partial t} + q_{i,i} = \gamma \tag{73}$$

where γ is the source density (the rate of injected fluid volume per unit volume of the porous solid). It should be noted that equation (73) is in a linearized form as the fluid density variation effect has been ignored.

5.4.2 Compatibility Equations

The strain field ε_{ij} defined in equation (1) must satisfy some compatibility requirements to ensure a single valued continuous displacement solution u_i. These compatibility relations are identical to those derived in elasticity [57]

$$\varepsilon_{ij,kl} + \varepsilon_{kl,ij} - \varepsilon_{ik,jl} - \varepsilon_{jl,ik} = 0 \tag{74}$$

From the above, the constitutive equation (equation 54), and the equilibrium equation (equation 72), the corresponding Beltrami–Michell compatibility equations for poroelasticity can be derived

$$\nabla^2\sigma_{ij} + \frac{1}{1+\nu}\sigma_{kk,ij} + 2\eta\left(\delta_{ij}\nabla^2 p + \frac{1-\nu}{1+\nu}p_{,ij}\right) = -\frac{\nu}{1-\nu}\delta_{ij}F_{k,k} - (F_{i,j} + F_{j,i}) \tag{75}$$

Linked to these compatibility equations, there are some very useful relations that satisfy the Laplace/Poisson equation. First, we can contract equation (75) to obtain

$$\nabla^2(\sigma_{kk} + 4\eta p) = -\frac{1+\nu}{1-\nu}F_{k,k} \tag{76}$$

For plane strain, this equation reduces to

$$\nabla^2(\sigma_{kk} + 2\eta p) = -\frac{1}{1-\nu}F_{k,k} \quad (k = 1, 2) \tag{77}$$

Next, we seek the harmonic relation between p and ε. Substituting the constitutive equation (equation 55) for σ_{ij} into the equilibrium equation (equation 72), and taking the divergence yields

$$\nabla^2\left(p - \frac{G}{\eta}\varepsilon\right) = \frac{F_{k,k}}{\alpha} \tag{78}$$

Using equation (59) to eliminate ε we obtain

$$\nabla^2(Sp - \zeta) = \frac{\eta}{G}F_{k,k} \tag{79}$$

Finally, the pore pressure p can be eliminated between equations (78) and (79) to derive an expression between ε and ζ

$$\nabla^2\left(\zeta - \frac{GS}{\eta}\varepsilon\right) = \frac{1}{\alpha M}F_{k,k} \tag{80}$$

Note that the right-hand member of equations (76)–(80) vanishes if the body force F_i derives from a harmonic potential (conservative loading). All these relations should actually be seen as one of the strain compatibility expressions (only one independent relation exists in plane strain).

5.4.3 Field Equations

Linear isotropic poroelastic processes are therefore described by: (i) the constitutive equations for the porous solid (one of the various forms in equations 54–57); (ii) the response for the fluid, either equation (58) or (59); (iii) Darcy's law (equation 66); (iv) the equilibrium equation (equations 72); and (v) the continuity equation (equation 73). A set of five material constants, G, ν, ν_u, α and κ, are needed to characterize fully a linear isotropic poroelastic system.

In this section, these governing equations are combined into field equations with a reduced number of variables. Only field equations that lead to a useful solution algorithm are investigated. Two fairly similar schemes are actually examined. In the first approach, the reduced variables are u_i and p and the field equations consist of a Navier-type equation for u_i and a diffusion equation for p (both containing a coupling term). The other approach is based on using u_i and ζ as reduced variables with a Navier-type equation for u_i and a diffusion equation for ζ. In the second approach the diffusion equation is uncoupled.

5.4.3.1 Navier equations

A Navier-type equation for the displacement u_i is obtained by substituting into the equilibrium equations (equations 72), the constitutive equations (equations 55 or 57), with ε_{ij} expressed in terms of the displacement gradient using equation (1). Two forms of the Navier equation exist, depending on which constitutive relation (equation 55 or 57) is used

$$G\nabla^2 u_i + \frac{G}{1-2\nu} u_{k,ki} = \alpha p_{,i} - F_i \tag{81a}$$

$$G\nabla^2 u_i + \frac{G}{1-2\nu_u} u_{k,ki} = \alpha M \zeta_{,i} - F_i \tag{81b}$$

The coupling term may be viewed as a 'body force', proportional either to the gradient of the pore pressure or the gradient of the variation of fluid content.

5.4.3.2 Diffusion equations

Two diffusion equations are derived, one for p, and the other for ζ. Consider first the diffusion equation for p. Combination of Darcy's law (equation 66), the continuity equation (equation 73), and the constitutive relation (equation 59) yields

$$\frac{\partial p}{\partial t} - \kappa M \nabla^2 p = -\alpha M \frac{\partial \varepsilon}{\partial t} + M(\gamma - \kappa f_{i,i}) \tag{82}$$

The diffusion of pore pressure is thus coupled with the rate of change of the volumetric strain. Under steady-state conditions, equation (82) certainly uncouples and becomes a Poisson equation. But there are other circumstances, discussed in Section 5.4.3.4, where the diffusion equation uncouples at all times.

The diffusion equation for ζ is deduced from equations (66) and (73), by taking into account equation (79). It has the form

$$\frac{\partial \zeta}{\partial t} - c\nabla^2 \zeta = \frac{\eta c}{G} F_{i,i} + \gamma - \kappa f_{i,i} \tag{83}$$

where the diffusivity coefficient c is given by [8, 32]

$$c = \frac{\kappa}{S} = \frac{2\kappa G(1-\nu)(\nu_u - \nu)}{\alpha^2 (1-2\nu)^2 (1-\nu_u)} \tag{84}$$

The coefficient c is also sometimes called the generalized consolidation coefficient [8], because it is identical to the Terzaghi consolidation coefficient under one-dimensional consolidation (see Section 5.6.1). The diffusion equation for ζ is thus uncoupled at all times, contrary to the diffusion equation for p.

It is of interest to note that the diffusivity coefficient for the pore pressure equation and the variation of fluid content can both be expressed as the ratio of the mobility coefficient κ to a storage coefficient, S or $1/M$. The storage coefficient is defined under the constraint of zero volumetric strain for p, and of uniaxial strain for ζ.

5.4.3.3 Irrotational displacement field

We consider now the particular case where the displacement field is irrotational, in the absence of body forces. According to the Helmholtz decomposition of a vector field, the displacement can then be expressed as the gradient of a scalar potential Φ

$$u_i = \Phi_{,i} \tag{85}$$

The Navier equation (equation 81a) then reduces to

$$\Phi_{,ikk} = \frac{\eta}{G} p_{,i} \tag{86}$$

Integration of this equation yields

$$u_{i,i} = \frac{\eta}{G} p + g(t) \tag{87}$$

where $g(t)$ is generally an unknown function of time. After insertion of equation (87), the contracted volumetric constitutive equation (equation 55) becomes

$$\sigma_{kk} + 4\eta p = \frac{2G(1+\nu)}{1-2\nu} g(t) \tag{88}$$

For plane strain, this relation gives

$$\sigma_{kk} + 2\eta p = \frac{2G}{1-2\nu} g(t) \quad (k = 1, 2) \tag{89}$$

Expressions similar to equations (87)–(89) can also be derived from equations (76)–(78) without the irrotationality condition. In this case, the function g is a function of both space and time variables (it satisfies the Laplace equation, $\nabla^2 g = 0$).

Alternative formulations of the pore pressure diffusion equation (equation 82) can now be written for the particular case of an irrotational displacement field. Taking into account equation (87) and recalling that body forces are ignored here, equation (82) becomes

$$\frac{\partial p}{\partial t} - c\nabla^2 p = -\frac{\alpha}{S}\frac{\mathrm{d}g}{\mathrm{d}t} + \frac{\gamma}{S} \tag{90}$$

or in view of equation (88)

$$\frac{\partial p}{\partial t} - c\nabla^2 p = -\frac{(1-\nu)\eta}{(1+\nu)GS}\frac{\mathrm{d}}{\mathrm{d}t}(\sigma_{kk} + 4\eta p) + \frac{\gamma}{S} \tag{91}$$

For the particular case of plane strain, equation (91) reduces to

$$\frac{\partial p}{\partial t} - c\nabla^2 p = -\frac{(1-\nu)\eta}{GS}\frac{\mathrm{d}}{\mathrm{d}t}(\sigma_{kk} + 2\eta p) + \frac{\gamma}{S} \quad (k = 1, 2) \tag{92}$$

5.4.3.4 Uncoupling of the pore pressure diffusion equation

Here, we examine the cases where the solid coupling term disappears from the governing equation (82) for the pore pressure.

(i) Irrotational displacement in infinite or semi-infinite domain

Under these conditions, the function $g(t)$ in equation (87) is identically zero, since both ε and p must vanish at infinity; thus equation (90) uncouples to become

$$\frac{\partial p}{\partial t} - c\nabla^2 p = \frac{\gamma}{S} \tag{93}$$

An important example for which the above conditions apply is the case of a fluid injection point source located in an infinite medium.

Note that under conditions where the function $g(t)$ vanishes, a one to one dependence exists between the various volumetric stress and strain quantities

$$\varepsilon = \frac{\eta}{G} p \tag{94}$$

Also, according to equation (88),

$$\sigma_{kk} = -4\eta p \tag{95}$$

and according to equations (59) and (94)

$$\zeta = Sp \tag{96}$$

(ii) Limit of very compressible pore fluid

As discussed in Section 5.4.1.1, $M \cong 1/S$, and the fluid equation of state (equation 65) has the same form as equation (96). In equation (82), the term $\partial\varepsilon/\partial t$ is of order $\varepsilon = K_f/\phi K$ as compared to $S\partial p/\partial t$. Or we can directly show from equations (65), (66) and (73) that the diffusion equation for p becomes

$$\frac{\partial p}{\partial t} - c\nabla^2 p = \frac{1}{S}(\gamma - \kappa f_{i,i}) \tag{97}$$

(iii) Steady state conditions

Finally, under steady state conditions, the equation governing the pore pressure field also uncouples

$$\kappa\nabla^2 p = \kappa f_{i,i} - \gamma \tag{98}$$

5.4.4 Solution of Initial/Boundary Value Problems

5.4.4.1 Initial/boundary conditions

Given the system of partial differential equations describing the response of a poroelastic material, a set of 'well-posed' initial and boundary conditions is needed to ensure the existence and the uniqueness of the mathematical solution.

The boundary condition generally consists of two types: a Dirichlet (potential) and a Neumann (gradient) type. For a poroelastic medium, boundary conditions are required for both the porous solid and the fluid. Dirichlet-type conditions consist in prescribing the solid displacement u_i and the pore pressure p, while Neumann-type conditions correspond to imposing the traction $t_i = \sigma_{ij} n_j$ and the normal flux $q = q_i n_i$. These conditions can also be alternated to form a mixed boundary value problem. Note, however, that a finite domain problem with exclusively Neumann conditions, namely tractions and fluid flux, is ill posed. The solution is then defined only within some arbitrary rigid body motions and constant fluid pressure.

For the initial conditions, we need either an initial stress field or displacement field, and a pressure field or a flux field. The conditions specified must themselves satisfy some constraints, such as the equilibrium equation and the compatibility equation. If the initial conditions are in an equilibrated state, namely satisfying the governing equations in steady state, they can simply be ignored as we need only to solve for the perturbed state.

5.4.4.2 *Convolutional technique*

The boundary conditions are generally functions of position and time. In one particular case, corresponding to proportional loading, we can utilize the convolutional technique to simplify the solution process. By proportional loading, we mean here a loading such that the time variation of the boundary conditions is uniformly characterized by the same evolutional function; it is symbolically written as

$$\mathscr{B}(x, t) = \mathscr{B}^0(x)\lambda(t) \tag{99}$$

where $\mathscr{B}(x, t)$ denotes the boundary condition, $\mathscr{B}^0(x)$ and $\lambda(t)$ are respectively the spatial and time dependent portions. The convolutional technique is based on the Duhamel principle of superposition. It requires first the solution of the 'influence function' $\mathscr{F}^*(x, t)$, which is obtained by solving the presumably simpler problem corresponding to the sudden application of constant boundary condition (step function)

$$\mathscr{B}^*(x, t) = \mathscr{B}^0(x)H(t) \tag{100}$$

where $H(t)$ is the Heaviside unit step function. The system response to an arbitrary time variation $\lambda(t)$ can then be evaluated by the following convolutional integral

$$\mathscr{F}(x, t) = \lambda(0)\mathscr{F}^*(x, t) + \int_0^t \frac{d\lambda(\tau)}{d\tau} \mathscr{F}^*(x, t - \tau)\, d\tau \tag{101}$$

5.5 METHODS OF SOLUTION

Due to the complexity of the poroelastic governing equations, it is generally difficult to derive closed form solutions of initial/boundary value problems, except for cases involving simple geometries (some of which are demonstrated in Section 5.6). Despite this difficulty, there are indeed some systematic analytical solution techniques, most notably the displacement function method proposed by McNamee and Gibson [58–60]. Otherwise, the solution relies on numerical techniques such as the finite element or the boundary element methods.

5.5.1 Method of Potentials

Several attempts have been made at expressing the equations of poroelasticity in terms of certain 'potentials', namely quantities satisfying Laplace or the diffusion equation [8, 19, 20, 58]. Three such formulations are examined here.

5.5.1.1 *Biot's decomposition*

Biot [19] suggested a decomposition of the displacement field which allows to some extent uncoupling of the Navier equation (equation 81b). According to Darcy's law (equation 66), the flux field q_i is irrotational, since it is expressible in terms of the gradient of a continuous field. It then follows, from the continuity equation (equation 73), that ζ can be written as

$$\zeta = \int_0^t [\kappa(\nabla^2 p - f_{i,i}) + \gamma]\, dt \tag{102}$$

If the fluid body force and source introduced can be expressed as the Laplacian of a potential (this is certainly the case if they are of the form of Dirac delta function), the same can be concluded for ζ

$$\zeta = \nabla^2 \Phi \tag{103}$$

Biot [19] proposed to write the displacement into two parts

$$u_i = u_i^0 + u_i^1 \tag{104}$$

where

$$u_i^{\mathrm{i}} = \frac{\eta}{GS}\Phi_{,i} \tag{105}$$

is an irrotational displacement and Φ, the displacement potential. On the other hand, u_i^0 looks like an undrained elastic displacement since substitution of equations (104) and (105) into equation (81b) reveals that u_i^0 satisfies the Navier equation with undrained Poisson ratio

$$G\nabla^2 u_i^0 + \frac{G}{1-2\nu_{\mathrm{u}}} u_{k,ki}^0 = -F_i \tag{106}$$

Consider first the irrotational component u_i^{i}. Using equation (103) in equation (83) produces

$$\frac{\partial \nabla^2 \Phi}{\partial t} - c\nabla^4 \Phi = \frac{\eta c}{G} F_{i,i} + \gamma - \kappa f_{i,i} \tag{107}$$

Relaxation of a Laplacian in equation (107) yields a simple diffusion equation for Φ

$$\frac{\partial \Phi}{\partial t} - c\nabla^2 \Phi = g_1 + g_2 + g_3 \tag{108}$$

in which the g_i functions are the body forces or source potentials satisfying the Poisson equations

$$\nabla^2 g_1 = \frac{\eta c}{G} F_{i,i} \tag{109a}$$

$$\nabla^2 g_2 = -\kappa f_{i,i} \tag{109b}$$

$$\nabla^2 g_3 = \gamma \tag{109c}$$

Equations (106) and (108) represent a system of field equations which is apparently uncoupled. After solving for u_i^0 and Φ, the displacement u_i is determined from equations (104) and (105). The stress and pore pressure also consist of two parts. They are calculated from the following formulae

$$\sigma_{ij}^0 = 2G\varepsilon_{ij}^0 + \frac{2G\nu_{\mathrm{u}}}{1-2\nu_{\mathrm{u}}}\varepsilon^0 \delta_{ij} \tag{110a}$$

$$p^0 = -\alpha M \varepsilon^0, \tag{110b}$$

$$\sigma_{ij}^{\mathrm{i}} = \frac{2\eta}{S}(\Phi_{,ij} - \delta_{ij}\nabla^2 \Phi) \tag{110c}$$

$$p^{\mathrm{i}} = \frac{1}{S}\nabla^2 \Phi \tag{110d}$$

This approach is however not suitable for the solution of general initial/boundary value problems. Indeed, as a matter of fact, the uncoupling of the new field equations in only apparent; coupling of the field quantities actually persists *via* the boundary conditions. As a consequence, u_i^0 is generally time dependent, even in the particular case where the boundary conditions remain constant for $t > 0$ (in this case, however, u_i^0 corresponds to the undrained solution at $t = 0$).

Nonetheless, this technique is extremely powerful for finding free-space Green's functions, such as the fundamental solution of a point force or a point source which correspond, respectively, to the replacement of the body force and source terms by the Dirac delta function. Since the domain is then without boundary, uncoupling of the system of equations (106) and (108) is truly achieved. This technique has been successfully applied to find various singular solutions in closed form [61–64].

5.5.1.2 Biot functions

Another approach due to Biot [20] leads to the definition of potentials that are analogous to the Papkovitch–Neuber functions in elasticity

$$u_i = (\varphi + x_j \psi_j)_{,i} - 4(1-\nu_{\mathrm{u}})\psi_i \tag{111a}$$

$$\zeta = \frac{GS}{\eta}\nabla^2\varphi \tag{111b}$$

where φ and ψ_i are usually referred to as the Biot functions. In the absence of body forces and sources, the components of the vector function ψ_i are harmonic

$$\nabla^2\psi_i = 0 \tag{112}$$

while φ satisfies the 'biharmonic diffusion equation'

$$\frac{\partial}{\partial t}(\nabla^2\varphi) - c\nabla^4\varphi = 0 \tag{113}$$

The completeness of the solution has been proven by Verruijt [65].

5.5.1.3 *Displacement functions*

The most successful analytical solution technique is the displacement function method developed by McNamee and Gibson [58]. It has been applied to the solution of constant loads exerted normally or horizontally over strip, circular or rectangular areas on top of semi-infinite, finite, single or multiple soil layer systems [59, 60, 66–69]. The original theory was derived for the incompressible constituents model, but the incompressible fluid assumption was later removed by Verruijt [70]. The theory is further extended below to the general case.

It has been pointed out by Verruijt [70] that the McNamee–Gibson displacement functions [58] can be deduced from the Biot functions. For plane strain, we use

$$\varphi = -\mathscr{E}(x, z, t) \tag{114a}$$

$$\psi_z = \mathscr{S}(x, z, t) \tag{114b}$$

$$\psi_x = \psi_y = 0 \tag{114c}$$

where $\mathscr{E}$ and $\mathscr{S}$ are displacement functions satisfying

$$\nabla^2\mathscr{S} = 0 \tag{115a}$$

$$\frac{\partial}{\partial t}(\nabla^2\mathscr{E}) - c\nabla^4\mathscr{E} = 0 \tag{115b}$$

The displacements, stresses, *etc.* are related to these functions as

$$u_x = -\frac{\partial\mathscr{E}}{\partial x} + z\frac{\partial\mathscr{S}}{\partial x} \tag{116a}$$

$$u_z = -\frac{\partial\mathscr{E}}{\partial z} + z\frac{\partial\mathscr{S}}{\partial z} - (3 - 4\nu_u)\mathscr{S} \tag{116b}$$

$$\zeta = -\frac{GS}{\eta}\nabla^2\mathscr{E} \tag{116c}$$

$$\sigma_{xx} = 2G\left[\nabla^2\mathscr{E} - \frac{\partial^2\mathscr{E}}{\partial x^2} + z\frac{\partial^2\mathscr{S}}{\partial x^2} - 2\nu_u\frac{\partial\mathscr{S}}{\partial z}\right] \tag{116d}$$

$$\sigma_{zz} = 2G\left[\nabla^2\mathscr{E} - \frac{\partial^2\mathscr{E}}{\partial z^2} + z\frac{\partial^2\mathscr{S}}{\partial z^2} - 2(1 - \nu_u)\frac{\partial\mathscr{S}}{\partial z}\right] \tag{116e}$$

$$\sigma_{xz} = 2G\left[-\frac{\partial^2\mathscr{E}}{\partial x\,\partial z} + z\frac{\partial^2\mathscr{S}}{\partial x\,\partial z} - (1 - 2\nu_u)\frac{\partial\mathscr{S}}{\partial x}\right] \tag{116f}$$

$$p = -\frac{G}{\eta}\left[\nabla^2\mathscr{E} - \frac{2(\nu_u - \nu)}{1 - \nu}\frac{\partial^2\mathscr{S}}{\partial z^2}\right] \tag{116g}$$

For the incompressible constituent model ($\nu_u = 1/2$ and $GS/\eta = 1$), the above expressions degenerate into McNamee–Gibson's [58]. The axial-symmetric displacement functions are obtained by assuming $\mathscr{E} = \mathscr{E}(r, z, t)$ and $\mathscr{S} = \mathscr{S}(r, z, t)$ with the Laplacian operator taking the form, in cylindrical coordinates

$$\nabla^2 = \frac{\partial^2}{\partial r^2} + \frac{1}{r}\frac{\partial}{\partial r} + \frac{\partial^2}{\partial z^2} \tag{117}$$

The displacement and stress expressions are formally equivalent to those in equation (116) with the symbol x replaced by r.

The system of equations (equations 115) is typically solved by a Laplace transform in time and a Fourier transform in space. The resultant is a set of linear algebraic equations in terms of the transformed parameters, $\mathscr{S}$ and $\mathscr{E}$, whose solution can easily be found. The difficulty resides in the inversion of the transformation, which is quite often done numerically.

5.5.2 Finite Element Method

The finite element techniques for poroelasticity were pioneered by Sandhu and Wilson [71] and Christian [72]. Later contributions include refs. 73–76. Most of the formulations use as basic nodal unknowns the displacement and the pore pressure. An alternative formulation [77] is based on the stress and the pore pressure. In the following, we briefly describe the finite element ideas following Zienkiewicz [76].

The similarity of the field equations (equations 81a and 82) to the conventional Navier and diffusion equations allows the direct application of the Galerkin weighted residual procedure. The discretized finite element equations, in matricial form, are then

$$[\boldsymbol{K}]\{\boldsymbol{u}\} + [\boldsymbol{L}]\{\boldsymbol{p}\} = \{\boldsymbol{f}\} \tag{118a}$$

$$[\boldsymbol{S}]\{\dot{\boldsymbol{p}}\} + [\boldsymbol{L}]^{\mathrm{T}}\{\dot{\boldsymbol{u}}\} + [\boldsymbol{H}]\{\boldsymbol{p}\} = \{\boldsymbol{q}\} \tag{118b}$$

where $\{\boldsymbol{u}\}$ is the column matrix of the nodal displacements, $\{\boldsymbol{p}\}$ the nodal pressure, $\{\boldsymbol{f}\}$ the body force, and $\{\boldsymbol{q}\}$ takes into account the fluid body force and source terms. The dot on top of a symbol denotes the time derivative. The square matrices are 'stiffness' matrices with their elements defined as

$$\boldsymbol{K} = \int_{\Omega} \boldsymbol{B}^{\mathrm{T}}\boldsymbol{D}\boldsymbol{B}\,\mathrm{d}x \tag{119a}$$

$$\boldsymbol{L} = \int_{\Omega} \boldsymbol{a}\boldsymbol{D}\boldsymbol{N}\,\mathrm{d}x \tag{119b}$$

$$\boldsymbol{H} = \int_{\Omega} \nabla^{\mathrm{T}}\boldsymbol{N}\boldsymbol{\kappa}\nabla\boldsymbol{N}\,\mathrm{d}x \tag{119c}$$

$$\boldsymbol{S} = \int_{\Omega} \boldsymbol{N}^{\mathrm{T}}\boldsymbol{\kappa}\boldsymbol{M}\boldsymbol{N}\,\mathrm{d}x \tag{119d}$$

where Ω denotes the domain of solution, $\boldsymbol{D}$ the elasticity coefficient matrix with drained parameters, $\boldsymbol{a}$, $\boldsymbol{\kappa}$ and $\boldsymbol{M}$ are material matrices corresponding to the same names, $\boldsymbol{N}$ is the shape function, $\boldsymbol{B}$ the strain differential operator matrix, and ∇ the gradient operator matrix (see Zienkiewicz [75] for detail of finite element notation). The system of equations (equations 118) can be solved using a regular time-stepping procedure. See refs. 78–80 for some typical applications.

5.5.3 Boundary Element Method

The boundary element method is a powerful numerical technique for solving systems governed by linear partial differential equations [81, 82]. Its formulation rests on the integral equation representation of the differential equation system. The boundary element technique has been widely applied to elasticity, potential and diffusion problems. This method has been implemented in poroelasticity using the Laplace transform [61, 83, 84], and the time stepping technique [85–88].

It is common in the boundary element literature to differentiate between a 'direct' and an 'indirect method'. The direct methods are from integral equations based on the generalized Green's theorem, which are sometimes expressed in the form of an energy reciprocity theorem. All the quantities appearing in the direct formulation are field variables such as potential, flux, displacement, stress, *etc.* On the other hand, the indirect methods are based on the distribution of influence functions such as source, dipole, point force, *etc.*, with 'fictitious densities'. A unification of the two formulations is presented below.

5.5.3.1 Direct method

The cornerstone of the direct formulation is the principle of reciprocity of work. Since the constitutive equations (equations 4) are constructed under the assumption of reversible thermodynamic process (equation 5), a reciprocal theorem similar to Betti's theorem in elasticity exists [64, 89, 90]

$$\sigma_{ij}^{(1)}\varepsilon_{ij}^{(2)} + p^{(1)}\zeta^{(2)} = \sigma_{ij}^{(2)}\varepsilon_{ij}^{(1)} + p^{(2)}\zeta^{(1)} \tag{120}$$

where superscripts $^{(1)}$ and $^{(2)}$ denote quantities under two independent stress and strain states. The first system has also to satisfy the governing equations (equations 66, 72 and 73). The second system is governed by the adjoint set, which corresponds to a change of sign in the time derivative term in the continuity equation (equation 73) [91]. Integrating equation (120) over the domain of solution and time, and performing an integration by parts, we arrive at the reciprocal integral equation

$$\int_0^t\int_\Gamma (\sigma_{ij}^{(1)} n_j u_i^{(2)} - \sigma_{ij}^{(2)} n_j u_i^{(1)})\,\mathrm{d}\chi\,\mathrm{d}\tau - \int_0^t\int_\Gamma (p^{(1)} v_i^{(2)} n_i - p^{(2)} v_i^{(1)} n_i)\,\mathrm{d}\chi\,\mathrm{d}\tau$$
$$+ \int_0^t\int_\Omega (F_i^{(1)} u_i^{(2)} - F_i^{(2)} u_i^{(1)})\,\mathrm{d}\chi\,\mathrm{d}r + \int_0^t\int_\Omega (p^{(1)}\theta^{(2)} - p^{(2)}\theta^{(1)})\,\mathrm{d}\chi\,\mathrm{d}\tau = 0 \tag{121}$$

where $\theta = \int_0^t \gamma\,\mathrm{d}t$ is the volume of source injection, and Ω the domain of solution with boundary Γ. For simplicity, we have ignored in equation (121) the fluid body force and the initial conditions. To obtain singular integral equations equivalent to the Somigliana equations in elasticity, the states corresponding to an instantaneous point force in the x_k direction, and an instantaneous fluid volume dilatation located at point x and time t

$$F_{ik}^{(2)} = \delta_{ik}\delta(\chi - x)\delta(\tau - t) \tag{122a}$$

$$\theta^{(2)} = \delta(\chi - x)\delta(\tau - t) \tag{122b}$$

are successively substituted for the second system in equation (121). The substitution yields the following expressions for the displacement $u_k(x, t)$ and pore pressure $p(x, t)$

$$bu_k(x,t) = \int_0^t\int_\Gamma [u_{ik}^{\mathrm{fi}}(\chi, t; x, \tau)\sigma_{ij}(\chi, \tau)n_j(\chi) - \sigma_{ijk}^{\mathrm{fi}}(\chi, t; x, \tau)n_j(\chi)u_i(\chi, \tau)]\,\mathrm{d}\chi\,\mathrm{d}\tau$$
$$- \int_0^t\int_\Gamma [q_{ik}^{\mathrm{fc}}(\chi, t; x, \tau)n_i(\chi)p(\chi, \tau) - p_k^{\mathrm{fc}}(\chi, t; x, \tau)q_i(\chi,\tau)n_i(\chi)]\,\mathrm{d}\chi\,\mathrm{d}\tau \tag{123a}$$

$$-bp(x,t) = \int_0^t\int_\Gamma [u_i^{\mathrm{li}}(\chi, t; x, \tau)\sigma_{ij}(\chi, \tau)n_j(\chi) - \sigma_{ij}^{\mathrm{li}}(\chi, t; x, \tau)n_j(\chi)u_i(\chi, \tau)]\,\mathrm{d}\chi\,\mathrm{d}\tau$$
$$- \int_0^t\int_\Gamma [q_i^{\mathrm{si}}(\chi, t; x, \tau)n_i(\chi)p(\chi, \tau) - p^{\mathrm{si}}(\chi, t; x, \tau)q_i(\chi,\tau)n_i(\chi)]\,\mathrm{d}\chi\,\mathrm{d}\tau \tag{123b}$$

In the above equations, the presence of body force and fluid source has been ignored, and b is a constant equal to 0, 1 or 1/2 depending on whether the base point x is located outside, inside of the domain, or on the boundary Γ (assumed here to be smooth). The quantities denoted by superscripts are the free-space poroelastic Green's functions, for which the following notational convention is adopted. The first superscript indicates the nature of the singularity: f for force, l fluid dilation, s for fluid source; the second characterizes the variation of the singularity strength with time: i refers to

instantaneous (Dirac delta function), c to continuous (Heaviside step function). These Green's functions are listed in Cheng *et al.* [90].

In an initial/boundary value problem for poroelasticity, either the boundary traction $t_i = \sigma_{ij}n_j$ or the displacement u_i, and either the fluid pressure p or the normal flux $q = q_i n_i$, are prescribed on a given part of the boundary. Equations (123) are applied at a set of boundary nodes, and a collocation procedure is performed. Due to the transient nature of the integral equations, the discretization takes place both in time and in space. The missing boundary data can be directly solved in terms of the physical quantities of traction, displacement, pressure or flux, through a time-stepping or convolutional integral process.

5.5.3.2 Indirect methods

Let Ω' denote the complement of the domain Ω, also bounded by the contour Γ. For the domain Ω', equations (123) become

$$0 = \int_0^t \int_\Gamma (u_{ik}^{\mathrm{fi}} \sigma'_{ij} n'_j - \sigma_{ijk}^{\mathrm{fi}} n'_j u'_i)\, \mathrm{d}\chi\, \mathrm{d}\tau - \int_0^t \int_\Gamma (q_{ik}^{\mathrm{fc}} n'_i p' - p_k^{\mathrm{fc}} q'_i n'_i)\, \mathrm{d}\chi\, \mathrm{d}\tau \tag{124a}$$

$$0 = \int_0^t \int_\Gamma (u_i^{\mathrm{li}} \sigma'_{ij} n'_j - \sigma_{ij}^{\mathrm{li}} n'_j u'_i)\, \mathrm{d}\chi\, \mathrm{d}\tau - \int_0^t \int_\Gamma (q_i^{\mathrm{si}} n'_i p' - p^{\mathrm{si}} q'_i n'_i)\, \mathrm{d}\chi\, \mathrm{d}\tau \tag{124b}$$

where a prime is used to denote quantities associated with Ω'. The left-hand sides of equations (124) are zero because the base point is located in Ω. Summing equations (124) with equations (123) and taking into account that $n'_i = -n_i$, we obtain

$$\begin{aligned} bu_k = & \int_0^t \int_\Gamma [u_{ik}^{\mathrm{fi}}(\sigma_{ij} - \sigma'_{ij}) n_j - \sigma_{ijk}^{\mathrm{fi}} n_j (u_i - u'_i)]\, \mathrm{d}\chi\, \mathrm{d}\tau \\ & - \int_0^t \int_\Gamma [q_{ik}^{\mathrm{fc}} n_i (p - p') - p_k^{\mathrm{fc}} (q_i - q'_i) n_i]\, \mathrm{d}\chi\, \mathrm{d}\tau \end{aligned} \tag{125a}$$

$$\begin{aligned} -bp = & \int_0^t \int_\Gamma [u_i^{\mathrm{li}}(\sigma_{ij} - \sigma'_{ij}) n_j - \sigma_{ij}^{\mathrm{li}} n_j (u_i - u'_i)]\, \mathrm{d}\chi\, \mathrm{d}\tau \\ & - \int_0^t \int_\Gamma [q_i^{\mathrm{si}} n_i (p - p') - p^{\mathrm{si}} (q_i - q'_i) n_i]\, \mathrm{d}\chi\, \mathrm{d}\tau \end{aligned} \tag{125b}$$

Two indirect methods can be devised from these equations: the single layer and the double layer methods.

Consider the single layer method first. For a problem defined in Ω, we can impose a complementary problem in Ω' with the displacement and pore pressure along the boundary identical to that of the primary problem. Equations (125) therefore reduce to

$$bu_k(x, t) = \int_0^t \int_\Gamma [u_{ki}^{\mathrm{fi}}(x, t; \chi, \tau) s_i(\chi, \tau) + p_k^{\mathrm{fc}}(x, t; \chi, \tau) d(\chi, \tau)]\, \mathrm{d}\chi\, \mathrm{d}\tau \tag{126a}$$

$$bp(x, t) = \int_0^t \int_\Gamma [u_i^{\mathrm{li}}(x, t; \chi, \tau) s_i(\chi, \tau) + p^{\mathrm{si}}(x, t; \chi, \tau) d(\chi, \tau)]\, \mathrm{d}\chi\, \mathrm{d}\tau \tag{126b}$$

The quantities s_i and d in equations (126) represent the traction and normal flux jumps across the boundary Γ as follows

$$s_i = (\sigma_{ij} - \sigma'_{ij}) n_j \tag{127a}$$

$$d = -(q_i - q'_i) n_i \tag{127b}$$

Equations (126) can be written in the physically more meaningful form

$$bu_k(x, t) = \int_0^t \int_\Gamma [u_{ki}^{\mathrm{fi}}(x, t; \chi, \tau) s_i(\chi, \tau) + u_k^{\mathrm{si}}(x, t; \chi, \tau) d(\chi, \tau)]\, \mathrm{d}\chi\, \mathrm{d}\tau \tag{128a}$$

$$bp(x, t) = \int_0^t \int_\Gamma [p_i^{\mathrm{fi}}(x, t; \chi, \tau) s_i(\chi, \tau) + p^{\mathrm{si}}(x, t; \chi, \tau) d(\chi, \tau)]\, \mathrm{d}\chi\, \mathrm{d}\tau \tag{128b}$$

where use has been made of certain relations among Green's functions [90]. These equations show that the displacement and pore pressure at a point x and time t can be evaluated by distributing along the boundary Γ poroelastic instantaneous point force and source solutions with 'fictitious densities' (which correspond to the traction and normal flux jumps). The above pair of equations are equivalent to the 'single layer' method in the potential theory [92] in which singularities of order $\ln r$ for 2-D and $1/r$ for 3-D are distributed.

In contrast to the single layer method, we now consider the case where the boundary traction and the normal flux for the interior and exterior domain problems are set equal. The following set of integral equations are then deduced from equations (124)

$$bu_k(x,t) = \int_0^t \int_\Gamma [\sigma_{ijk}^{fi}(x,t;\chi,\tau)n_j(\chi)d_i(\chi,\tau) + \frac{1}{\kappa} q_{ki}^{fc}(x,t;\chi,\tau)n_i(\chi)s(\chi,\tau)]\,d\chi\,d\tau \tag{129a}$$

$$bp(x,t) = \int_0^t \int_\Gamma [\sigma_{ij}^{li}(x,t;\chi,\tau)n_j(\chi)d_i(\chi,\tau) + \frac{1}{\kappa} q_i^{si}(x,t;\chi,\tau)n_i(\chi)s(\chi,\tau)]\,d\chi\,d\tau \tag{129b}$$

In the above

$$d_i = u_i - u_i' \tag{130a}$$

$$s = -\kappa(p - p') \tag{130b}$$

correspond respectively to displacement and pore pressure discontinuities. The alternative form of equations (129) is

$$bu_k(x,t) = \int_0^t \int_\Gamma [u_{kji}^{di}(x,t;\chi,\tau)n_j(\chi)d_i(\chi,\tau) + u_{ki}^{pi}(x,t;\chi,\tau)n_i(\chi)s(\chi,\tau)]\,d\chi\,d\tau \tag{131a}$$

$$bp(x,t) = \int_0^t \int_\Gamma [p_{ji}^{di}(x,t;\chi,\tau)n_j(\chi)d_i(\chi,\tau) + p_i^{pi}(x,t;\chi,\tau)n_i(\chi)s(\chi,\tau)]\,d\chi\,d\tau \tag{131b}$$

where the superscript d refers to displacement discontinuity and the superscript p to a fluid dipole. The above formulae thus define another indirect method in which the influence functions correspond to displacement discontinuity and fluid dipole singularities. It may be viewed as the equivalent of the double layer method in potential theory, or the displacement discontinuity method [93] in elasticity.

5.5.4 Method of Singularities

Problems involving infinite or semi-infinite domains can sometimes be elegantly solved using superposition of singularities that captures the essential aspect of the problem at stake. In contrast to the indirect integral method, the strength of the singularity is here always a physically meaningful quantity. Examples of such an approach are the use of the source solution to model subsidence problems due to pumping, and the displacement discontinuity to create fracture opening. A brief presentation of the application of this method, for solving consolidation, subsidence, and fracture propagation problems, is given below.

5.5.4.1 Modeling consolidation and subsidence

In this class of problems, the basic interest is to compute the progressive settlement of the ground surface caused either by the application of surface surcharge (consolidation) or by the withdrawal of pore fluid (subsidence). For a homogeneous half-space, this calculation can be achieved by the superposition of the fundamental solution of an impulsive point surface force for the consolidation problem and impulsive point source for the subsidence problem (respectively line force and line source for plane strain problems). The same approach has also been extended to the analysis of consolidation in layered soil [69].

The singular solutions have been derived using the displacement function formalism of McNamee and Gibson for boundary conditions corresponding to a traction-free surface under either zero pore pressure or zero flux [59, 66, 94, 95]. Note that these solutions are obtained by applying a double

integral transformation to the field equations (Laplace–Hankel or Laplace–Fourier) and that at least one of the inversions is performed numerically; thus none of these solutions are presented in closed form.

5.5.4.2 Modeling fractures

(i) Fracture model

A fracture in a poroelastic medium is a surface across which the solid displacement and the normal fluid flux are generally discontinuous. Such a discontinuity surface can mathematically be simulated by a distribution over time and space of impulse point displacement discontinuities (DD) and sources. If the density of these singularities is known, integral representations of the field quantities, such as displacement, flux, stress, and pore pressure, can be evaluated using the principle of superposition. As an example, consider a linear hydraulic fracture which is pressurized by the injection of a fluid. The integral representations of the normal stress and pore pressure on the crack surface are [63,88]

$$\sigma_n(x,t) = \int_0^t \int_{-L}^{+L} d_n(\chi,\tau)\sigma_{nn}^{di}(x-\chi,t-\tau) + d(\chi,\tau)\sigma_n^{si}(x-\chi,t-\tau)\,d\chi\,d\tau \tag{132a}$$

$$p(x,t) = \int_0^t \int_{-L}^{+L} d_n(\chi,\tau)p_n^{di}(x-\chi,t-\tau) + d(\chi,\tau)p^{si}(x-\chi,t-\tau)\,d\chi\,d\tau \tag{132b}$$

where σ_n denotes the normal stress on the fracture, d_n is the normal displacement discontinuity density, and d the flux discontinuity density (source density, or the rate of fluid leakoff per unit fracture length). The quantities marked with a 'di' and a 'si' superscript are the influence functions of an instantaneous point displacement discontinuity, and an instantaneous source, respectively: σ_{nn}^{di} is the normal stress and p_n^{di} the pressure generated by a unit normal displacement discontinuity; σ_n^{si} and p^{si} are those caused by a unit fluid source. The singular integral equations (equations 132) can be exploited directly to solve for the discontinuity densities d_n and d, as a function of both space and time, from the known fluid pressure in the fracture [87]. However, the kernel function σ_{nn}^{di} contains a 'hypersingularity', $1/(x-\chi)^2$, which needs to be interpreted in the Hadamard sense [96]. It is more convenient to reduce the level of singularity in the kernels to Cauchy singular. By performing an integration by parts on the terms containing the displacement discontinuity, we obtain the 'edge dislocation' formulation

$$\sigma_n(x,t) = \int_0^t \int_{-L}^{+L} d_n'(\chi,\tau)\sigma_{nn}^{ei}(x-\chi,t-\tau) + d(\chi,\tau)\sigma_n^{si}(x-\chi,t-\tau)\,d\chi\,d\tau \tag{133a}$$

$$p(x,t) = \int_0^t \int_{-L}^{+L} d_n'(\chi,\tau)p_n^{ei}(x-\chi,t-\tau) + d(\chi,\tau)p^{si}(x-\chi,t-\tau)\,d\chi\,d\tau \tag{133b}$$

where $d_n' = \partial d_n/\partial\chi$ is the slope of the fracture profile, and σ_{nn}^{ei} is the influence function of normal stress due to an instantaneous opening edge dislocation (a semi-infinite discontinuity line with constant displacement jump), with the kernel p_n^{ei} as the pressure influence function. Note that an auxiliary condition of fracture closure needs to be introduced to determine the free term resulting from the integration by parts,

$$\int_{-L}^{+L} d_n'(\chi,t)\,d\chi = 0 \tag{134}$$

Numerical solution of equations (133) and (134) has been accomplished with the aid of the Laplace transform for a nonpropagating fracture [17].

For the same problem of a pressurized fracture but with impermeable surfaces, the integral equation to be solved reduces to

$$\sigma_n(x,t) = \int_0^t \int_{-L}^{+L} d_n(\chi,\tau)\sigma_{nn}^{di}(x-\chi,t-\tau)\,d\chi\,d\tau \tag{135}$$

Indeed the normal displacement discontinuity (and likewise the opening edge dislocation) naturally satisfies the condition of zero flux across the x axis (the dislocation line). This 'natural' boundary

condition for the fluid (in the case of shear dislocation, it corresponds to a zero pore pressure) emerges from the requirement of symmetry across the dislocation line (antisymmetry for the shear mode) for a solution constrained to have the pore pressure and its gradient continuous across the x axis. Fundamental solutions of the continuous edge dislocation have been obtained by Rice and Cleary [8] and Detournay and Cheng [63] for the natural fluid boundary condition and by Rudnicki [97] for conditions corresponding to a zero pore pressure along the x axis for the opening mode and a zero flux across the x axis for the shear mode. It is interesting to note that the poroelastic solution of an edge dislocation with the natural fluid boundary condition is simply the superposition of the elastic solution with undrained Poisson's ratio and a fluid dipole oriented perpendicular to the Burger's vector, *i.e.* respectively parallel and perpendicular to the x axis for the opening and shear mode.

(ii) Propagating fractures

The steady state propagation of a fracture can be modeled using steadily moving singularities in an infinite poroelastic medium [16]. For this class of problems, time does not enter into consideration if a moving coordinate system is used and if the problem remains self-similar in that system. With these assumptions, the fluid mass balance equation (equation 73), which is the only governing equation that contains a time derivative, transforms into

$$-v\frac{\partial\zeta}{\partial x} + q_{i,i} = \gamma \tag{136}$$

in a moving coordinates system with the x axis in the same direction as the velocity v.

The solution of a moving singularity can be deduced from the corresponding impulsive solution through superposition (integration), or alternatively by direct solution of the singular differential equations in the moving coordinates system. The pore pressure field induced by a moving source is given by Carslaw and Jaeger [98], while moving edge dislocation solutions have been obtained by Rudnicki and Roeloffs [99]. Moving dislocation solutions have been used to analyze pore pressure changes and stabilizing effects associated with the propagation of slip on permeable and impermeable faults [10, 99–102], and the mechanism of retardation of a propagating hydraulic tensile fracture with impermeable [16] or permeable walls [103].

5.6 SOME FUNDAMENTAL PROBLEMS

In this section we study a few fundamental problems: one-dimensional loading of a layer, pressurization of a cylinder, far-field loading of a borehole, and hydraulic fracturing. These problems involve simple geometries but are instructive for understanding the role of poroelastic effects.

In all these problems at least one of the boundaries is subject to a particular condition: a prescribed constant normal stress and/or pore pressure suddenly applied at $t = 0^+$. In such cases, it is actually convenient to consider two fundamental loading modes: mode 1 with $\sigma_n^{(1)} = -p^*H(t)$ and $p^{(1)} = 0$, and mode 2 with $\sigma_n^{(2)} = 0$ and $p^{(2)} = p^*H(t)$, where, as a convention, the superscripts $^{(1)}$ and $^{(2)}$ are used to designate the corresponding mode. These two loadings can later on be superposed to match any boundary conditions where pore pressure and normal stress are arbitrarily imposed.

5.6.1 Uniaxial Strain Problems

Here we consider a particular class of 'one-dimensional' problems, characterized by only one nonzero normal strain and by field quantities varying only in that direction. Let this privileged orientation coincide with the x direction (ε_{xx} being thus the nonzero strain). First we examine how some of the governing and field equations transform under uniaxial strain conditions.

5.6.1.1 Governing equations

Under uniaxial strain condition, the constitutive equations (equations 54–57) become

$$\sigma_{xx} = \frac{2G(1-\nu)}{1-2\nu}\varepsilon_{xx} - \alpha p \tag{137a}$$

$$\sigma_{yy} = \sigma_{zz} = \frac{\nu}{1-\nu}\sigma_{xx} - 2\eta p \tag{137b}$$

or

$$\sigma_{xx} = \frac{2G(1-\nu_u)}{1-2\nu_u}\varepsilon_{xx} - \alpha M\zeta \tag{138a}$$

$$\sigma_{yy} = \sigma_{zz} = \frac{\nu_u}{1-\nu_u}\sigma_{xx} - 2\eta M\zeta \tag{138b}$$

depending on whether p or ζ is chosen as the coupling term. Under undrained conditions, the pore pressure is proportional to σ_{xx}

$$p = -\frac{B(1+\nu_u)}{3(1-\nu_u)}\sigma_{xx} = -\frac{\eta}{GS}\sigma_{xx} \tag{139}$$

There is only one nontrivial equilibrium equation (equation 72), which shows that, in the absence of body force, σ_{xx} is independent of x (although it can still be a function of time). The differential equation for u_x (the Navier equation) is simply deduced from equations (137a) or (138a), by expressing ε_{xx} as $\partial u_x/\partial x$, *i.e.*

$$\frac{2G(1-\nu)}{1-2\nu}\frac{\partial^2 u_x}{\partial x^2} - \alpha\frac{\partial p}{\partial x} = 0 \tag{140}$$

By expressing ε_{xx} in terms of p and σ_{xx} using equation (137a), the diffusion equation for the pore pressure (equation 82) simplifies to

$$\frac{\partial p}{\partial t} - c\frac{\partial^2 p}{\partial x^2} = -\frac{\eta}{GS}\frac{\mathrm{d}\sigma_{xx}}{\mathrm{d}t} \tag{141}$$

This equation could have been alternatively deduced from the particular pore pressure diffusion equation (equation 90) – applicable for irrotational displacement field – by noting that $g = \eta\sigma_{xx}/\alpha G$, in uniaxial deformation.

For problems with a specified stress condition, equation (141) is an inhomogeneous diffusion equation with a known right-hand side. The pore pressure can therefore be solved independently of the displacement in this particular class of problems.

5.6.1.2 Terzaghi's one-dimensional consolidation

First we analyze the classical one-dimensional consolidation problem of Terzaghi [1] in light of the Biot theory. Consider a soil layer of thickness L, resting on a rigid impermeable base. A constant load is applied on the surface of the layer under drained conditions. The boundary conditions are therefore $\sigma_{xx} = -p^*H(t)$ and $p = 0$ at $x = 0$ and $u_x = 0$ and $\partial p/\partial x = 0$ at $x = L$. The surface loading clearly corresponds to what has been identified as mode 1 loading.

Since the stress is a constant, the right-hand side of equation (141) drops out to give a homogeneous diffusion equation

$$\frac{\partial p}{\partial t} - c\frac{\partial^2 p}{\partial x^2} = 0 \tag{142}$$

This equation is identical to that found in the Terzaghi's consolidation theory. The two theories are therefore consistent for this particular geometry and loading condition. In the literature, the homogeneous diffusion equation for p has often been extended to other situations. This, however, cannot be done as, in general, a term proportional to the rate of change of the mean stress needs to be included in the pore pressure diffusion equation. This term corresponds to the 'Skempton' pore pressure generation mechanism, that continues to feed the diffusion process.

The solution of the consolidation problem now involves solving equation (142) with boundary conditions $p^{(1)} = 0$ at $x = 0$ and $\partial p^{(1)}/\partial x = 0$ at $x = L$. (The superscripts $^{(1)}$ and $^{(2)}$ are from now on used to associate the solution with the corresponding loading mode.) The initial pore pressure field p^u, induced upon loading of the layer, is given by $p^u = \eta p^*/GS$ (see equation 139). Note that in the

limiting case of incompressible fluid and solid constituents (which is a good approximation for water-saturated soils), $p^u = p^*$, which is also consistent with Terzaghi's solution.

The two fields $p^{(1)}$ and $u_x^{(1)}$ can be expressed in terms of the dimensionless coordinate $\chi = x/L$ and the dimensionless time $\tau = ct/4L^2$. Solving equation (142) with the above initial and boundary conditions yields

$$p^{(1)} = \frac{\eta p^*}{GS}[1 - F_1(\chi, \tau)] \tag{143}$$

where

$$F_1(\chi, \tau) = 1 - \sum_{m=1,3,\ldots}^{\infty} \frac{4}{m\pi} \sin\left(\frac{m\pi\chi}{2}\right) \exp(-m^2\pi^2\tau) \tag{144}$$

Note that $F_1(\chi, 0^+) = 0$ and $F_1(\chi, \infty) = 1$.

The displacement $u_x^{(1)}$ is found by integrating equation (140) and substituting the resulting expression in the boundary conditions. It can be expressed as $u_x^{(1)} = u_x^u + \Delta u_x^{(1)}$ where u_x^u is the initial undrained elastic displacement and $\Delta u_x^{(1)}$ a time-dependent incremental component

$$u_x^u = \frac{p^* L(1 - 2\nu_u)}{2G(1 - \nu_u)}(1 - \chi) \tag{145a}$$

$$\Delta u_x^{(1)} = \frac{p^* L(\nu_u - \nu)}{2G(1 - \nu)(1 - \nu_u)} F_2(\chi, \tau) \tag{145b}$$

where

$$F_2(\chi, \tau) = \sum_{m=1,3,\ldots}^{\infty} \frac{8}{m^2\pi^2} \cos\left(\frac{m\pi\chi}{2}\right)[1 - \exp(-m^2\pi^2\tau)] \tag{146}$$

We note that $F_2(\chi, 0) = 0$ and $F_2(\chi, \infty) = (1 - \chi)$, hence the large time asymptotic solution of the displacement field is indeed the drained elastic solution. The layer thus deforms instantaneously with an elastic response characterized by the undrained Poisson ratio ν_u, and progressively consolidates into another elastic state, characterized by a displacement field similar to u^u, but for ν_u replaced by ν. The pore pressure field, initially equal to p^u, dissipates continuously to vanish at $\tau = \infty$.

At the top of the layer, the settlement $u^*(\tau) = u_x(0, \tau)$ is

$$u^{*(1)} = \frac{p^* L(1 - 2\nu_u)}{2G(1 - \nu_u)}\left[1 + \frac{\nu_u - \nu}{(1 - \nu)(1 - 2\nu_u)} f(\tau)\right] \tag{147}$$

where $f(\tau) = F_2(0, \tau)$, *i.e.*

$$f(\tau) = \sum_{m=1,3,\ldots}^{\infty} \frac{8}{m^2\pi^2}[1 - \exp(-m^2\pi^2\tau)] \tag{148}$$

The function $f(\tau)$, which varies between 0 and 1 as τ increases from 0 to ∞, is plotted in Figure 1.

5.6.1.3 Loading by a fluid

We consider next a similar problem, where the upper surface of the layer is now in contact with a fluid at pressure p^*. In this case, the boundary conditions at $x = 0$ are $\sigma_{xx} = -p^* H(t)$ and $p = p^* H(t)$. These boundary conditions correspond, therefore, to the superposition of mode 1 (the Terzaghi's consolidation problem) and mode 2. Only mode 2 needs to be solved.

The initial pore pressure field for mode 2 loading is everywhere zero. The solution of $p^{(2)}$ is thus given by

$$p^{(2)} = p^* F_1(\chi, \tau) \tag{149}$$

The pore pressure in the layer increases with time until it reaches the constant value p^* at $\tau = \infty$. The displacement field is again found by integrating equation (140)

$$u_x^{(2)} = -\frac{\eta p^* L}{G} F_2(\chi, \tau) \tag{150}$$

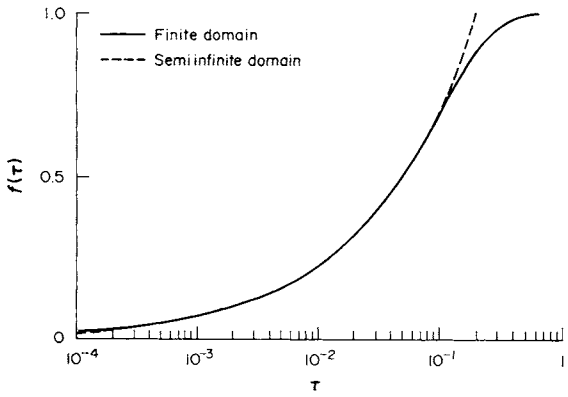

Figure 1 Response function for the surface displacement

with the surface displacement given by

$$u^{*(2)} = -\frac{\eta p^* L}{G} f(\tau) \tag{151}$$

We observe that the surface displacement is zero at $\tau = 0^+$, and gradually rebounds (instead of consolidating) to the long-term value of $u^{*(2)}(\infty) = -\eta p^* L/G$. The rebound is a consequence of the dilation of the porous solid induced by an increase of the pore pressure.

The solution of this problem is then obtained by superposition of the solutions of the two modes. For example, the surface displacement is given by the sum of equations (147) and (151). At the instant of loading, the layer immediately consolidates to $u^* = p^* L(1 - 2\nu_u)/2G(1 - \nu_u)$. Two opposing processes then follow: one consolidates to the maximum value $p^* L(\nu_u - \nu)/2G(1 - \nu)(1 - \nu_u)$, and the other rebounds to the asymptotic value of $-p^* L\eta/G$. It can be shown that the second process is always greater in magnitude than the first, but that it is never able to overcome the initial settlement. Hence the layer ends up with a positive settlement which is smaller than the initial one.

5.6.1.4 Early time solution

Considering the above equations, it is obvious that the time-dependent component of mode 1 and 2 loading corresponds to the same generic process: one-dimensional diffusion triggered by step difference between the boundary condition of the pore pressure and its initial value. A simpler expression of the early time solution for these two modes can be derived.

At early time, the pore pressure perturbation (with respect to the initial conditions) is virtually confined to a region (growing with time) adjacent to the boundary; in other words, the layer appears semi-infinite from the point of view of the pore pressure perturbation near the boundary. The early time solution corresponds therefore to the half-space solution.

The pore pressure field induced in a semi-infinite domain by the application of a constant pore pressure p^* at time $t = 0^+$ on the surface of a half-space is well known [98]; it is a self-similar solution, which is only a function of the coordinate x scaled by the characteristic length $\sqrt{ct}$

$$p = p^* \operatorname{erfc}\left(\frac{x}{2\sqrt{ct}}\right) \tag{152}$$

Although the pore pressure is instantly perturbed everywhere at time $t = 0^+$ (due to the infinite propagation velocity of the pressure wave), the decay property of the complementary error function is such that beyond the distance $4\sqrt{ct}$, the pore pressure is less than 0.5% of the boundary value p^*. It is thus convenient to speak of a 'pressure front' located at $\delta = 4\sqrt{ct}$, progressively moving inside the domain. We expect the half-space solution to be applicable to the finite domain problem, as long as the pressure front has not reached the bottom of the layer, *i.e.* when $4\sqrt{ct} < L$, or equivalently, when the dimensionless time τ (defined earlier as $ct/4L^2$) is less than about 2×10^{-2}.

The displacement field is found through integration of the Navier equation (equation 140), using the pore pressure solution (equation 152) and $\sigma_{xx} = 0$. In particular, we find that the dimensionless function $f(\tau)$, appearing in equations (147) and (151) for the surface displacement u^*, takes the simplified form

$$f(\tau) \cong 4\sqrt{\frac{\tau}{\pi}} \text{ for } \tau < 2 \times 10^{-2} \tag{153}$$

A plot of the early time approximation (equation 153) of $f(\tau)$ is shown in Figure 1, where it can be compared to the full solution (equation 148). This plot clearly shows the divergence between the two solutions at about $\tau \cong 5 \times 10^{-2}$.

5.6.1.5 *Harmonic excitation*

As demonstrated in equation (141), the one-dimensional pressure diffusion equation based on the poroelastic theory differs from that of the *ad hoc* consolidation theory by a term proportional to the rate of stress variation. While this effect is nonexistent for constant loading, a departure from the consolidation theory is expected for transient loading. In particular, we will examine the one-dimensional harmonic loading of a layer. Considering here only mode 1 loading, the top boundary conditions are (using complex variable notation): at $x = 0$, $\sigma_{xx} = -p^* \exp(i\omega t)$ and $p = 0$, where $i = \sqrt{-1}$ and ω is the frequency. The governing equation for the steady state periodic solution is

$$i\omega\tilde{p} - c\frac{d^2\tilde{p}}{dx^2} = \frac{i\omega\eta p^*}{GS} \tag{154}$$

in which $\tilde{p}$ denotes the complex amplitude of the periodic pressure response. Now the solution can be expressed in terms of the coordinate $\chi = x/L$ and the dimensionless frequency $\omega^* = \omega L^2/c$.

With the same bottom boundary conditions as in the Terzaghi's problem, the pore pressure solution is

$$\tilde{p}^{(1)} = \frac{\eta p^*}{GS}(1 + \tanh\lambda \sinh\lambda\chi - \cosh\lambda\chi) \tag{155}$$

where $\lambda = \sqrt{i\omega^*}$. To draw a parallel with the early time solution discussed in Section 5.6.1.4, it is interesting to compare equation (155) with the solution obtained for a half-space subject to the same surface harmonic loading. This solution

$$\tilde{p} = \frac{\eta p^*}{GS}\left[1 - \exp\left(-\sqrt{\frac{i\omega}{c}}x\right)\right] \tag{156}$$

indicates that beyond the distance $\delta = 3\sqrt{c/\omega}$ from the surface, the pore pressure is virtually in phase and proportional by a factor η/GS to the surface loading. In other words, departure of the pore pressure fluctuations from the trivial undrained solution is virtually confined to a boundary layer of thickness δ. We expect therefore the half-plane solution to be applicable to the finite domain problem provided $\delta < L$, or equivalently $|\lambda| > 3$ (*i.e.* $\omega^* > 9$). Refer to refs. 104–108 for more discussion on the concept of boundary layer and its application.

Note that the right-hand side of equation (154) vanishes in the consolidation theory, thus yielding the trivial zero solution. The consolidation theory therefore predicts that there is no pressure response generated in the formation other than some initial transients that will dissipate in time.

For the poroelastic theory, the displacement $u^{*(1)}$ at $x = 0$ is given by

$$\tilde{u}^{*(1)} = \frac{p^* L(1 - 2\nu_u)}{2G(1 - \nu_u)}\left[1 + \frac{(\nu_u - \nu)}{(1 - \nu)(1 - 2\nu_u)}\frac{\tanh\lambda}{\lambda}\right] \tag{157}$$

while in the consolidation case, we find

$$\tilde{u}^{*(1)} = \frac{p^* L(1 - 2\nu)}{2G(1 - \nu)} \tag{158}$$

The consolidation theory predicts a purely elastic settlement with a stiffness characterized by the

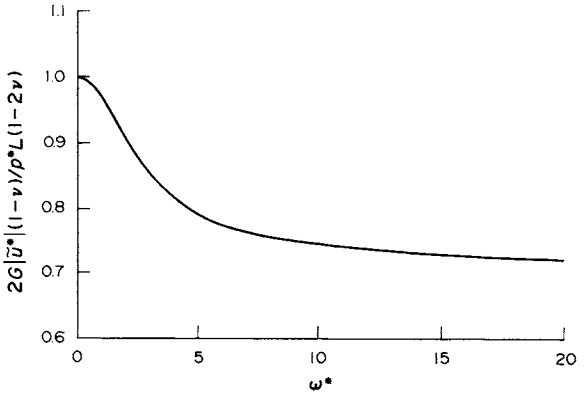

Figure 2 Maximum settlement as function of loading frequency

drained Poisson ratio. That settlement is also completely in phase with the applied load. For the poroelasticity case, the apparent stiffness of the formation is a function of the loading frequency. As $\omega \to \infty$, the material behaves as an undrained one (it should be remarked that as the frequency becomes large, the dynamic (inertia) effect will manifest itself [28, 109], a topic, however, which is beyond the scope of this presentation), i.e. $\tilde{u}^{*(1)}(\infty) = p^*L(1 - 2\nu_u)/2G(1 - \nu_u)$; as $\omega \to 0$, its behavior evolves to that of drained material, $\tilde{u}^{*(1)}(0) = p^*L(1 - 2\nu)/2G(1 - \nu)$; this last relation being identical to equation (158). It should also be pointed out that the settlement is generally not in phase with the loading. Figure 2 illustrates the normalized maximum settlement $|\tilde{u}^{*(1)}|$ *versus* the dimensionless frequency ω^* for the particular case $\nu = 0.15$ and $\nu_u = 0.31$.

5.6.2 Cylinder Problem

5.6.2.1 Problem definition and solution methodology

We consider now the problem of a cylinder with radius a deforming, under plane strain conditions, after sudden application of a constant fluid pressure p^* on the boundary $r = a$. Under conditions of planar deformation and axisymmetry, the displacement field is obviously irrotational, and characterized by the only nonzero component, $u_r(r, t)$. It then follows from equation (92) that the pore pressure diffusion equation takes the particular form

$$\frac{\partial p}{\partial t} - c\left(\frac{1}{r}\frac{\partial p}{\partial r} + \frac{\partial^2 p}{\partial r^2}\right) = -\frac{\eta(1-\nu)}{GS}\frac{\mathrm{d}}{\mathrm{d}t}(\sigma_{rr} + \sigma_{\theta\theta} + 2\eta p) \tag{159}$$

where the quantity $\sigma_{rr} + \sigma_{\theta\theta} + 2\eta p$ on the right-hand side is a function of time only (see Section 5.4.3.3). However, in contrast to the uniaxial deformation problems discussed previously, the inhomogeneous term in the diffusion equation is here unknown; equation (159) is thus not really suitable to be used for solving this boundary value problem.

In an alternative approach, we start with the uncoupled diffusion equation (equation 83) for the variation of fluid content ζ. If the general solution ζ can be obtained for the particular symmetries involved, the volumetric strain ε can then be readily determined up to a function of time only. Indeed ε and ζ are related according to

$$\frac{\partial \varepsilon}{\partial r} = \frac{\eta}{GS}\frac{\partial \zeta}{\partial r} \tag{160}$$

which is simply a reduced form of the Navier equation (equation 81b). In turn, the displacement u_r is found by an integration of ε, from the relation

$$\varepsilon = \frac{1}{r}\frac{\partial}{\partial r}(ru_r) \tag{161}$$

The stress and pressure solutions follow from the constitutive equations. The various constants appearing in the solution are eliminated using the boundary conditions.

The solution can be obtained explicitly for the Laplace transform of the various quantities. The solution in time is then calculated using a numerical inversion technique. Application of the Laplace transformation to the diffusion equation for ζ (to eliminate the time derivative operator) yields, taking the symmetry conditions into account,

$$\frac{d^2\tilde{\zeta}}{dr^2} + \frac{1}{r}\frac{d\tilde{\zeta}}{dr} - \frac{s}{c}\tilde{\zeta} = 0 \tag{162}$$

where the tilde overbar denotes the Laplace transform and s is the transform parameter. The solution will depend on two dimensionless variables: $\rho = r/a$ and $\beta = a\sqrt{s/c}$. The general solution of equation (162) is

$$\tilde{\zeta} = D_1 I_0(\xi) \tag{163}$$

where $\xi = \beta\rho$, I_0 is the modified Bessel function of first kind of order 0, and D_1 is a constant to be determined. The volumetric strain is obtained by integrating equation (160)

$$\tilde{\varepsilon} = \frac{\eta}{GS} D_1 I_0(\xi) + D_2 \tag{164}$$

Finally, integrating equation (161) using equation (164) yields the general solution for the radial displacement $\tilde{u}_r$

$$\tilde{u}_r = \frac{\eta a}{\beta GS} D_1 I_1(\xi) + \frac{D_2}{2} r \tag{165}$$

All the elements are now in place to solve the cylinder problem for mode 1 and 2 loading.

5.6.2.2 Mode 1 loading

The boundary conditions for mode 1 loading are $\sigma_{rr}^{(1)} = -p^*$ and $p^{(1)} = 0$, at $r = a$. After fulfillment of these boundary conditions, equation (165) becomes

$$\frac{2G}{ap^*} s\tilde{u}_r^{(1)} = -\rho \frac{(1-2\nu_u)(1-\nu)I_0(\beta) + 2(\nu_u - \nu)\xi^{-1}I_1(\xi)}{(1-\nu)I_0(\beta) - 2(\nu_u - \nu)\beta^{-1}I_1(\beta)} \tag{166}$$

The asymptotic behavior of the solution can easily be checked: as $t \to \infty$, $s \to 0$, hence

$$\frac{2G}{ap^*} u_r^{(1)}(r, \infty) = -(1-2\nu)\rho \tag{167}$$

which is the drained elastic solution. As $t \to 0$, $s \to \infty$, and we obtain an expression similar to equation (167) but with ν replaced by ν_u.

Consider now the pore pressure field. At $t = 0^+$, there is a uniform pressure rise due to the Skempton effect

$$p^{(1)}(r, 0^+) = p^u \tag{168}$$

where

$$p^u = \tfrac{2}{3}(1+\nu_u)Bp^* \tag{169}$$

As $t \to \infty$, the pressure is fully dissipated, *i.e.* $p^{(1)}(r, \infty) = 0$. The transform solution of the pore pressure field is given by

$$\frac{s\tilde{p}^{(1)}}{p^u} = \frac{(1-\nu)[I_0(\beta) - I_0(\xi)]}{(1-\nu)I_0(\beta) - 2(\nu_u - \nu)\beta^{-1}I_1(\beta)} \tag{170}$$

It is of interest to compare the poroelastic solution with the solution based on the simple diffusion equation which ignores the right-hand side of equation (159). With the same initial condition (equation 168), the pore pressure solution based on the homogeneous diffusion equation is given by

$$\frac{s\tilde{p}}{p^u} = \left[1 - \frac{I_0(\xi)}{I_0(\beta)}\right] \tag{171}$$

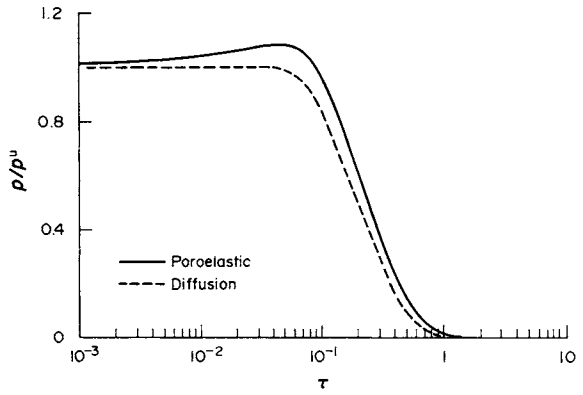

Figure 3 Pressure at the center of a cylindrical core under axisymmetric stress load

Figure 3 presents plots of the pressure history at the center of the cylinder ($r = 0$) for the case $\nu = 0.15$, $\nu_u = 0.31$ following the two theories. (The time domain solutions presented in these figures were calculated using a simple inversion scheme devised by Stehfest [110]; this technique relies only on real values of the Laplace parameter s.) The diffusion solution is characterized by a monotonic decline of the pore pressure while the poroelastic theory predicts a rise of pressure above its initial value before its dissipation. This phenomenon, known as the Mandel–Cryer effect [111, 112] in the soil mechanics literature, can be explained as follows. At the instant of loading, a uniform pore pressure is generated in the cylinder due to the Skempton effect. As the pressure starts to dissipate near the surface, the outer layer effectively softens. Due to the compatibility requirement, there is a load transfer to the inner and effectively harder material, which causes an additional pore pressure rise. This pore pressure generation mechanism, accomplished by the right-hand side of equation (159), is lacking in the consolidation theory.

5.6.2.3 Mode 2 loading

For the boundary conditions $p^{(2)} = p^*$ and $\sigma_{rr}^{(2)} = 0$, at $r = a$, the solution for the radial displacement in mode 2 loading is

$$\frac{2G}{ap^*} s\tilde{u}_r^{(2)} = \alpha(1-2\nu)\rho \frac{\xi^{-1}\mathrm{I}_1(\xi) + (1-2\nu_u)\beta^{-1}\mathrm{I}_1(\beta)}{(1-\nu)\mathrm{I}_0(\beta) - 2(\nu_u - \nu)\beta^{-1}\mathrm{I}_1(\beta)} \tag{172}$$

and the pressure

$$\frac{s\tilde{p}^{(2)}}{p^*} = \frac{(1-\nu)\mathrm{I}_0(\xi) - 2(\nu_u - \nu)\beta^{-1}\mathrm{I}_1(\beta)}{(1-\nu)\mathrm{I}_0(\beta) - 2(\nu_u - \nu)\beta^{-1}\mathrm{I}_1(\beta)} \tag{173}$$

We notice that as $t \to \infty$, $p^{(2)} = p^*$ and

$$\frac{2G}{ap^*} u_r^{(2)}(r, \infty) = \alpha(1-2\nu)\rho \tag{174}$$

5.6.2.4 Applications

The complete solution for the cylinder, in contact with a fluid at pressure p^*, is given by the superposition of the two fundamental modes. The cylinder will initially deform inward and then rebound to recover a portion of the initial volume loss. In particular, for materials with incompressible constituents ($\alpha = 1$ and $\nu_u = 0.5$) it can be shown that changes in confining fluid pressure cause no deformation in the sample at any time (*i.e.* $u_r(r, t) = 0$).

As an application of this solution, we investigate the evolution of the tangential stress $\sigma_{\theta\theta}$ in an 'instantaneously' retrieved cylindrical core. The core, initially under a uniform confining stress $\sigma_{rr} = -P_0$ and a pore pressure $p = p_0$, is instantly exposed to the atmosphere. The sudden removal

of the load causes a nonmonotonic evolution of stresses and displacement. In particular, the tangential stress is given by

$$s\tilde{\sigma}_{\theta\theta}(r,s) = P_0\left\{-1+\frac{(1-\nu)I_0(\beta)-2(\nu_u-\nu)[I_0(\xi)-\xi^{-1}I_1(\xi)]}{(1-\nu)I_0(\beta)-2(\nu_u-\nu)\beta^{-1}I_1(\beta)}\right\}$$
$$-p_0\alpha(1-2\nu)\frac{\xi^{-1}I_1(\xi)+\beta^{-1}I_1(\beta)-I_0(\xi)}{(1-\nu)I_0(\beta)-2(\nu_u-\nu)\beta^{-1}I_1(\beta)} \tag{175}$$

The normalized tangential stress profile in the cylinder at various times is plotted in Figure 4, for the case $\nu = 0.18$, $\nu_u = 0.28$ and $p_0 = 0.5P_0$. At the instant of unloading, the cylinder is stress-free $\sigma_{\theta\theta}(r, 0^+) = 0$, except at the wall, $r = a$, where a tensile stress immediately develops due to the effective softening of material by pressure diffusion

$$\sigma_{\theta\theta}(a,0) = -\frac{2(\nu_u-\nu)}{1-\nu}P_0 + 2\eta p_0 \tag{176}$$

The stress then goes through a non-monotonic evolution and finally settles down to the stress-free state again. Of interest to failure analysis is the Terzaghi effective stress $\sigma'_{\theta\theta} = \sigma_{\theta\theta} + p$. Figure 5 shows its history: it is entirely in the tensile range, with a maximum value reached at $t = 0^+$

$$\sigma'_{\theta\theta}(r,0^+) = -\tfrac{2}{3}B(1+\nu_u)P_0 + p_0 \tag{177}$$

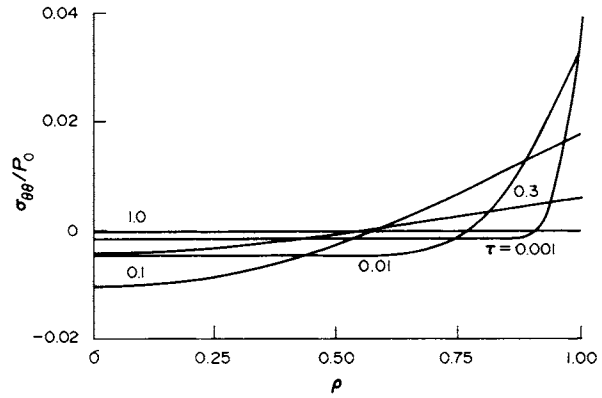

Figure 4 Evolution of tangential stress in an instantly retrieved cylindrical core

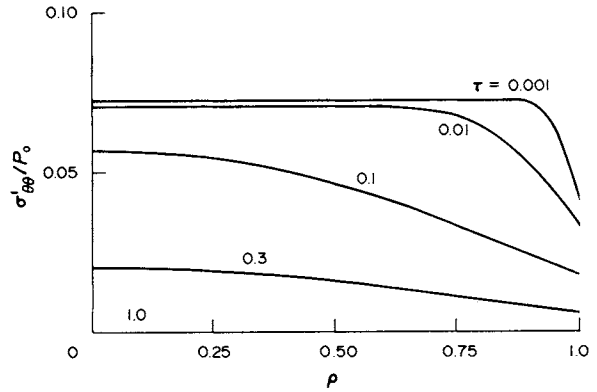

Figure 5 Evolution of Terzaghi effective tangential stress in an instantly retrieved cylindrical core

5.6.3 Borehole Problem

5.6.3.1 Problem definition

Now we consider the problem of a vertical borehole drilled in a porous rock layer subjected to a non-hydrostatic horizontal *in situ* stress field

$$\sigma_{xx} = -(P_0 - S_0) \tag{178a}$$

$$\sigma_{yy} = -(P_0 + S_0) \tag{178b}$$

$$\sigma_{xy} = 0 \tag{178c}$$

$$p = p_0 \tag{178d}$$

In the above P_0 and S_0 are the far-field mean stress and stress deviator, respectively, and p_0 is the virgin pore pressure. This problem is analyzed by assuming plane strain conditions and 'instantaneous' drilling of the borehole, simulated by removing at $t = 0^+$ the stresses and pore pressure that were initially acting on the borehole boundary.

To facilitate the physical interpretation of this problem, the loading is decomposed into three fundamental modes: (i) a far-field isotropic stress; (ii) a virgin pore pressure; and (iii) a far-field stress deviator. Denoting by the superscript (i), the stress induced by loading mode i, the boundary conditions at the borehole wall for each of the loading modes can be written as follows

Mode 1
$$\sigma_{rr}^{(1)} = P_0 \quad \sigma_{r\theta}^{(1)} = 0 \quad p^{(1)} = 0 \tag{179}$$

Mode 2
$$\sigma_{rr}^{(2)} = 0 \quad \sigma_{r\theta}^{(2)} = 0 \quad p^{(2)} = -p_0 \tag{180}$$

Mode 3
$$\sigma_{rr}^{(3)} = -S_0 \cos 2\theta \quad \sigma_{r\theta}^{(3)} = S_0 \sin 2\theta \quad p^{(3)} = 0 \tag{181}$$

Both the induced stress and pore pressure vanish at infinity. Solutions for the induced stress, pore pressure and displacement are derived below for each of the fundamental loading modes.

5.6.3.2 Mode 1 loading

For loading mode 1, the solution corresponds to the classical Lamé solution in elasticity

$$\frac{2Gu_r^{(1)}}{P_0 a} = -\frac{1}{\rho} \tag{182a}$$

$$\frac{\sigma_{rr}^{(1)}}{P_0} = \frac{1}{\rho^2} \tag{182b}$$

$$\frac{\sigma_{\theta\theta}^{(1)}}{P_0} = -\frac{1}{\rho^2} \tag{182c}$$

where ρ is the dimensionless radial coordinate r/a. Since the displacement field is characterized by zero volumetric strain, there is no mechanism for pore pressure generation and its subsequent diffusion. The displacement and stress fields are therefore independent of time.

5.6.3.3 Mode 2 loading

In the case of mode 2, the pressure field is governed by a homogeneous diffusion equation (the right-hand side of equation 159 drops out because of the vanishing stress condition at infinity)

$$\frac{\partial^2 p}{\partial r^2} + \frac{1}{r}\frac{\partial p}{\partial r} = \frac{1}{c}\frac{\partial p}{\partial t} \tag{183}$$

The pressure, stress and displacement fields are again solved by taking the Laplace transform

$$\frac{s\tilde{p}^{(2)}}{p_0} = -\frac{\mathrm{K}_0(\xi)}{\mathrm{K}_0(\beta)} \tag{184a}$$

$$\frac{2Gs\tilde{u}_r^{(2)}}{p_0 a} = 2\eta\left[\frac{K_1(\xi)}{\beta K_0(\beta)} - \frac{K_1(\beta)}{\xi K_0(\beta)}\right] \tag{184b}$$

$$\frac{s\tilde{\sigma}_{rr}^{(2)}}{p_0} = -2\eta\left[\frac{K_1(\xi)}{\xi K_0(\beta)} - \frac{K_1(\beta)}{\xi\rho K_0(\beta)}\right] \tag{184c}$$

$$\frac{s\tilde{\sigma}_{\theta\theta}^{(2)}}{p_0} = 2\eta\left[\frac{K_1(\xi)}{\xi K_0(\beta)} - \frac{K_1(\beta)}{\xi\rho K_0(\beta)} + \frac{K_0(\xi)}{K_0(\beta)}\right] \tag{184d}$$

where K_ν is the modified Bessel function of second kind of order ν, β is the dimensionless parameter $a\sqrt{s/c}$, and $\xi = \beta\rho$.

5.6.3.4 *Mode 3 loading*

The solution for mode 3 is somewhat more involved (the details of the solution procedure – similar to the technique used for the cylinder problem – can be found in ref. 113). Using symmetry considerations, it can be shown that the dependence of the displacement and stress upon the polar angle θ is of the following form

$$\{\tilde{u}_r^{(3)}, \tilde{\sigma}_{rr}^{(3)}, \tilde{\sigma}_{\theta\theta}^{(3)}, \tilde{p}^{(3)}\} = \{\tilde{U}_r, \tilde{S}_{rr}, \tilde{S}_{\theta\theta}, \tilde{P}\}\cos 2\theta \tag{185a}$$

$$\{\tilde{u}_\theta^{(3)}, \tilde{\sigma}_{r\theta}^{(3)}\} = \{\tilde{U}_\theta, \tilde{S}_{r\theta}\}\sin 2\theta \tag{185b}$$

where $\tilde{U}_r$, $\tilde{U}_\theta$, $\tilde{S}_{rr}$, $\tilde{S}_{r\theta}$, $\tilde{S}_{\theta\theta}$ and $\tilde{P}$ are solely functions of r and s (or ρ and β). The solution is given by

$$\frac{2Gs\tilde{U}_r}{S_0 a} = -\frac{1}{\beta}C_1\left[K_1(\xi) + \frac{2}{\xi}K_2(\xi)\right] + \frac{C_2}{\rho} + \frac{C_3}{\rho^3} \tag{186a}$$

$$\frac{2Gs\tilde{U}_\theta}{S_0 a} = -\frac{2C_1}{\beta\xi}K_2(\xi) - \frac{1-2\nu_u}{2(1-\nu_u)}\frac{C_2}{\rho} + \frac{C_3}{\rho^3} \tag{186b}$$

$$\frac{s\tilde{P}}{S_0} = \frac{2C_1}{\eta}K_2(\xi) + \frac{\eta}{GS}\frac{C_2}{\rho^2} \tag{186c}$$

$$\frac{s\tilde{S}_{rr}}{S_0} = C_1\left[\frac{1}{\xi}K_1(\xi) + \frac{6}{\xi^2}K_2(\xi)\right] - \frac{1}{1-\nu_u}\frac{C_2}{\rho^2} - \frac{3C_3}{\rho^4} \tag{186d}$$

$$\frac{s\tilde{S}_{\theta\theta}}{S_0} = -C_1\left[\frac{1}{\xi}K_1(\xi) + \left(1 + \frac{6}{\xi^2}\right)K_2(\xi)\right] + \frac{3C_3}{\rho^4} \tag{186e}$$

$$\frac{s\tilde{S}_{r\theta}}{S_0} = 2C_1\left[\frac{1}{\xi}K_1(\xi) + \frac{3}{\xi^2}K_2(\xi)\right] - \frac{1}{2(1-\nu_u)}\frac{C_2}{\rho^2} - \frac{3C_3}{\rho^4} \tag{186f}$$

in which

$$C_1 = -\frac{4\beta(\nu_u - \nu)}{D_2 - D_1} \tag{187a}$$

$$C_2 = \frac{4(1-\nu_u)D_2}{D_2 - D_1} \tag{187b}$$

$$C_3 = -\frac{\beta(D_2 + D_1) + 8(\nu_u - \nu)K_2(\beta)}{\beta(D_2 - D_1)} \tag{187c}$$

and

$$D_1 = 2(\nu_u - \nu)K_1(\beta) \tag{188a}$$

$$D_2 = \beta(1-\nu)K_2(\beta) \tag{188b}$$

5.6.3.5 *Applications*

With the above basic solutions, various borehole excavation, pressurization and production problems can be examined.

We first examine the stress concentration at the wall of a borehole, 'instantaneously' drilled at $t = 0$ to become stress- and pressure-free. Upon unloading, a compressive tangential stress concentration is immediately induced on the borehole wall. As indicated by equations (182c), (184d) and (186e), the contributions of the stress concentration from modes 1 and 2 are time-independent, while that from mode 3 is transient and is a function of the polar angle θ. The largest compressive stress concentration takes place at $\theta = 0, \pi$, *i.e.* at points connected by a diameter orthogonal to the direction of the most compressive far-field stress. Initially, the stress concentration at $\theta = 0, \pi$ is given by

$$\sigma_{\theta\theta}(a, 0^+) = -2P_0 + 2\eta p_0 - 4\frac{1-\nu_u}{1-\nu} S_0 \tag{189}$$

As time elapses, the tangential stress becomes more compressive and eventually reaches the large time asymptotic value

$$\sigma_{\theta\theta}(a, \infty) = -2P_0 + 2\eta p_0 - 4S_0 \tag{190}$$

This increase of stress concentration with time following drilling may account for delayed borehole failure.

We will now investigate the conditions leading to shear failure around the borehole. The stress evolution in the medium can be represented, in relation to a failure criterion, by plotting, along a given radial direction and at selected times, the maximum planar shear stress S, defined by

$$S = \tfrac{1}{2}\sqrt{(\sigma_{\theta\theta} - \sigma_{rr})^2 + 4\sigma_{r\theta}^2} \tag{191}$$

as a function of the mean planar Terzaghi effective compressive stress P''

$$P'' = -\tfrac{1}{2}(\sigma_{\theta\theta} + \sigma_{rr}) - p \tag{192}$$

Figure 6 presents such a plot for the following values of the stress parameters, $P_0 = 7S_0$, $p_0 = p^* = 4S_0$ (p^* is the pressure in the borehole), and the material constants, $\nu = 0.2$, $\nu_u = 0.4$ and $B = 0.8$. The solid curves indicate the stress profile at a given dimensionless time $\tau = ct/a^2$ for the whole range of dimensionless radial distance $1 \leq \rho < \infty$. The left end of the curves corresponds to $\rho = \infty$, where $P'' = 3S_0$ and $S = S_0$. The curves terminate at $\rho = 1$ where $P'' = S$. The lower envelope corresponds to $\tau \to \infty$; it coincides with the elastic solution. Also in the same diagram are dashed curves, representing the stress history at fixed ρ, for $0 < \tau < \infty$.

In a simple failure analysis based on the Mohr–Coulomb criterion, the failure condition can be expressed as

$$S = \frac{K_p - 1}{K_p + 1}\left(P'' + \frac{q}{K_p - 1}\right) \tag{193}$$

where q is the uniaxial compressive strength, and K_p the coefficient of passive stress, given in terms of

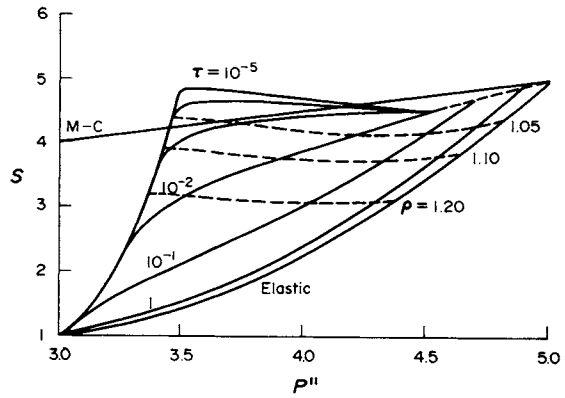

Figure 6 Isochrone of stress profile in the radial direction $\theta = 0, \pi$ and stress history at selected points

the friction angle φ by

$$K_p = \frac{1 + \sin \varphi}{1 - \sin \varphi} \tag{194}$$

The straight line in Figure 6 represents a Mohr–Coulomb criterion characterized by a friction angle $\varphi = 30°$ and a uniaxial strength $q = 10S_0$. A stress state above this line implies failure. As indicated on the figure, the parameters have been chosen in such a way that a state of impending failure exists at the borehole wall (at $\theta = 0$) according to the elastic solution (*i.e.* the Mohr–Coulomb line intersects with the right end of the elastic stress profile). The figure clearly indicates that failure can indeed initiate at some distance away from the borehole, and not right at the borehole wall as predicted on the basis of the elastic stress distribution. According to the stress history curves (dashed lines), failure occurs away from the wall at a distance ranging from 5% to 10% of the borehole radius. The poroelastic effects associated with mode 3 thus provide a potential mechanism for the formation of borehole breakouts, a pervasive feature of deep wells.

5.6.4 Early Time Evolution of Stress near a Permeable Boundary

Short time asymptotic expressions have been previously derived for the stress concentration at the outer boundary of a cylinder and at the borehole wall. Both cases are actually particular expressions of a generic process taking place near the permeable boundary of a poroelastic domain. An analysis of this near-boundary process is outlined below; it is followed by a discussion of the problem of rate effects in the tensile failure of fluid-pressurized cavities.

5.6.4.1 Early time stress concentration

We will now investigate the early time evolution of the stress concentration in that part of a poroelastic domain adjacent to a segment of boundary Γ. For simplicity, the domain is assumed to be under condition of plane strain and initially stress and pore pressure free. Let ρ denote the local radius of curvature of the boundary and let (l, n) refer to a local orthogonal curvilinear system of coordinates with the n axis in the same direction as the outward normal to Γ. At time $t = 0^+$, the boundary of the poroelastic domain is suddenly put in contact with a fluid, maintained at a constant pressure p^* for $t \geq 0$. As done earlier, this loading is decomposed in mode 1 and 2 loading.

Consider first mode 2 loading. At early time, the depth of penetration δ of the 'diffusion front' is very small compared to the radius of curvature ρ (and any other relevant length characterizing the problem); *i.e.* $\delta/\rho \ll 1$ and all other dimensions then appear infinite at the length scale δ. Therefore a one-dimensional solution of the poroelastic equations is expected in the neighborhood of the boundary. The early time evolution of the stress near the boundary can be deduced directly from the results obtained in Section 5.6.1. In particular, the following local relationship between the tangential stress and the pore pressure applies at early time

$$\sigma_{ll} = -2\eta p \qquad -\delta < n < 0 \tag{195}$$

In mode 1 loading, we generally have to take into account the existence of a pore pressure induced by application of a mechanical loading on the poroelastic solid. This induced pore pressure, denoted as p^u, is proportional to the mean stress σ^u_{kk} computed from an 'undrained' elastic analysis (see equation 63). At the boundary, the 'undrained' pore pressure is given by

$$p^u = -\frac{B(1 + \nu_u)}{3}(\sigma^u_{ll} - p^*) \tag{196}$$

Since p^u is a harmonic function (see equation 79 with $\zeta = 0$), the induced pore pressure field is internally equilibrated. (The only case for which the condition $\nabla^2 p^u = 0$ is not met, is when the mechanical loading includes a body force which does not derive from an harmonic potential.) However, p^u does not generally satisfy the boundary condition $p = 0$ and pore pressure adjustment will therefore take place at $t > 0$. Again, we expect a one-dimensional solution for the incremental field quantities near the boundary, during the initial phase of the pore pressure change; hence, in mode 1, at early time

$$\sigma_{ll} - \sigma^u_{ll} = -2\eta(p - p^u) \tag{197}$$

At the boundary, the readjustment of the pore pressure to the boundary condition takes place 'instantaneously' for either loading mode. The instantaneously adjusted value of the boundary tangential stress, σ_{ll}^{0+}, can thus be deduced from equation (197) (where $p = 0$ and p^u has been eliminated using equation 196) for mode 1 and from equation (195) (with $p = p^*$) for mode 2. Finally, the two expressions for the early time stress concentration are given by

Mode 1
$$\sigma_{ll}^{0+} = \frac{1 - \nu_u}{1 - \nu}\sigma_{ll}^u + \frac{\nu_u - \nu}{1 - \nu}p^* \tag{198}$$

Mode 2
$$\sigma_{ll}^{0+} = -2\eta p^* \tag{199}$$

As an example, the stress concentration at the boundary of a poroelastic cylinder (equation 176) is immediately recovered from equations (198) and (199).

For mode 2, the early time stress concentration is thus the result of a purely local phenomenon (its magnitude depends only on the local pressure p^*). For mode 1, there is a global influence on σ_{ll}^{0+} due to the presence of σ_{ll}^u in equation (199) (σ_{ll}^u is an 'elastic' contribution).

5.6.4.2 Strain compatibility argument

Equations (199) and (198) can actually be derived from a somewhat different point of view. In Section 5.4.3.3, it was mentioned that integration of the plane strain compatibility equation (equation 78) yields the expression

$$\sigma_{ll} + \sigma_{nn} + 2\eta p = f \tag{200}$$

where the harmonic function f generally depends on position and time (only on time if the displacement field is irrotational). Using the constitutive relation (equation 62), equation (200) can alternatively be written along the boundary as

$$2G\varepsilon_{ll} + \sigma_{nn} = (1 - \nu)f \tag{201}$$

Let us now focus on the situation arising when under constant stress on the boundary there is an 'instantaneous' adjustment of the pore pressure, as that occurring during the transition 'u' to '0^+' in mode 1 loading or at $t = 0^+$ in mode 2 loading. During the sudden transition of the pore pressure along the boundary of the domain, f remains unchanged (indeed f is an harmonic and thus a smooth function) and so does the tangential strain ε_{ll} since σ_{nn} is constant. Equations (198) and (200) can then be derived from equation (201), noting that along the boundary at $t = 0^+$, $f = \sigma_{ll}^u + \sigma_{nn}^u$ for mode 1 and $f = 0$ for mode 2.

Simply stated, the sudden variation of the tangential stress along the boundary takes place in order to preserve the tangential strain during the 'instantaneous' equilibration of the pore pressure to the imposed boundary value.

5.6.4.3 Application to tensile failure

(i) General considerations

Elastic stress concentrations are often used in conjunction with a failure criterion to predict the elastic limit of the system under consideration. This is done on the ground that the critical conditions are usually reached on the boundary of the domain. There is, however, a hidden assumption in this approach, namely that the stress concentration is representative of the stress 'averaged' over the length scale λ that underpins the failure process (*e.g.* the length of a microcrack for tensile failure). This condition is met in elastic boundary value problems, provided that λ is small compared to the radius of curvature ρ of the boundary. An example of this approach is the condition of propagation of a small 'edge' crack of length $\lambda \ll \rho$ which can be written as [114]

$$\sigma_{ll} = T \tag{202}$$

where the 'tensile strength' T is given by

$$T \cong \frac{K_{Ic}}{1.12\sqrt{\pi\lambda}} \tag{203}$$

with K_{Ic} denoting the material toughness.

In elasticity, this approach is therefore justified provided $\lambda \ll \rho$. In poroelasticity, however, we need to take into account an additional length scale, δ, the distance of propagation of the pore pressure perturbation from the boundary. When the diffusion length δ (which at early time is proportional to $\sqrt{ct}$) is smaller than or of the same order as the length scale λ, significant variation of the stress over the distance λ is expected, implying that the stress concentration does not properly reflect the stress controlling the tensile failure process.

It is possible to acknowledge in simple terms the existence of this length scale λ by considering a tangential stress $\bar{\sigma}_{tt}$ averaged in a boundary layer of thickness λ [115]

$$\bar{\sigma}_{tt} = \frac{1}{\lambda}\int_0^{-\lambda} \sigma_{tt}\, dn \tag{204}$$

As an illustration, we consider the case where mode 2 loading introduces the only significant poroelastic (time-dependent) contribution. On account that the induced stress in this boundary layer is given at early time by the one-dimensional solution (equation 195), the average Terzaghi effective stress $\bar{\sigma}'_{tt}$ (the relevant stress for tensile failure) is given by

$$\bar{\sigma}'_{tt} = \sigma^e_{tt} + \frac{1-2\eta}{\lambda}\int_0^{-\lambda} p\, dn \tag{205}$$

In the above, σ^e_{tt} is the elastic stress concentration, corresponding to mode 1 loading (no averaging on a boundary layer is necessary if $\lambda \ll \rho$). As an example, $\sigma^e_{tt} = -P_0 + p^*$ for the problem of a pressurized borehole with a far-field isotropic stress. Using equation (152) for the pore pressure solution, equation (205) for $\bar{\sigma}'_{tt}$ becomes

$$\bar{\sigma}'_{tt} = \sigma^e_{tt} + (1-2\eta)p^* g(\tau) \tag{206}$$

where τ is the dimensionless time $4ct/\lambda^2$ and the dimensionless response function $g(\tau)$ is defined as

$$g(\tau) = \sqrt{\frac{\tau}{\pi}}\left[1 - \exp\left(\frac{-1}{\tau}\right)\right] + \left[1 - \operatorname{erf}\left(\frac{1}{\sqrt{\tau}}\right)\right] \tag{207}$$

This function, which varies between 0 and 1 as τ increases from 0 to ∞, is plotted in Figure 7. From this figure, it is seen that $g(\tau)$ reaches about 60% of its asymptotic value at $\tau = 1$. At $\tau \cong 100$, $\bar{\sigma}'_{tt}$ is virtually equal to the boundary value which was attained 'instantaneously'. Thus by introducing a length scale λ, it has become possible to introduce a time lag between the boundary pressure and the tangential stress.

This simple analysis suggests that rate effects that are sometimes observed in the tensile failure following pressurization of a hole – 'breakdown' – are actually linked to a mechanism of fluid diffusion and are the consequence of the interaction of two length scales: the diffusion length δ and the 'microstructural' length λ. In essence, the mere existence of a rate effect can be seen as evidence of the existence of a certain length scale λ in the failure mechanism. Only when the pressurization rate is 'slow' enough, is the underlying length scale λ concealed; this asymptotic behavior corresponds to the case when the stress, averaged in the boundary layer of thickness λ, is at all times proportional to the boundary fluid pressure.

(ii) Breakdown criterion

Using this approach, Detournay and Cheng [116] have investigated the influence of the pressurization rate on the magnitude of the breakdown pressure p_b (the critical pressure at which 'breakdown' takes place during pressurization of a borehole). An expression for p_b was derived which depends explicitly on a dimensionless pressurization rate γ

$$\gamma = \frac{A\lambda^2}{4cS} \tag{208}$$

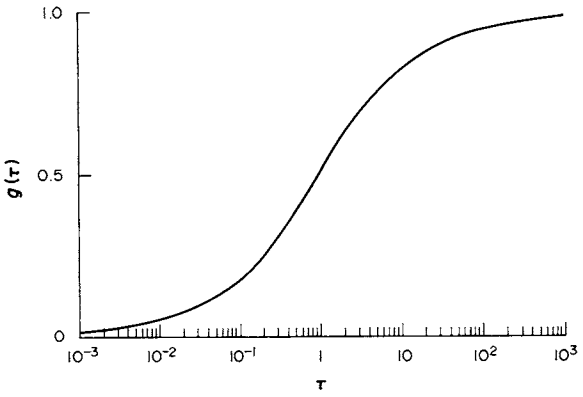

Figure 7 Response function for average tangential stress in the boundary layer

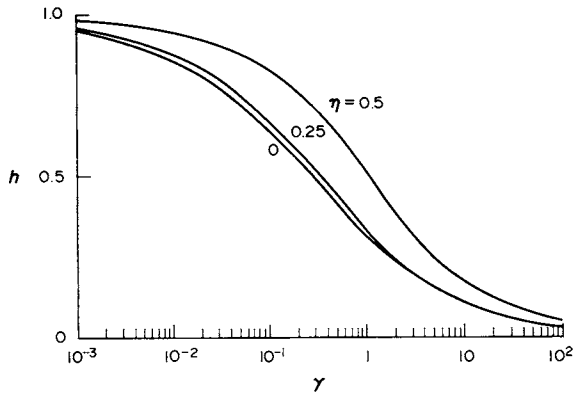

Figure 8 Plot of $h(\gamma)$ *versus* γ for $\eta = 0, 0.25, 0.5$

where A is the rate of increase of the borehole pressure and S a stress quantity defined as

$$S = 2P_0 - 4S_0 - 2p_0 + T \tag{209}$$

(P_0, S_0, and p_0 have the meaning defined in Section 5.6.3). The breakdown criterion can then be written as follows [116]

$$p_b - p_0 = \frac{S}{1 + (1 - 2\eta)h(\gamma)} \tag{210}$$

where the dimensionless function $h(\gamma)$ decreases from 1 to 0 as γ varies from 0 to ∞. The form of $h(\gamma)$ depends only on η (see Figure 8 where $h(\gamma)$ is plotted for $\eta = 0, 0.25, 0.5$).

On the basis of the characteristics of the function $h(\gamma)$, three different pressurization regimes can be identified: slow, transient, and fast.

(a) Slow regime ($\gamma < \gamma_l$). The slow asymptotic regime corresponds to the limit $\gamma \to 0$. In practice, this regime is approximately reached for $\gamma < \gamma_l(\eta)$ ($\gamma_l \cong 0.001$ for $\eta = 0.25$, corresponding to $h(\gamma_l) \cong 0.95$). The slow pressurization limit yields a lower bound value of the breakdown pressure p_{bl}, given by

$$p_{bl} - p_0 = \frac{S}{2(1 - \eta)} \tag{211}$$

This expression is equivalent to the Haimson–Fairhurst (H–F) breakdown equation [7].

(b) Fast regime ($\gamma > \gamma_u$). The fast asymptotic regime corresponds to the limit $\gamma \to \infty$ and thus to $h(\gamma) \to 0$. In practice, this regime is approximately reached for $\gamma > \gamma_u(\eta)$ ($\gamma_u \cong 100$ for $\eta = 0.25$, corresponding to $h(\gamma_u) \cong 0.05$). The fast pressurization limit yields an upper bound value of the

breakdown pressure p_{bu}, given by

$$p_{bu} - p_0 = S \tag{212}$$

This expression is identical to the Hubbert–Willis (H–W) breakdown equation [117].

(c) Transient regime ($\gamma_1 < \gamma < \gamma_u$). In this regime, p_b depends on the pressurization rate A. The breakdown pressure varies between the H–F and the H–W limit as γ increases between γ_1 and γ_u.

The H–F and H–W expressions for the breakdown pressure correspond, therefore, to the asymptotically slow and fast pressurisation regimes, respectively. It can be shown [116] that the H–F limit is actually the appropriate breakdown criterion for 'permeable' rocks, as hydraulic fracturing experiments in these rocks are practically always in the slow regime. However, rate effects are potentially significant in low permeability/low porosity rocks. Furthermore, it is in these rocks that the difference between the H–F and the H–W values is the largest (since α and thus $\eta \to 0$ when $\phi \to 0$). In this case, both the H–F and the H–W expressions are practically reachable limits, depending on the pressurization rate.

5.6.5 Hydraulic Fracture

5.6.5.1 Preamble

To conclude this overview of poroelastic mechanisms, we now study their roles in the context of a hydraulic fracture. Hydraulic fracturing involves several strongly coupled processes: fracture opening, viscous fluid flow in the fracture, diffusion of fracturing fluid in the porous formation and propagation of the fracture. Only one of the mechanisms involved in the modeling of the complete process will be addressed here; namely the relationship between the fracture width and the fluid pressure in the fracture. First, we study the fundamental response of a stationary fracture embedded in an infinite, two-dimensional, poroelastic medium. The response of a vertical hydraulic fracture bounded by impermeable elastic layers will be analyzed next.

5.6.5.2 Griffith crack

As an introduction to this analysis of poroelastic effects in hydraulic fracturing, we begin with the problem of a Griffith crack with length L, internally loaded by a fluid at pressure p^* [17]. Our main objective is to calculate the time evolution of the average fracture width w.

As before, the fluid pressure loading is decomposed into modes 1 and 2; the poroelastic response of the fracture to a step loading is expressed in terms of two functions of the dimensionless time $\tau = 4ct/L^2$, $w^{(1)}(\tau)$ and $w^{(2)}(\tau)$.

(i) Mode 1 loading

The instantaneous average fracture aperture at $t = 0^+$ is given by Sneddon's solution [118] with undrained elastic constants

$$w^{(1)}(0^+) = \pi L(1 - \nu_u)p^*/4G \tag{213}$$

while the long-term value $w^{(1)}(\infty)$ is given by the same expression with ν_u replaced by ν. The final fracture aperture is greater than the initial one (this is expected since the poroelastic material is softer when drained). The maximum time-dependent width increase, $\Delta w^{(1)}(\infty)$, experienced by the fracture is thus given by

$$\Delta w^{(1)}(\infty) = \pi L(\nu_u - \nu)p^*/4G \tag{214}$$

It is convenient to introduce the dimensionless width response function $f^{(1)}(\tau)$, which varies between 0 and 1 as τ increases from 0 to ∞

$$w^{(1)}(\tau) = w^{(1)}(0^+) + \Delta w^{(1)}(\infty) f^{(1)}(\tau) \tag{215}$$

The response function can be computed by modeling the fracture using a distribution of singularities to account for the discontinuity of flux and displacement that characterize the crack [17] (see also Section 5.5.4.2). The function $f^{(1)}(\tau)$ depends on the values of ν, ν_u and α; it is plotted in Figure 9 for

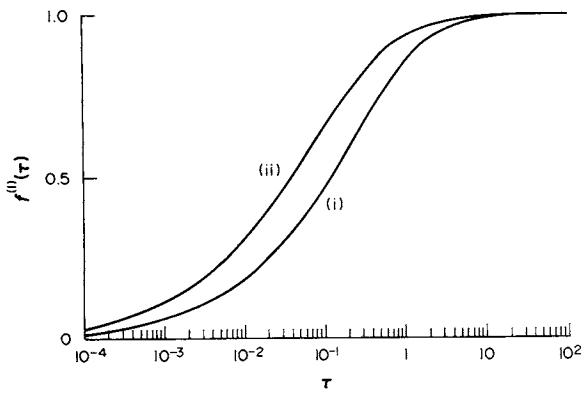

Figure 9 Mode 1 response function for average fracture width in the Griffith crack problem

two limiting cases: (i) the 'soil mechanics' case ($\nu_u = 0.5$, $\alpha = 1$) and (ii) the uncoupled case ($\nu_u \cong \nu$) (in the limit $\nu_u \to \nu$, $\Delta w^{(1)}(\infty) \to 0$, but the response function $f^{(1)}(\tau)$ remains defined).

(ii) Mode 2 loading

When a constant pore pressure p^* is applied on the fracture faces, the crack width decreases from 0 to the asymptotic value

$$w^{(2)}(\infty) = -\pi(1-\nu)L\eta p^*/4G \tag{216}$$

The crack thus closes under mode 2 loading as a result of the dilation of the porous solid around the fracture, caused by an increase of the pore pressure (of course it is assumed that the crack remains open under combined mode 1 and 2 loading).

The asymptotic value (equation 216) can be obtained using the following line of argumentation. In doing so, we first pretend that the fracture is closed or does not exist (while retaining the 'boundary' condition $p = p^*$) and calculate the stress induced across the fracture path at $t = \infty$. In a second stage, we calculate the fracture width induced by the removal of this stress along the fracture, as in a simple superposition problem.

At large time, the pore pressure diffusion equation (equation 82) uncouples from the volumetric strain rate (eventually to degenerate into the Laplace equation) and, as a consequence, the induced displacement field becomes irrotational. It has been shown earlier (see Sections 5.4.3.3 and 5.4.3.4) that in these circumstances the relationship between the stress and the pore pressure is given by

$$\sigma_{xx} + \sigma_{yy} = -2\eta p \tag{217}$$

As $t \to \infty$, the pore pressure p in the region around the fracture approaches the asymptotic value of p^* and induces, by symmetry, a uniform confining stress $\sigma_{xx} = \sigma_{yy}$. It then follows from equation (217) that

$$\sigma_{xx} = \sigma_{yy} = -\eta p^* \quad \text{as} \quad t \to \infty \tag{218}$$

A compressive stress of magnitude ηp^* (sometimes called 'back-stress' [119]) is thus generated across the fracture path at $\tau \to \infty$ by mode 2 loading. To obtain the solution of a fracture with zero stresses on the surface, we must superpose the solution of a Griffith fracture in a drained medium with a tensile stress $\sigma_n = \eta p^*$ applied on the fracture faces. The asymptotic value of the fracture width is hence given by equation (216), or equivalently by

$$w^{(2)}(\infty) = -\eta w^{(1)}(\infty) \tag{219}$$

The dimensionless response function $f^{(2)}(\tau) = w^{(2)}(\tau)/w^{(2)}(\infty)$ can be calculated in the same manner as $f^{(1)}(\tau)$ [17]; it is plotted in Figure 10 for the two limiting cases described above.

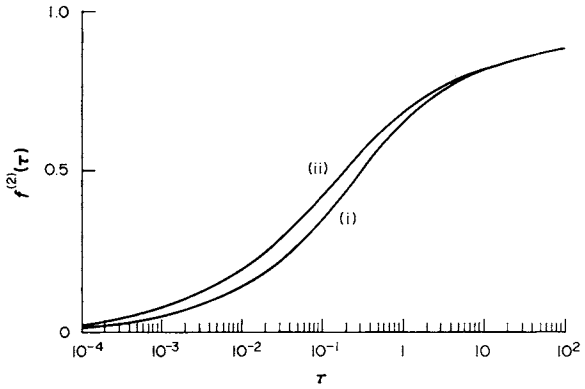

Figure 10 Mode 2 response function for average fracture width in the Griffith crack problem

(iii) Discussion

Figure 10 shows little difference in the response function $f^{(2)}$ computed for the two limiting poroelastic cases. This implies that the elastic coupling in the pore pressure diffusion equation is weak. (Note that the elastic coupling vanishes as $t \to \infty$, with the consequence that the uncoupled solution is asymptotically the correct solution for the coupled case, as time becomes large.) Furthermore, in taking into account the existence of a far-field compressive stress σ_0 perpendicular to the fracture plane, and a far-field pore pressure p_0 with $p^* > \sigma_0 > p_0$, we observe that the time-dependent part associated with mode 1 loading is generally overshadowed by mode 2 [17]. Indeed the term $(\nu_u - \nu)(p^* - \sigma_0)$ is typically much smaller than $\eta(p^* - p_0)$. Hence, we can conclude that the influence of the coupling 'solid to fluid' (as embodied in the difference between ν_u and ν or by the departure of the Skempton B coefficient from 0) does not generally play an important role for this class of problems; in other words, these problems can satisfactorily be solved within the framework of 'uncoupled' poroelasticity (*i.e.* only with a coupling 'fluid to solid').

5.6.5.3 Vertical hydraulic fracture bounded by impermeable layers

We now turn toward the somewhat more realistic geometry of a vertical hydraulic fracture, of height H, confined within a horizontal permeable layer bounded by impermeable semiinfinite strata (see Figure 11). (In practice this type of geometry can occur when a permeable sandstone, saturated with oil, is bounded by quasi-impermeable shales.) If a sufficiently high contrast in horizontal stress exists between the permeable and impermeable layers, the hydraulic fracture remains confined to the reservoir layer, and propagates laterally with a constant height.

In these conditions, provided the length of the fracture is much larger than its height, propagation of the hydraulic fracture can be simulated using the 'one-dimensional' model, developed by Perkins and Kern [120], and Nordgren [121], and known as the PKN model. The PKN model can be used to predict the transient evolution of the fracture length and the 'fracturing pressure' (the pressure at the fracture inlet). One of the ingredients needed for the PKN model is the relation between the average fracture width and the fluid pressure in a plane cross section perpendicular to the fracture direction (such as shown in Figure 11). This relation, which incorporates poroelastic effects, is calculated below.

We assume the existence of a far-field compressive stress σ_0 and pore pressure p_0 ($< \sigma_0$) in the poroelastic layer (see Figure 11). Starting at time $t = 0$, a fluid of the same compressibility and viscosity as the pore fluid is injected into the fracture at a pressure $p^* > \sigma_0$. As for the Griffith fracture, the analysis of the poroelastic response is here restricted to the determination of the evolution in time of the average fracture width w.

The loading provided by the fluid in the fracture is again decomposed into two modes; and the modal response functions are calculated for conditions where the far-field stress and pore pressure are both zero. Details on the solution of this problem can be found elsewhere [122]. Here we analyze this problem within the restricted framework of uncoupled poroelasticity, and under the particular conditions where the bounding layers have the same elastic properties as the permeable layer (as in the case of the Griffith crack problem, the elastic coupling in the diffusion equation governing the pore pressure can be shown to be weak [122]).

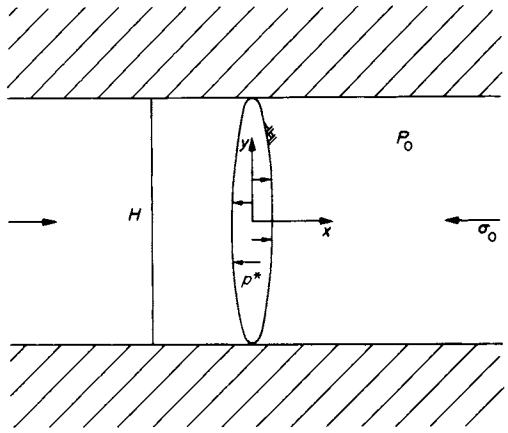

Figure 11 Vertical hydraulic fracture bounded by semi-infinite impermeable elastic layers

(i) Mode 1 loading

Under the approximation $\nu_u \cong \nu$, the response of the fracture to mode 1 loading is simply elastic. Hence

$$w^{(1)} = \frac{\pi(1 - \nu)Hp^*}{4G} \tag{220}$$

(ii) Mode 2 loading

A special form of the reciprocal theorem for the uncoupled quasi-static theory of poroelasticity leads to the following form of the average fracture width $w^{(2)}$ (see Timoshenko and Goodier [123] for derivation of this theorem for the mathematically equivalent theory of thermal stress)

$$w^{(2)} = \frac{2\alpha}{H}\int_0^{\infty}\int_{-H/2}^{H/2} p^{(2)}(x, t)\varepsilon^*(x, y)\,dx\,dy \tag{221}$$

where ε^* is the elastic volumetric deformation induced by a unit normal stress in the fracture, and $p^{(2)}(x, t)$ is the pore pressure field corresponding to mode 2 loading. Note that the volume integral extends only over the permeable layer, because the pore pressure is zero everywhere else.

Since p is here governed by an homogeneous diffusion equation and given the boundary conditions controlling the diffusion problem, the pore pressure field in the permeable layer is actually given by the one-dimensional solution (equation 152). Also, using a distribution of dislocation to model the fracture, ε^* can be expressed in the following integral form

$$\varepsilon^*(x, y) = \frac{1 - 2\nu}{\pi G}\int_{-H/2}^{+H/2} \frac{2\xi(y - \xi)\,d\xi}{\sqrt{H^2 - 4\xi^2}[(y - \xi)^2 + x^2]} \tag{222}$$

As before, we can express the response function $w^{(2)}$ as

$$w^{(2)} = w^{(2)}(\infty)f(\tau) \tag{223}$$

where $w^{(2)}(\infty)$ is the long-term asymptotic fracture width and $f(\tau)$ a dimensionless response function (varying between 0 and 1) of the normalized time $\tau = 4ct/H^2$. The asymptotic value of $w^{(2)}$ can be obtained by setting the pore pressure field equal to p^* in equation (221). The integration yields

$$w^{(2)}(\infty) = -2\eta w^{(1)} \tag{224}$$

In a situation similar to the Griffith crack, the diffusion of pore pressure acts therefore to close the fracture, by inducing a volumetric expansion of the rock in the permeable layer. It is interesting to note, however, that the asymptotic value given by equation (224) is exactly twice the limit derived for the poroelastic Griffith crack problem. The reasons are elaborated below, using heuristic arguments.

The influence function $f(\tau)$ can be expressed as follows, using equations (221), (152) and (222),

$$f(\tau) = \frac{4}{\pi}\int_0^\infty \operatorname{erfc}\left(\frac{\chi}{2\sqrt{\tau}}\right) g(\chi)\, d\chi \tag{225}$$

where $\chi = 2x/H$ and $g(\chi)$ is a 'spatial' influence function. (Note that $\chi = 2x/H$ is introduced to allow the interpretation of g as a spatial influence function.)

$$g(\chi) = 1 - \sqrt{\frac{\chi}{2}(\sqrt{4+\chi^2} - \chi)} \tag{226}$$

The function $g(\chi)$ decays monotonically from the value of 1 at $\chi = 0$ to 0 at $\chi = \infty$ (see Figure 12). This figure clearly indicates that beyond a distance $4H$ from the fracture, there is hardly any contribution from the rock volumetric deformation (due to pore pressure change) to the fracture volume.

Figure 13 presents a plot of the response function $f(\tau)$. Comparison with Figure 10 clearly indicates an increase of the characteristic time (which can loosely be defined as the time required to reach about 70% of the asymptotic effect) for the fracture bounded by impermeable barriers with respect to the Griffith crack. This difference is directly attributable to the presence of impermeable interfaces which are responsible for a one-dimensional diffusion process, in contrast to the two-dimensional one characterizing the poroelastic Griffith crack problem.

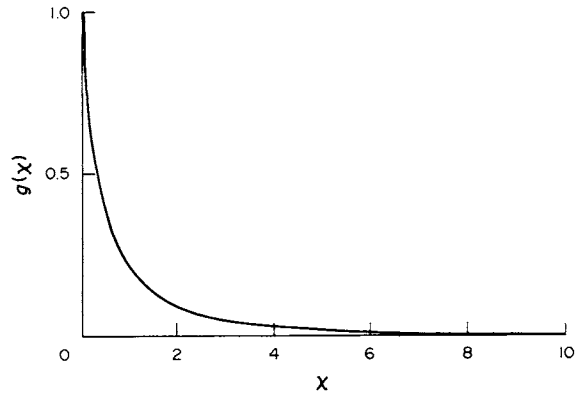

Figure 12 Spatial influence function giving the contribution to the fracture width change caused by a unit change of the pore pressure at distance $\chi = 2x/H$

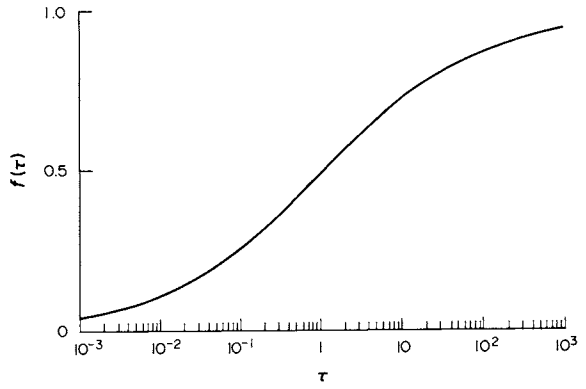

Figure 13 Mode 2 response function for average fracture width in the problem of a vertical hydraulic fracture bounded by impermeable elastic layers

(iii) Heuristic arguments for the mode 2 asymptotic limit

A simple mechanical model is now developed to calculate the asymptotic value $w^{(2)}(\infty)$. We use the same artifice as before; first we calculate the stress induced across the fracture by pretending that the fracture is closed, then we determine the change in fracture width induced by the removal of this stress.

We now contend that at large time (assuming the fracture closed), mode 2 loading induces a uniaxial strain state in the poroelastic layer such that

$$\varepsilon_{xx}^{\infty} = \varepsilon_{xy}^{\infty} = \sigma_{yy}^{\infty} = 0 \tag{227}$$

where the superscript $^{\infty}$ indicates that this state of deformation applies only at $t = \infty$. As a consequence of the infinite horizontal extent of the permeable layer and of the uniform pore pressure rise taking place throughout that layer at $t = \infty$, only a vertical strain can exist in the permeable layer at large time. The vanishing of the vertical stress at $t = \infty$ can be argued using the model of a one-dimensional column. The vertical stress σ_{yy} induced in the permeable layer is proportional to $H\varepsilon_{yy}/H_b$, where H_b is the height of the impermeable layer; since $H_b = \infty$, $\sigma_{yy}^{\infty} = 0$.

From the results of Section 5.6.1, we can immediately conclude that an increase of the pore pressure to p^* under conditions of uniaxial strain and constant axial stress induces in the poroelastic layer a compressive horizontal stress of magnitude $2\eta p^*$. Employing the principle of superposition, it is then deduced that

$$w^{(2)}(\infty) = -2\eta w^{(1)} \tag{228}$$

The asymptotic fracture closure for the three layer system (with uniform elastic properties) is thus twice as much as for the infinite homogeneous system. Note that the argument embedded in equation (228) is quite general, in so far as it also applies to the case where the bounding layers are characterized by different elastic properties; in other words, the effect of a contrast in elastic properties on the asymptotic value of $w^{(2)}$ is taken into account by the term $w^{(1)}$, which can be evaluated from an elastic analysis [122]. (In the context of a fully coupled poroelastic analysis, $w^{(1)}$ should be understood as $w^{(1)}(\infty)$, *i.e.* the elastic analysis must be carried out using the drained constant.)

In closing, it is worthwhile to point out that contrast in value of elastic constants between the permeable and impermeable layers appears to have a large effect on the response function $f(\tau)$ [122]. Impermeable layers that are stiffer than the permeable one cause an acceleration of fracture closure at early time, while softer impermeable layers have the opposite effect.

5.6.5.4 Applications

Taking into account the existence of a far-field stress σ_0 and a far-field pore pressure p_0 in the permeable layer, the expression for the average fracture width corresponding to a step loading of the internal fluid pressure p^* becomes

$$w = \frac{\pi(1-\nu)H}{4G}\left[(p^* - \sigma_0) - 2\eta\,(p^* - p_0)f(\tau)\right] \tag{229}$$

This equation can be substituted to the elastic fracture compliance equation in a PKN model of a hydraulic fracture [124]. Such a model has been used to investigate the impact of poroelastic effects on the time evolution of the fracture length and the fracturing pressure.

Note that the asymptotic fracture closure $w^{(2)}(\infty)$ for the case of the fracture in an infinite medium and the fracture bounded by impermeable layers were derived on the assumption that the fracture surface is directly exposed to a fracturing fluid of the same viscosity and compressibility as the reservoir fluid. This restriction can actually be overcome by interpreting $(p^* - p_0)$ in equation (229) as the difference between the pressure at the fracturing/reservoir fluid interface and the far-field pore pressure p_0 [124]. This approximation is acceptable as long as the penetration distance of the fracturing fluid in the rock remains small compared to the fracture height, which is the characteristic length controlling the poroelastic process.

An evaluation of the impact of poroelastic effects in hydraulic fracturing must address the issues of both magnitude and time-scale. Poroelastic mechanisms will play a significant role, only if: (i) its maximum potential effect is of the same order of magnitude as the elastic effect; and (ii) its

characteristic time is not small compared to the injection time. Here we have focused attention on the fracture closure induced by pore pressure diffusion in the permeable medium (rock). (There are other issues that need to be considered, such as the impact of poroelastic effects on the magnitude of the stress intensity factor.) It has been shown that the long-term closure (the 'magnitude') and the characteristic time (the 'time-scale') depend on the geometry of the fracture–rock system.

Under conditions where the poroelastic effects are important, it can be shown [124, 125] that they lead to an increase of the injection pressure and the closure pressure. (The closure pressure is the pressure at which the fractures close after the pumping is stopped and the well shut-in). This last point is of particular importance, since the closure pressure is generally interpreted as the far-field stress σ_0; neglect of poroelastic effects then leads to a systematic overestimation of the far-field stress perpendicular to the fracture plane.

5.7 APPENDIX A: EQUIVALENCE BETWEEN POROELASTIC CONSTANTS

In his landmark 1941 paper on poroelasticity [4], Biot introduced the following bulk dynamic and kinematic variables (in the current notation): the total stress tensor σ_{ij}, the fluid pressure p, the solid strain tensor ε_{ij}, and the variation of fluid volume content ζ. This theory was reformulated in 1955 [18] using the concept of partial stresses. In that formulation, the constitutive variables are: the solid partial stress tensor τ_{ij}, the fluid partial stress τ, the solid strain tensor ε_{ij}, and the fluid dilatation $\varepsilon = U_{i,i}$, where U_i is the fluid displacement vector. The relations between the two sets of variables are

$$\sigma_{ij} = \tau_{ij} + \delta_{ij}\tau \tag{230a}$$

$$p = -\frac{\tau}{\phi} \tag{230b}$$

$$\zeta = \phi(\varepsilon - \varepsilon) \tag{230c}$$

In this paper, we have followed the Biot 1941 formulation in terms of total stress, which was also adopted by Rice and Cleary [8]. There are however a large number of papers that follow the Biot 1955 convention (see also Biot [19], and Biot and Willis [31]). It is therefore necessary to clarify the equivalence between the constitutive constants introduced in the various formulations.

5.7.1 Biot, 1941

The constitutive constants H, R and Q (two of them are independent) introduced by Biot in 1941 [4] are here denoted as H', R' and Q' to avoid confusion, as these same symbols were redefined by Biot in 1955 [18]. The equivalence between $\{H', R', Q'\}$ and the present set $\{\alpha, K, K_u\}$ is

$$B = \frac{R'}{H'} \tag{231a}$$

$$K_u = \frac{KQ'}{R'} \tag{231b}$$

$$\alpha = \frac{K}{H'} \tag{231c}$$

Note that $Q' = M$, where M is defined in Biot and Willis [31].

5.7.2 Biot, 1955

The Biot 1955 [18] constants Q, R, M were discussed in detail by Biot and Willis [31]. The conversion to and from the present set follows the formulas below

$$R = \frac{\phi^2 B^2 K_u^2}{K_u - K} = \frac{\phi^2(K_u - K)}{\alpha^2} \tag{232a}$$

$$Q = \phi B K_u \left(1 - \frac{\phi B K_u}{K_u - K}\right) = \frac{\phi(\alpha - \phi)(K_u - K)}{\alpha^2} \tag{232b}$$

and

$$B = \frac{Q + R}{\phi\left[\dfrac{(Q+R)^2}{R} + K\right]} = \frac{\alpha M}{K + \alpha^2 M} \tag{233a}$$

$$K_u = \frac{(Q+R)^2}{R} + K = K + \alpha^2 M \tag{233b}$$

$$\alpha = \frac{\phi(Q+R)}{R} \tag{233c}$$

where $M = R/\phi^2$.

5.7.3 Biot and Willis, 1957

Biot and Willis [31] also introduced the following micromechanical parameters: κ' = jacketed compressibility (prime is added to avoid confusion with the permeability coefficient), δ = unjacketed compressibility and γ = coefficient of fluid content. They are related to the current micromechanical constants as

$$\kappa = \frac{1}{K} \tag{234a}$$

$$\delta = \frac{1}{K_s'} \tag{234b}$$

$$\gamma = \phi\left(\frac{1}{K_f} - \frac{1}{K_s''}\right) \tag{234c}$$

5.8 APPENDIX B: NOTATION

c	diffusivity coefficient
d	flux discontinuity
d_i	displacement discontinuity
e_{ij}	deviatoric strain tensor
f_i	fluid body force component
k	intrinsic permeability
n_i	unit outward normal vector
p	pore pressure
p'	Π-pressure
q	normal flux
q_i	specific discharge
s	pressure discontinuity
s_i	stress discontinuity
s_{ij}	deviatoric stress tensor
t_i	traction vector
u_i	solid displacement vector
B	Skempton pore pressure coefficient
C_{bc}, C_{bp}	bulk compressibilities
C_{pc}, C_{pp}	pore compressibilities
C_s, C_s', C_s''	solid phase compressibilities
F_i	bulk body force component
G	shear modulus
G_s	shear modulus of the solid phase
H', H''	poroelastic constants (see equation 4)
K	drained bulk modulus of elasticity
K_f	bulk modulus of fluid

K_p	bulk modulus of pores
K_s, K_s', K_s''	bulk modulus of solid phase (see equations 23 and 37)
K_u	undrained bulk modulus of elasticity
K_ϕ	bulk modulus of porosity
M	Biot modulus
P	total pressure (isotropic compressive stress)
P_s	pressure on the solid phase
P'	Terzaghi effective pressure
R	poroelastic constant
R'	poroelastic constant (see equation 4)
S	storage coefficient
V	total volume
V_f	volume of fluid
V_p	volume of interconnected pores
V_s	volume of solid phase
α	Biot coefficient of effective stress
β	effective stress coefficient for pore volume strain
γ	fluid source density
δ	Dirac delta function
δ_{ij}	Kronecker delta
ε	solid volumetric strain
ε_{ij}	solid strain tensor
ζ	variation of fluid content per unit volume of porous media
η	poroelastic stress coefficient
θ	volume of source injection
κ	mobility coefficient
μ	fluid viscosity
ν	drained Poisson ratio
ν_u	undrained Poisson ratio
σ_{ij}	total stress tensor
σ'_{ij}	Terzaghi effective stress tensor
ϕ	porosity
ω	frequency
ω^*	dimensionless frequency
τ	dimensionless time

ACKNOWLEDGEMENTS

E.D. would like to express his grateful thanks to the Department of Civil and Mineral Engineering of the University of Minnesota for granting him the MTS Visiting Professorship in Geomechanics during the fall quarter of 1990, as this gave him the opportunity to work on the first draft of this chapter. He also would like to acknowledge Schlumberger Cambridge Research for its support. Both authors wish to thank Dr. Christine Detournay and Dr. Anthony Pearson for their careful review of the manuscript and for their suggestions.

5.9 REFERENCES

1. Terzaghi K. Die berechnung der durchlassigkeitsziffer des tones aus dem verlauf der hydrodynamischen spannungserscheinungen. *Sitzungsber. Akad. Wissen., Wien Math. Naturwiss. Kl., Abt. IIa* **132**, 105–124 (1923).
2. Rendulic L. Porenziffer und Porenwasserdrunk in Tonen. *Der Bauingenieur* **17**, 559–564 (1936).
3. Biot M. A. Le problème de la consolidation des matières argileuses sous une charge. *Ann. Soc. Sci. Bruxelles* **B55**, 110–113 (1935).
4. Biot M. A. General theory of three-dimensional consolidation. *J. Appl. Phys.* **12**, 155–164 (1941).
5. Verruijt A. Elastic storage of aquifers. In *Flow Through Porous Media* (Edited by R. J. M. DeWiest). Academic Press, New York (1969).
6. Lewis R. W. and Schrefler B. A. *The Finite Element Method in the Deformation and Consolidation of Porous Media.* Wiley, London (1987).
7. Haimson B. C. and Fairhurst C. Hydraulic fracturing in porous-permeable materials. *J. Pet. Technol.* **21**, 811–817 (1969).

8. Rice J. R. and Cleary M. P. Some basic stress–diffusion solutions for fluid saturated elastic porous media with compressible constituents. *Rev. Geophys. Space Phys.* **14**, 227–241 (1976).
9. Rudnicki J. Effects of pore fluid diffusion on deformation and failure of rock. In *Mechanics of Geomaterials, Proc. IUTAM William Prager Symp. on Mechanics of Geomaterials: Rocks, Concrete, Soils* (Edited by Z. P. Bazant), Chap. 15, pp. 315–347. Wiley (1985).
10. Rudnicki J. W. and Hsu T,-C. Pore pressure changes induced by slip on permeable and impermeable faults. *J. Geophys. Res.* **93**, 3275–3285 (1988).
11. Detournay E., Cheng A. H.-D., Roegiers J.-C. and McLennan J. D. Poroelasticity considerations in *in situ* stress determination by hydraulic fracturing. *Int. J. Rock Mech. Min. Sci. & Geomech. Abstr.* **26**, 507–513 (1989).
12. Madsen O. S. Wave-induced pore pressure and effective stresses in a porous bed. *Geotechnique* **28**, 377–393 (1978).
13. Yamamoto T., Koning H. L., Sellmeijer H. and Van Hijum E. On the response of a poro-elastic bed to water waves. *J. Fluid Mech.* **87**, 193–206 (1978).
14. Cheng A. H.-D. and Liu P. L.-F. Seepage force on a pipeline buried in a poroelastic seabed under wave loadings. *Appl. Ocean Res.* **8**, 22–32 (1986).
15. Ruina A. Influence of coupled deformation–diffusion effects on the retardation of hydraulic fracture. In *Proc. 19th U.S. Rock Mech. Symp.*, Lake Tahoe, NV, pp. 274–282 (1978).
16. Cleary M. P. Moving singularities in elasto-diffusive solids with applications to fracture propagation. *Int. J. Solids Struct.* **14**, 81–97 (1978).
17. Detournay E. and Cheng A. H.-D. Plane strain analysis of a stationary hydraulic fracture in a poroelastic medium. *Int. J. Solids Struct.* **37**, 1645–1662 (1991).
18. Biot M. A. Theory of elasticity and consolidation for a porous anisotropic solid. *J. Appl. Phys.* **26**, 182–185 (1955).
19. Biot M. A. General solutions of the equations of elasticity and consolidation for a porous material. *J. Appl. Mech., Trans. ASME* **78**, 91–96 (1956).
20. Biot M. A. Thermoelasticity and irreversible thermodynamics. *J. Appl. Phys.* **27**, 240–253 (1956).
21. Biot M. A. Mechanics of deformation and acoustic propagation in porous media. *J. Appl. Phys.* **33**, 1482–1498 (1962).
22. Crochet M. J. and Naghdi P. M. On constitutive equations for flow of fluid through an elastic solid. *Int. J. Eng. Sci.* **4**, 383–401 (1966).
23. Morland L. W. A simple constitutive theory for a fluid-saturated porous solid. *J. Geophys. Res.* **77**, 890–900 (1972).
24. Atkin R. J. and Craine R. E. Continuum theories of mixtures: basic theory and historical development. *Q. J. Mech. Appl. Math.* **29**, 209–244 (1976).
25. Bowen R. M. Compressible porous media models by use of the theory of mixtures. *Int. J. Eng. Sci.* **20**, 697–735 (1982).
26. Katsube N. and Carroll M. M. The modified mixture theory for fluid-filled porous materials: theory. *J. Appl. Mech.* **54**, 35–40 (1987).
27. Coussy O. *Mécanique des Milieux Poreux*, p. 437. Editions Technip, Paris (1991).
28. Biot M. A. Theory of propagation of elastic waves in a fluid-saturated porous solid, part I: low frequency range. *J. Acoust. Soc. Am.* **28**, 168–178 (1956).
29. Carroll M. M. An effective stress law for anisotropic elastic deformation. *J. Geophys. Res.* **84**, 7510–7512 (1979).
30. Skempton A. W. The pore pressure coefficients A and B. *Geotechnique* **4**, 143–147 (1954).
31. Biot M. A. and Willis D. G. The elastic coefficients of the theory of consolidation. *J. Appl. Mech.* **24**, 594–601 (1957).
32. Green D. H. and Wang H. F. Specific storage as a poroelastic coefficient. *Water Resour. Res.* **26**, 1631–1637 (1990).
33. Geertsma J. The effect of fluid pressure decline on volumetric changes of porous rocks. *Trans. Am. Inst. Min. Metall. Pet. Eng.* **210**, 331–340 (1957).
34. Brown R. J. S. and Korringa J. On the dependence of the elastic properties of a porous rock on the compressibility of the pore fluid. *Geophysics* **40**, 608–616 (1975).
35. Carroll M. M. Mechanical response of fluid-saturated porous materials. In *Theoretical and Applied Mechanics, 15th Int. Cong. Theoretical and Appl. Mech.*, Toronto (Edited by F. P. J. Rimrott and B. Tabarrok), pp. 251–262 (1980).
36. Nur A. and Byerlee J. D. An exact effective stress law for elastic deformation of rock with fluids. *J. Geophys. Res.* **76**, 6414–6419 (1971).
37. Gassmann F. Elastic waves through a packing of spheres. *Geophysics* **16**, 673 (1951)
38. Carroll M. M. and Katsube N. The role of Terzaghi effective stress in linearly elastic deformation. *J. Energy Resour. Technol.* **105**, 509–511 (1983).
39. Katsube N. The constitutive theory for fluid-saturated porous materials. *J. Appl. Mech.* **52**, 185–189 (1985).
40. Mackenzie J. K. The elastic constants of a solid containing spherical holes. *Proc. Phys. Soc. London, Sect. B* **63**, 2–11 (1950).
41. Hill R. The elastic behavior of a crystalline aggregate. *Proc. Phys. Soc. London, Sect. A* **65**, 349–354 (1952).
42. Walsh J. B. The static deformation of rock. *J. Eng. Mech. Div., Am. Soc. Civ. Eng.* **106**, 1005–1019 (1965).
43. Zimmerman R., Somerton W. and King M. Compressibility of porous rock. *J. Geophys. Res.* **91**, 12 765–12 777 (1986).
44. Hughes D. S. and Cooke C. E. The effect of pressure on the reduction of pore volume of consolidated sandstones. *Geophysics* **18**, 298–309 (1953).
45. Knutson C. F. and Bohor B. F. Reservoir rock behavior under moderate confining pressure. *Proc. 5th U.S. Symp. Rock Mech.*, Minneapolis, MN (Edited by C. Fairhurst), pp. 627–659. Pergamon Press, Oxford (1963).
46. Hashin Z. and Shreikman S. Note on a variational approach to the theory of composite elastic materials. *J. Franklin Inst.* **271**, 336–341 (1961).
47. Zimmerman R. W., Haraden J. L. and Somerton W. H. The effects of pore pressure and confining pressure on pore and bulk volume compressibilities of consolidated sandstones. In *Measurement of Rock Properties at Elevated Pressures and Temperatures*, ASTM STP 869 (Edited by H. J. Pincus and E. R. Hoskins), pp. 24–36 (1985).
48. Green D. H. and Wang H. F. Fluid pressure response to undrained compression in saturated sedimentary rock. *Geophysics* **51**, 948–958 (1986).
49. Wissa A. E. Z. Pore pressure measurement in saturated stiff soils. *J. Soil Mech. Found. Div., Am. Soc. Civ. Eng.* **95** (SM4), 1063–1073 (1969).
50. Fatt I. The Biot–Willis elastic coefficients for a sandstone. *J. Appl. Mech.* **26**, 296–297 (1958).
51. Yew C. H. and Jogi P. N. The determination of Biot's parameters for sandstones, Part 1: Static tests. *Exp. Mech.* **18**, 167–172 (1978).

52. Yew C. H., Jogi P. N. and Gray K. E. Estimation of the mechanical properties of fluid-saturated rocks using the measured wave motions. *J. Energy Resour. Technol.* **101**, 112–116 (1979).
53. Bear J. *Dynamics of Fluids in Porous Media.* Elsevier, New York (1972).
54. Hubert M. K. The theory of groundwater motion. *J. Geol.* **48**, 785–944 (1940).
55. Scheidegger A. E. *The Physics of Flow Through Porous Media*, 3rd edn. University of Toronto Press, Toronto (1974).
56. Torquato S. Random heterogeneous media: microstructure and improved bounds on effective properties. *Appl. Mech. Rev.* **44**, 37–76 (1991).
57. Sokolnikoff I. S. *Mathematical Theory of Elasticity*, 2nd edn. McGraw-Hill, New York (1956).
58. McNamee J. and Gibson R. E. Displacement functions and linear transforms applied to diffusion through porous elastic media. *Q. J. Mech. Appl. Math.* **13**, 98–111 (1960).
59. Gibson R. E. and McNamee J. Plane strain and axially symmetric problems of the consolidation of a semi-infinite clay stratum. *Q. J. Mech. Appl. Math.* **13**, 210–227 (1960).
60. Gibson R. E. and McNamee J. A three-dimensional problem of the consolidation of a semi-infinite clay stratum. *Q. J. Mech. Appl. Math.* **16**, 115–127 (1963).
61. Cheng A. H.-D. and Liggett J. A. Boundary integral equation method for linear poroelasticity with applications to soil consolidation. *Int. J. Numer. Meth. Eng.* **20**, 255–278 (1984).
62. Cheng A. H.-D. and Liggett J. A. Boundary integral equation method for linear poroelasticity with applications to fracture propagation. *Int. J. Numer. Meth. Eng.* **20**, 279–296 (1984).
63. Detournay E. and Cheng A. H.-D. Poroelastic solution of a plane strain point displacement discontinuity. *J. Appl. Mech.* **54**, 783–787 (1987).
64. Cheng A. H.-D. and Predeleanu M. Transient boundary element formulation for poroelasticity. *Appl. Math. Model.* **11**, 285–290 (1987).
65. Verruijt A. The completeness of Biot's solution of the coupled thermoelastic problem. *Q. Appl. Math.* **26**, 485–490 (1969).
66. Schiffman R. L. and Fungaroli A. A. Consolidation due to tangential loads In *Proc. 6th Int. Conf. Soil Mech. Foundation Eng.*, Montreal, vol. 1, pp. 188–192 (1965).
67. Gibson R. E., Schiffman R. L. and Pu S. L. Plane strain and axially symmetric consolidation of clay layer on a smooth impervious base. *Q. J. Mech. Appl. Math.* **23**, 505–519 (1970).
68. Shanker N. B., Karma K. S. and Ratnam M. V. Consolidation due to shear loads distributed over a rectangular area. *Int. J. Numer. Anal. Meth. Geomech.* **2**, 329–342 (1978).
69. Vardoulakis I. and Harnpattanapanich T. Numerical Laplace–Fourier transform inversion technique for layered-soil consolidation problems: I. Fundamental solutions and validation . *Int. J. Numer. Anal. Meth. Geomech.* **10**, 347–365 (1986).
70. Verruijt A. Displacement functions in the theory of consolidation or in thermoelasticity. *J. Appl. Math. Phys.* **22**, 891–898 (1971).
71. Sandhu R. S. and Wilson E. L. Finite element analysis of seepage in elastic media. *J. Eng. Mech. Div., Am. Soc. Civ. Eng.* **95**, 641–652 (1969).
72. Christian J. T. Undrained stress distribution by numerical methods. *J. Soil Mech. Found. Div., Am. Soc. Civ. Eng.* **94**, 1333–1345 (1968).
73. Ghaboussi J. and Wilson E. L. Flow of compressible fluid in porous elastic solids. *Int. J. Numer. Meth. Eng.* **5**, 419–442 (1973).
74. Booker J. R. and Small J. C. An investigation of the stability of numerical solution of Biot's equations of consolidation. *Int. J. Solids Struct.* **2**, 907–917 (1975).
75. Zienkiewicz O. C. *The Finite Element Method*, 3rd edn. McGraw-Hill, New York (1977).
76. Zienkiewicz O. C. Basic formulation of static and dynamic behaviour of soil and other porous media. In *Numerical Methods in Geomechanics* (Edited by J. Martinus), pp. 39–56 (1982).
77. Cividini A. and Rossi A. Z. The consolidation problem treated by a consistent (static) finite element approach. *Int. J. Numer. Anal. Meth. Geomech.* **7**, 435–455 (1983).
78. Zienkiewicz O. C. and Shiomi T. Dynamic behavior of saturated porous media: the generalized Biot formulation and its numerical solution. *Int. J. Numer. Anal. Meth. Geomech.* **8**, 71–96 (1984).
79. Sandhu R. S., Lee S. C. and The H.-I. Special finite elements for analysis of soil consolidation. *Int. J. Numer. Anal. Meth. Geomech.* **9**, 125–147 (1985).
80. Boone T. J. and Ingraffea A. R. Numerical procedure for simulation of hydraulically driven fracture propagation in poroelastic media. *Int. J. Numer. Anal. Meth. Geomech.* **14**, 27–47 (1990).
81. Brebbia C. A., Telles J. C. F. and Wrobel L. C. *Boundary Element Techniques – Theory and Applications in Engineering.* Springer-Verlag, Berlin (1984).
82. Banerjee P. K. and Butterfield R. *Boundary Element Methods in Engineering Science.* McGraw-Hill, New York (1981).
83. Cheng A. H.-D. and Detournay E. A direct boundary element method for plane strain poroelasticity. *Int. J. Numer. Anal. Meth. Geomech.* **12**, 551–572 (1988).
84. Badmus T., Cheng A. H.-D. and Grilli S. A Laplace-transform based three-dimensional BEM for poroelasticity. *Int. J. Numer. Meth. Eng.* **36**, 67–85 (1993).
85. Dargush G. F. and Banerjee P. K. A time domain boundary element method for poroelasticity. *Int. J. Numer. Meth. Eng.* **28**, 2423–2449 (1989).
86. Nishimura N and Kobayashi S. A boundary integral equation method for consolidation problems. *Int. J. Solids Struct.* **25**, 1–21 (1989).
87. Vandamme L., Detournay E. and Cheng A. H.-D. A two-dimensional poroelastic displacement discontinuity method for hydraulic fracture simulation. *Int. J. Numer Anal. Meth. Geomech.* **13**, 215–224 (1989).
88. Curran J. H. and Carvalho J. L. A displacement discontinuity model for fluid-saturated porous media. In *Proc. 6th Int. Congr. Rock Mech.*, Montreal (Edited by G. Herget and S. Vongpaisal), pp. 73–78. Balkema, Rotterdam (1987).
89. Nowacki W. *Thermoelasticity*, 2nd end. Pergamon, Oxford (1986).
90. Cheng A. H.-D., Carvalho J. L. and Detournay E. Equivalence between direct and indirect boundary integral equations for linear poroelasticity. In *Computational Engineering with Boundary Elements*, 2: *Solid and Computational Problems* (Edited by A. H.-D. Cheng, C. A. Brebbia and S. Grilli), pp. 199–209. Comp. Mech. Publ., Southhampton (1990).
91. Morse P. and Feshbach H. *Methods of Theoretical Physics*, Parts I and II. McGraw-Hill, New York (1953).

92. Jaswon M. A. and Symm G. T. *Integral Equation Methods in Potential Theory and Elastostatics.* Academic Press, New York (1977).
93. Crouch S. L. and Starfield A. M. *Boundary Element Methods in Solid Mechanics*, Allen and Unwin, London (1983).
94. Booker J. R. and Carter J. P. Analysis of a point sink embedded in a porous clastic half space. *Int. J. Numer. Anal. Meth. Geomech.* **10**, 137–150 (1986).
95. Kanok-Nukulchai W. and Chau K. T. Point sink fundamental solutions for subsidence prediction, *J. Eng. Mech. Div., Am. Soc. Civ. Eng.* **116**, 1176–1182 (1990).
96. Hadamard J. *Lectures on Cauchy's Problem in Linear Differential Equations.* Dover, New York (1952).
97. Rudnicki J. W. Plane strain dislocations in linear elastic diffusive solids. *J. Appl. Mech.* **109**, 545–552 (1987).
98. Carslaw H. S. and Jaeger J. C. *Conduction of Heat in Solids*, 2nd edn. Clarendon Press, Oxford (1959).
99. Rudnicki J. W. and Roeloffs E. plane-strain shear dislocations moving steadily in linear elastic diffusive solids. *J. Appl. Mech.* **57**, 32–39 (1990).
100. Roeloffs E. and Rudnicki J. W. Coupled deformation–diffusion effects on water-level changes due to propagating creep events. *Pure Appl. Geophys.* **122**, 560–582 (1984/85).
101. Rudnicki J. W. Slip on an impermeable fault in a fluid-saturated rock mass. In *Earthquake Source Mechanics* (Edited by S. Das, J. Boatwright and C. H. Scholz), Geophys. Monogr. no. 37, pp. 81–89. American Geophysical Union, Washington, D.C. (1986).
102. Rudnicki J. W. and Koutsibelas D. Steady propagation of plane strain shear cracks on an impermeable plane in an elastic diffusive solid. *Int. J. Solids Struct.* **27**, 205–225 (1991).
103. Cheng A. H.-D., Badmus T. and Detournay E. Singular integral equation method for cracks embedded in poroelastic space. In *Boundary Elements X*, vol. 3: *Stress Analysis* (Edited by C. A. Brebbia).
104. Kenyon D. E. Transient filtration in a porous elastic cylinder. *J. Appl. Mech., ASME* **98**, 594–598 (1976).
105. Kenyon D. E. A mathematical model for water flux through aortic tissue. *Bull. Math. Biol.* **41**, 79–90 (1979).
106. Mei C. and Foda M. Wave-induced responses in a fluid-filled poroelastic solid with a free surface – a boundary layer theory. *Geophys. J. R. Astron. Soc.* **66**, 597–631 (1981).
107. Mei C. and Foda M. Boundary layer theory of waves in a poroelastic sea bed. In *Soil Mechanics – Transient and Cyclic Loads* (Edited by G. N. Pande and O. C. Zienkiewicz), Chap. 2. Wiley, New York (1982).
108. Verruijt A. Approximations of cyclic pore pressures caused by sea waves in a poroelastic half-plane. In *Soil Mechanics – Transient and Cyclic Loads* (Edited by G. N. Pande and O. C. Zienkiewicz), Chap. 3. Wiley, New York (1982).
109. Cheng A. H.-D., Badmus T. and Beskos D. E. Integral equation for dynamic poroelasticity in frequency domain with BEM solution. *J. Eng. Mech. Div., Am. Soc. Civ. Eng.* **117**, 1136–1157 (1991).
110. Stehfest H. Numerical inversion of Laplace transforms. *Commun. ACM* **13**, 47–49 and 624 (1970).
111. Mandel J. Consolidation des sols (étude mathematique). *Geotechnique* **3**, 287–299 (1953).
112. Cryer C. W. A comparison of the three-dimensional consolidation theories of Biot and Terzaghi. *Q. J. Mech. Appl. Math.* **16**, 401–412 (1963).
113. Detournay E. and Cheng A. H.-D. Poroelastic response of a borehole in a nonhydrostatic stress field. *Int. J. Rock Mech. Min. Sci. & Geomech. Abstr.* **25**, 171–182 (1988).
114. Wigglesworth L. A. Stress distribution in a notched plate. *Mathematika*, **4** (1957).
115. Whitney J. M. and Nuismer R. J. Stress fracture criterion for laminated composites containing stress concentration. *J. Compos. Mater.* **8**, 253–265 (1974).
116. Detournay E. and Cheng A. H.-D. Influence of pressurization rate on the magnitude of the breakdown pressure. *Proc. 33rd U.S. Symp. Rock. Mech.* pp. 325–333. Balkema, Rotterdam (1992).
117. Hubbert M. K. and Willis D. G. Mechanics of hydraulics fracturing. *Trans. Am. Inst. Min. Metall. Pet. Eng.* **210**, 153–163 (1957).
118. Sneddon I. N. The distribution of stress in the neighborhood of a crack in an elastic solid. *Proc. Roy. Soc. London, Ser. A* **187**, 229–260 (1946).
119. Cleary M. P. Analysis of mechanisms and procedures for producing favorable shapes of hydraulic fractures. In *Proc. 55th Annu. Fall Meeting, SPE-AIME*, Dallas, paper 9260 (1980).
120. Perkins T. K. and Kern L. R. Widths of hydraulic fractures. *Trans. Am. Inst. Min. Metall. Pet. Eng.* **220**, 937–949 (1961).
121. Nordgren R. P. Propagation of a vertical hydraulic fracture. *Trans. Soc. Pet. Eng. AIME* **253**, 306–314 (1972).
122. Boone T. J., and Detournay E. Response of a vertical hydraulic fracture intersecting a poroelastic formation bounded by semi-infinite impermeable elastic layers. *Int. J. Rock Mech. Min. Sci. & Geomech. Abstr.* **27**, 189–197 (1990).
123. Timoshenko S. P. and Goodier J. N. *Theory of Elasticity*, 3rd edn. McGraw-Hill, New York (1970).
124. Detournay E., Cheng A. H.-D. and McLennan J. D. A poroelastic PKN hydraulic fracture model based on an explicit moving mesh algorithm. *J. Energy Resour. Technol.* **112**, 224–230 (1990).
125. Boone T. J., Kry P. R., Bharatha S. and Gronseth J. M. Poroelastic effects related to stress determination by micro-frac tests in permeable rock. *Proc. 32nd U. S. Symp. Rock Mech.* pp. 25–34. Balkema, Rotterdam (1991).